# Sheffield Hallam University

*High temperature cracking of nickel chromium austenitic steels.*

HEMSWORTH, Brian.

Available from the Sheffield Hallam University Research Archive (SHURA) at:

http://shura.shu.ac.uk/19782/

## A Sheffield Hallam University thesis

HIGH TEMPERATURE CRACKING OF NICKEL CHROMIUM AUSTENITIC STEELS.


by BRIAN HEMSWORTH, A.C.T. (SHEFFIELD), M.MET.


A Dissertation submitted to the
C.N.A.A. for the Degree DOCTOR
OF PHILOSOPHY.


JANUARY, 1970.
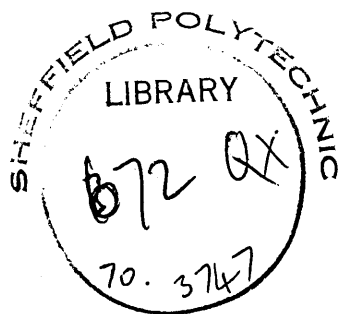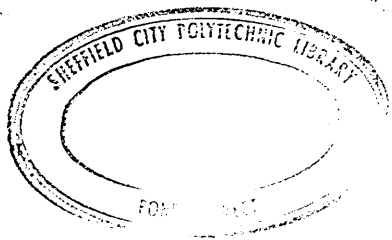
<u>PREFACE.</u>

This dissertation on the 'High Temperature Weld Cracking of Nickel Chromium Austenite Steels' is submitted for the degree Doctor of Philosophy of the Council for National Academic Awards under the guidance of the Department of Metallurgy, Sheffield Polytechnic. The research described was carried out in the period October, 1966, to October, 1969, at the Research and Development Department of British Steel Corporation, Midland Group, (formerly English Steel Corporation Limited); and at the Marchwood Engineering Laboratories, Central Electricity Generating Board, Southampton. Industrial Supervision of the work was initially undertaken by Mr. G.B. Allen, (British Steel Corporation) from October, 1966, to January, 1968, and finally by Dr. N.F. Eaton (C.E.G.B.) from January, 1968 to January, 1970. The Academic Supervisor and Director of Studies was Dr. R.P. Stratton of the Department of Metallurgy, Sheffield Polytechnic. Prior to carrying out the research programme the candidate has studied in the Post-Graduate School of Physical Metallurgy, University of Sheffield, and was awarded the degree Master of Metallurgy 1965. In addition, various advanced courses and conferences have been attended.

1. Martensite-fundamentals and technology. Sheffield Polytechnic, 1967.

2. Electron Microscopy. Sheffield Polytechnic, 1967.

3. Statistical Methods. Sheffield Polytechnic, 1967.

4. Fabrication of Austenitic Steels at the University of Birmingham, 1968.

5. Autumn Meeting of the Institute of Welding, October, 1968.
   Cracking of Welds.

To the best of my knowledge, the results, apparatus, and the theories described are original, except where reference is made to other work.

B. Hemsworth,
<u>January, 1970.</u>

# CONTENTS.

Figure 20.  Close up of tungsten inert gas (TIG) welding torch in position for carrying out melt runs.

Figure 21.  Shows overall set up of tensile machine and the X-Y recorder.

Figure 22.  Electrical circuit for measurement of applied stress and extension.

Figure 23.  Shows read out of applied stress against overall extension for a melt run.

Figure 24.  Schematic representation of the set up for evaluating manual arc electrodes.

Figure 25.  HAZ ductility dip cracking in AlSl 304 steel (18Cr 10Ni steel). X 270.

Figure 26.  Relationship between applied stress to initiate HAZ ductility dip cracking and grain size in AlSl 304 (18Cr 10Ni stainless steel).

Figure 27.  Relationship between overall extension at which HAZ cracking occurs and grain size in AlSl 304 (18Cr 10Ni stainless steel).

Figure 28.  Graph of Vickers hardness plotted against ageing time for A286.

Figure 29.  Bead on plate testing of A286 using the W.R. K S10 experimental manual metal arc electrode.

Figure 30.  Shows rosette shaped cavities associated with "Chinese script" orientated liquation phases in thw HAZ.  Unetched.  X 1000.

Figure 31.  HAZ liquation region associated with straighter edged cracking which is presumably wetted by the excess liquid.  Unetched.  X750.

Figure 32.  Non-metallic films in the HAZ of A286.  Unetched.  X 750.

Figure 33.  Shows HAZ cracks propagating normal, to the fusion boundary.  Note their jagged morphology in the region of the fusion boundary and their more straight edged morphology in the colder regions. Etched in Metharegia.  X 150.

Figure 34.  Shows detail of jagged shaped liquation cracks in the HAZ.  Note their association with a titanium carbonitride particle.  X 550.

Figure 35.  Shows the heavily microsegregated parent metal after etching in the selective mixed acids reagent.  Note the strong remains of the dendritic structure of A286 even after heavy hot deformation. (Selectively etched).  X 25.

Figure 36.  Shows the fusion boundary and HAZ in A286.  The white etching regions are the interdendritic interstices which are locally enhanced in low melting point elements.  (Selectively etched). X 150.

Figure 37.  Detail of white etching regions show that they are a preferential paths for crack propogation.  (Selectively etched).  X 300.

Figure 38.  Showing rosette shaped liquation cracks in the white etching regions.  (Selectively etched).  X 480.

Figure 39.  Shows liquation cracking associated with titanium rich phase. Compare with figures 30, 31.    Unetched.

Figure 40.  Shows the regions which liquate are enriched in Ti and Mo but they are not necessarily at grain boundaries where the cracks initiate.

Figure 41.  Film like arrays of possible Y-phase ($M_2CS$) or titanium sulphide which are too thin to detect by electron-micro-probe analysis.

Figure 42.  Shows the composition of the white etching region to be enhanced in titanium and nickel and depleted in iron and chromium. (See figures 37 and 38).

Figure 43.  Shows liquated titanium sulphide in the Zone 1 of the HAZ of A286.  Electron-microscope micro analysis indicates Ti and S.

Figure 44. Zone 1 of HAZ. Shows fern shaped $Ti_5S_4$. Indexed selected area electron diffraction pattern sheet 1 Appendix 1. Electron-microscope-micro-analysis also indicates Ti and S.

Figure 45. Dendritic sulphides of titanium indicated by electron-microscope-micro-analysis.

Figure 46. Dendritic $Ti_5S_4$ selected area electron diffraction pattern indexed sheet 2 Appendix 1.

Figure 47. Selected area electron diffraction indicates the particles are dendritic arrays of $M_6C$. Sheet 3, Appendix 1.

Figure 48. Detail of $M_6C$ in the HAZ of A286. (See figure 49 and sheet 3, Appendix 1) for selected area electron diffraction pattern.

Figure 49. Indexed diffraction pattern of $[001]$ zone of $M_6C$.

Figure 50. Shows liquated iron titanium phase.

Figure 51. Electron-microscope-micro-analysis indicates Fe-Ti phase.

Figure 52. Dendritic liquated Fe-Ti phase.

Figure 53. Liquated Fe-Ti phase associated with thermal faceting.

Figure 54. Unsolved selected area electron diffraction pattern of Fe-Ti phase. Possibly a $[123]$ zone of the F.C.C. crystal Appendix 1 Sheet 7.

Figure 55. Show titanium vanadium carbosulphide ( Y-phase) in HAZ of A286. This particular region is near the fusion boundary.

Figure 56. Shows detail of titanium vanadium sulphide or carbosulphide (Y-phase) in the HAZ of A286.

Figure 57. Selected area electron diffraction pattern indicates $[0001]$ zone basal plane of hexagonal close packed crystalof the phase. (Appendix 1, sheets 4-6).

## SUMMARY.

On the basis of published work and the experimental results of this investigation, a detailed classification of high temperature weld cracking is proposed. Two major types of cracking are recognised: Type 1 - separations along boundaries decorated with liquated second phase resulting from microsegregation, (solidification cracking in the weld metal and liquation cracking in the HAZ (Heat Affected Zone) ): Type 2 - separations associated with relatively clean grain boundaries caused by grain boundary sliding in the solid state and they are synonymous with creep rupture. This form of cracking is referred to as ductility dip cracking because it is believed to be associated with a ductility minimum which occurs in some alloys.

In order to study high temperature weld cracking in detail, a reliable and reproducible means of producing cracks is required. To fulfil this need, an experimental horizontal tensile machine was designed and constructed. The high temperature weld cracking resistance is expressed in terms of the applied stress and overall extension necessary to initiate cracking. Using this apparatus, the effect of grain size on the HAZ (Heat Affected Zone) cracking of AISI 304 (an 18Cr 10Ni non-hardenable austenitic steel in which the grain boundaries are free to migrate) was investigated. A linear relationship between applied cracking stress and the reciprocal of the square root of the grain size was found. This is consistent with the cracking theories.

Bead on plate tests carried out on a more complex alloy, A286 (a 25Ni 15Cr intermetallic strengthened austenitic steel in which the grain boundaries are not free to migrate) verified the adverse effect of a coarse grain size. Cracking occurred in the HAZ (Heat Affected Zone) without an

applied stress being required, and this was due to the formation of titanium rich liquid phases which wet the grain boundaries and render the steel hot short. Detailed light and electron microscopy complemented by electron-micro-probe-analysis revealed the cracking mechanism to be two stage: Initiation by liquation (Type 1) and propagation by a solid state creep rupture process (Type 2). A 0.39 wt% boron addition to the basic composition of A286 was found to improve the cracking resistance by refining the parent metal grain size and making the steel more resistant to grain coarsening during welding. The boron was also found to alter the elemental solidification sequence of A286 and it avoids the formation of the white etching hot short regions.

# 1. GENERAL INTRODUCTION.

Austenitic nickel-chromium steels have excellent corrosion resistances and elevated temperature properties and they are used extensively in the chemical and power generating industries. Modern plant requirements have resulted in the development of steels with improved creep resistances (i.e. increased resistance to time dependent hot deformation which often results in a decrease in the resistance to high temperature cracking. This has led to an increase in the incidence of cracking during casting, hot working and welding and the application of these alloys has therefore been limited.

During fusion welding of creep resistant alloys a complex form of cracking may take place both in the heat affected zone (HAZ) and in the weld metal. The cracking is always intergranular and it is generally referred to by such terms as hot tearing and hot cracking. In austenitic steels the cracks may be so small (micro-fissures) that they are not detected by non-destructive testing. However, the cracks can be sufficiently extensive to provide notches and preferential corrosion paths for premature failure in service. The lack of knowledge of the mode of formation and the methods of eliminating intergranular cracking coupled with the cost of weldment failures were the main reasons for commencing this programme of work.

Unfortunately an ambiguous terminology has evolved to describe weldment cracking and the first task of this investigation is to systematically classify the possible forms of high temperature cracking based on the literature and the experimental results. The proposed classification of cracking is consistent with the cracking theories which postulate a liquid-solid as well as a solid state cracking mechanism. The exact cause of cracking is not yet fully understood but it is thought to be caused by a

combination of mechanical and metallurgical factors.  The mechanical factor takes the form of the shrinkage stresses and strains induced during the welding thermal cycle and the metallurgical factor is influenced by the degree of microsegregation and the grain size.  It is known that both weld metal cracking and heat affected zone (HAZ) cracking are often caused by liquid films which wet the grain boundaries and embrittle the steel.  Both the mechanical and metallurgical factors can be adjusted.  A suitable pre-heat will reduce the thermal strains whereas a fine grain size and a restriction in the amount of impurities will increase the high temperature cracking resistance.  The introduction of a second phase such as delta ferrite or the eutectic boride may also reduce the incidence of cracking by reducing the grain size.

In the literature describing the various methods of estimating the hot cracking resistance, no single method has been universally accepted. An alternative method of assessing the hot cracking resistance of steels has been developed in this investigation.  This necessitated the construction of a horizontally opposed tensile machine of original design.  The test consists of loading a test plate in the machine, to a stress at which cracking occurs during welding.  The cracking is reflected by an increase in the extension of the test specimen.  It is believed that this test procedure is a more sensitive and reproducible means of assessing the high temperature weld cracking resistance of steels than tests which rely on the difficult and debatable measurement of crack length.

Two austenitic steels were used in this investigation having widely differing weld cracking resistances.  AISI 304 is an 18Cr10Ni, non-hardenable steel in which the grain boundaries are free to migrate and only when the

steel is coarse grained is weld cracking a problem. The experimental tensile machine was used to investigate the effect of grain size on the high temperature weld cracking of this steel. By sharp contrast A286 is an intermetallic strengthened, 25Ni, 15Cr steel, in which the grain boundaries are not free to migrate and cracking is most likely during fusion welding. The various methods of reducing cracking in this steel have been fully investigated. Detailed light microscopy, electron microscopy complemented by a electron micro-probe-analysis have provided the evidence to postulate a cracking mechanism.

A 0.39 wt% boron addition was found to improve the high temperature weld cracking resistance and the reasons for the beneficial effects of boron are described. The full details of the literature survey and the experimental results are contained in the following report.

## CHAPTER 1.   CRACKING TERMINOLOGY.

### 1.1  Introduction.

The general phenomenon of ferrous and non-ferrous alloys exhibiting low ductility when stressed in the vicinity of their solidus temperature has been a problem since the early days of metal manufacture. Over the years, as each stage of metal production has developed, an ambiguous often confusing terminology has evolved to describe the same intergranular cracking. In the casting bay, cracking is referred to by such terms as Ingotism and Panel Cracking (1). Unfortunately, these terms only convey the location of cracking along the flat faces of the ingots and they do not indicate their micro-structural nature. In the foundry industry, a similar form of cracking is referred to by the most mis-used term Hot Tearing, (2,3). This term attempts to convey the temperature of formation and the mode of fracture. Other terms

used to describe the separations which occur during the solidification of metals are Shrinkage Cracking (3) and Contraction Cracking (3). During the hot deformation of metals, intergranular cracks often form and terms such as Hot Shortness (4), Hot Short Cracking, (8, 20), Forge Cracking (8), Over-heating (5,6) and Burning (5,6) are used. When the intergranular fracture surfaces have a dull appearance the fracture is said to be Matt-Faceted (7). Burnt steels when fractured show a texture which is often referred to as "Coaky" (8) in appearance. In nickel base alloys during hot working the surfaces of the metal may exude a silicon rich liquid phase which is described as "Freckle Formation" (9). In the manufacture of tin bronzes and grey cast irons a similar effect is referred to as "Tin Sweat" (3,10) when a tin rich liquid containing sulphur and phosphorus exudes from the cast surfaces.

## 1.2 Terminology used in Welding Literatures.

Unfortunately the technology of welding has developed later than casting and hot working industries and the evolution of the various terms to describe intergranular cracking has been insular. It is therefore not surprising to find a whole new range of technical jargon to describe the same basic form of intergranular cracking. As with the other stages of metal production original descriptive terms have evolved such as Crater Cracking (11), Star Cracking (11), Root Notch Cracking (11) and Underbead Cracking (11). In the special case of electroslag welding, which is basically a continuous casting process, the cracking which occurs at the start and the finish of welding is described as the Start and Finish Defect (12). This form of defect is not unlike the Piping (13) which occurs during the solidification of ingots. Orientation with respect to the welding

direction is thought important (14) and terms such as Longitudinal cracking and Centre-line cracking refer to cracks propagating in the direction of welding whereas the term Transverse Cracking applies to cracks propagating normal to the welding direction. Size is considered to be relevant and terms such as Macro-Cracks for the large cracks and Micro-Cracks or Fissures for small cracks are used. Radiography has also evolved a descriptive term for the type of intergranular cracking which appear to ignore the welding direction and terms such as Check Cracking (14) or Multi-Directional Cracking (14) are often used.

Since the various technologies have developed separately, it is not surprising to find such a confusing terminology. In an attempt to place welding on a more scientific basis, terms such as Hot Tearing (15,16), Hot Cracking (17), Super-Solidus Cracking (17,18) and Sub-Solidus Cracking (17,18) have been applied. According to the Welding Institute (15), heat affected zone hot tears can be distinguished by the following characteristics:

(i)     The path of hot tears is always intergranular with respect
        to the prior austenitic grains.

(ii)    Hot tears are usually accompanied by redistribution of non-
        metallic inclusions and the formation of arrays of non-
        metallic particles at prior austenite grain boundaries.

(iii)   Hot tears form short microcracks often confined to a portion
        of the prior austenite grain boundary and seldom exceeding a
        few prior austenite grain diameters in length.

(iv)    Hot tears can be observed in the heat affected zones having
        ferritic-pearlitic microstructures which would not be expected
        to show cold cracking.

Foundry technologists would modify the Welding Institute description

of hot tearing and Middleton (2) has defined this form of cracking as follows.

"Hot tears can always be distinguished by their discontinuity, i.e. the irregular and jagged appearance of the crack, and often the connection of small unconnected ruptures. They are interdendritic and follow the dendritic solidification pattern. The surfaces of hot tears are oxidized and discoloured and they may exhibit decarburization and a coarse dendritic structure".

From these two descriptions it is obvious that the word 'Hot Tearing' has a different meaning to different people, and it is in the welding literature where the confusion exists because this term has been used for many years in the foundry industry. Even though there are major discrepancies between the respective definitions, there are basic similarities. For example, both cracks are associated with microsegregation, formed at high temperature, and they are intergranular.

To help clear up this apparent confusion Borland (17) proposed a generalised theory on which cracks which form in weld metals and castings in the presence of a liquid films are referred to as Super-Solidus Cracks. Brockhurst and Muir (18) have extended this classification to distinguish three main types of cracking which are as follows:

(1) Rupture occurring at temperatures which are above the equilibrium solidus temperature of the alloy concerned. This can be referred to as "hot tearing".

(2) Rupture at temperatures which may be considered below the apparent equilibrium solidus temperature for the alloy in question, but which may still involve the presence of liquid in the form of low melting point impurity constituents. The term 'hot cracking' may be reserved for this mode of failure.

(3) Rupture may also occur at temperatures which are sufficiently low to
eliminate the possibility of a liquid phase. Failure may be due to
the presence of solid phases of low ductility, or to the operation of
creep deformation mechanisms. This form of cracking may be referred
to as "stress rupture", "creep rupture" or "hot brittleness".

There is evidence to suggest that the first two modes of rupture
involve very similar mechanisms. The distinction between them may be based
partly on the morphology of the crack - hot tears being more jagged than
hot cracks and partly on the fact that hot tearing is "super-solidus" while
hot cracking is "sub-solidus" cracking, at least as far as the main
intentional constituents of the alloy are concerned. In both cases the
fracture path is intergranular". From Brockhurst and Muir's analysis,
temperature is the main criterion on which to classify cracking. At
high temperature (super-solidus) hot tearing occurs in the presence of
a liquid phase whereas in the fully solidified mass hot cracking occurs
at some (sub-solidus) temperature and at even lower temperature stress
rupture occurs. The issue is even further confused by Hull (19) who
considers hot cracking to only occur at "super-solidus" temperatures.

In the author's opinion this commitment to a time at temperature
is unnecessary and impracticable, and this is the weakness of using
temperature as the classification parameter.

In an attempt to rationalize a classification of cracking Kammer
et al (14) have proposed that the appearance and their condition of
formation are the most important parameters of cracking. The essence of
this classification has been summarised in Table 1. In the literature up
to 1967, this is the most systematic analysis of the various forms of high
temperature cracking during welding. Unfortunately the classification is

ambiguous and complicated and includes nearly every possible parameter which may affect weld cracking.  There is therefore a need for an unambiguous classification of high temperature cracking which the author has attempted to compose.  The classification is presented in Chapter 3.

# CHAPTER 2.   THEORIES OF HIGH TEMPERATURE WELDMENT CRACKING.

## 2.1 Introduction

The theories of hot cracking are not very well developed. Many of these theories are of a foundry technology origin and they have been modified to explain weldment cracking. The theories may be divided into two basic groups. In the first main group, the SOLID-LIQUID THEORIES, the effect of a low melting point liquid spreading along a grain boundary is considered. From the observations of weldment cracking, the solid-liquid theories are far more likely to explain the type 1 cracking, as explained in Table 2. At temperatures which are sufficiently low to exclude the possibility of intergranular liquids, the cracking can be accounted for by the second main group; the SOLID STATE THEORIES. Such theories are related to creep rupture and are relevant to type 2 ductility dip cracking as summarised in Table 2.

## 2.2 Requirements of a Comprehensive Cracking Theory.

A theory of cracking must be related to practical circumstances and it should be valid over the high temperature range ( $>0.5$ $T_m$, where $T_m$ is the melting point in $^{\circ}K$). The theory should predict the conditions by which the two basic cracking types form and also explain the relative significance of liquated films, solid films, thermal faceting, and slip lines on the crack surfaces. Finally, a comprehensive theory should take into account the various physical parameters which may influence the mode of cracking. They are as follows:-

(1) Property of the intergranular microsegregates.

Such factors as the spreading tendency of the liquid films, thickness and the dihedral angle the films make with the grain boundaries.

(2) <u>Relationship with basic fracture theory.</u>

According to fracture theory a relationship should exist between

fracture stress, grain size and the surface energy of the crack

over the high temperature range.

(3) <u>High temperature properties of the alloy.</u>

The relative intergranular strength to intragranular strength for

a given alloy and the tendency of the grain boundaries to slide or

migrate over the high temperature range.

Needless to say, no comprehensive theory of weldment cracking has

been proposed. It is beyond the scope of this chapter to deal in great

detail with standard theories of high temperature cracking which are

contained in numerous reviews (14,17,20,21) but to give a brief outline of

the main theories which have been proposed.

## 2.3 Group 1 - Solid-Liquid Theories.

### 2.3.1 Descriptive Theories

Three main pictorial theories of cracking have been developed on

the basis of observations of solidifying castings. All three propose that

cracking is due to mechanical and metallurgical factors. The mechanical

factor increases as the restraint or hindrance to contraction increases

whereas the metallurgical factor is the formation of intergranular micro-

segregates in the form of liquid films.

(a) <u>The Shrinkage Brittle Theory</u> (22,23)

This theory has been mainly used to describe the cracking of

solidifying castings but it can be suitably modified for a weld metal.

The sequence of solidification is as follows:

(i) Of the liquid alloy a percentage is parent metal mixed with the weld

metal.

(ii) A solid skin first forms by rapid cooling. Solidification cracks form at the weakest point, the solid-liquid interface, and are healed by the remaining liquid. Dendrites nucleate and grow but a <u>coherent network</u> is <u>not</u> formed.

(iii) As the temperature decreases further, a coherent network of cells or dendrites is formed. Since the weldment is restrained the shrinkage stresses developed may exceed the rupture stress of the cored weld metal and solidification cracks can form. The cracks cannot be healed because the solidification structure is torn apart and there is insufficient liquid available for healing.

In the case of large castings and electroslag welds where there may be a hot spot (high temperature region), the shrinkage stresses are greatest and the cracking is most pronounced. Van Eeghem (24) has extended this theory to include cracks which form in the solid state along the impurity enriched prior austenite grain boundaries.

(b) <u>Strain Theory of Pellini</u> (25)

This theory proposes that cracking is due to the high strains which are set up by the steep temperature gradients and these tend to pull apart solid masses separated by a continuous film of liquid. Like the shrinkage brittle theory cracking occurs at or near the bulk solidus. A schematic drawing of the solidification sequence leading to cracking is shown in Figure 1.

(c) <u>Borlands Generalised Theory</u> (17)

The Borland generalised theory is a combination of the Shrinkage Brittle Theory plus the Strain Theory and also stresses the importance of dihedral angle. In this cracking model the solidification sequence is proposed in four main stages:

Stage 1     Primary dendrite formation

Stage 2     Dendrite interlocking

Stage 3     Grain boundary development

Stage 4     Complete solidification

The theory proposes that during stages 2 and 3 cracking occurs but liquid healing may take place in stage 2, whereas in stage 3 the dihedral angle is important.  A low contact angle will give a small solid to solid contact area and high stresses can build up which can result in cracking.

### 2.3.2 Interfacial Energy - Dihedral Angle Relationships (26)

Smith (26) has suggested that the distribution of a liquid particle at a grain boundary depends on the interfacial energies between the liquid and the solid.  The interfacial or surface energies operating can be approximated to simple surface tension or surface forces and by simple geometry (triangle or forces).

$$\gamma_{SS} = \gamma_{LS} \cos \theta/2$$

$$\tau = \frac{\gamma_{LS}}{\gamma_{SS}} = \frac{1}{2 \cos \theta/2}$$

where $\gamma_{LS}$ ------is the solid-liquid interface energy

$\gamma_{SS}$·········is the grain boundary solid-solid interface energy

$\theta$ --------is the dihedral angle

$\tau$----------is the ratio of the solid-liquid interface energy

$\gamma_{LS}$ to the solid solid interface energy $\gamma_{SS}$.

The relative interface energy ratio can be measured in terms of the dihedral angle of the solid-liquid interface as shown in the Figure 2a, 2b.  Smith et al have shown by micro-radiography that:

(1) When $180^\circ > \theta < 60^\circ$ the liquid takes the form of isolated particles on the grain boundaries and at triple points.

(2) When $\theta = 60^{\circ}$ the liquid forms a continuous film around the grain edges.

(3) When $\theta < 60^{\circ}$ the liquid film spreads out over the grain faces as the angle decreases giving complete coverage at $\theta = 0$.

### 2.3.3  The Saveiko Model (27)

Saveiko has suggested that a solidifying casting is analogous to a set of glass blocks separated by water films.  The force necessary to separate these two blocks of glass is given by the relationship.

$$P \approx \frac{A\gamma}{gb} \qquad \dots\dots (2)$$

where:

      P    is the force

      $\gamma$    is the surface energy

      A    is the surface area

      g    is the value for gravity

      b    is the film thickness

### 2.3.4  Liquid Filled Crack Theories (29,30,31,32)

All the liquid filled theories of cracking relate applied stress to initiate cracking with a surface energy term.  This is the basis of the Griffith's crack criterion which postulates the existence of pre-existing cracks.

$$f = \left(\frac{E\gamma}{C}\right)^{\frac{1}{2}}$$

where:

      f -    stress required to propagate a crack of length C

      $\gamma$ -    surface energy of the fractured faces

      C -    crack length

      E -    Youngs modulus

At the high temperatures in the HAZ or in the last stages of alloy solidification, low melting point liquid films appear at the grain boundaries and Eborall et al (29) have proposed that these are effectively <u>crack nuclei or notches</u> having no strength. The presence of these films reduces the solid-solid contact area which are the only regions possessing strength. Several workers (29-32) have applied similar relationships to the Griffith's (28) criterion incorporating the effect of liquid films which reduces the surface energy term. According to Rostoker (30) and Stoloff (31) crack propagation can only be continued by the flow of liquid metal to the crack tip. If this passage of liquid ceases the crack is arrested.

All of the liquid filled crack models relate a fracture stress to a surface energy term and by a simple mathematical development, Williams (20) has related the fracture stress to the reciprocal of the square root of the grain size. This is in essence the relationship derived by Stroh (33) and McLean (34) for solid state creep cracking

$$f = \gamma \left( \frac{K}{D} \right)^{\frac{1}{2}} \quad \ldots \ldots (20)$$

where:  f  -  fracture stress

K  -  constant dependent on dihedral angle

$\gamma$  -  effective fracture surface energy (energy of the exposed surface plus the energy due to plastic deformation at the tip).

D  -  grain size

### 2.3.5 Prohkorov Grain Boundary Displacement Mechanism (35)

This model assumes complete liquid coverage of the grain boundary faces. The theory then postulates grain boundary rotation takes place and the grains are able to move freely in the liquid until they eventually impinge

on one another. Further deformation can only occur if the surface tension
and the resistance to liquid flow is sufficient to accommodate the stresses
required for plastic strain in the grains. The conclusions from this theory
are:-

(i)     An increase in film thickness increases the fracture strain.
        The work of Medovar (36) agrees with this conclusion.

(ii)    A decrease grain size increases the fracture strain. This is
        also consistent with experimental findings in this report.

(iii)   A mixed grain size decreases the fracture strain. This is also
        consistent with practical experience because the centre line of
        ingots where there can be the greatest variation in grain size
        is the most crack prone.

2.4  Summary of the Solid-Liquid Theories.

        The descriptive theories (2.3.1) are of little scientific value
and at best are only a pictorial representation of type 1 cracking. All
three theories also overlook the possibility of the cracks initiating and
propagating in the solid state along impurity embrittled grain boundaries.
Such impurity decorated boundaries are known to promote intergranular
separations in the solid state (temper brittleness) and Van Eegham (24)
has evidence which indicates that a large percentage of cracking in
solidifying castings occurs in the solid state.

        The model proposed by Smith (26) has great practical importance
especially when the last liquid to solidifying has a low melting point and
spreads along the grain boundaries and can result in complete intergranular
disintegration. An interesting example of this effect is caused by the
addition of a small amount of phosphorus to the molten weld pool of an
18Cr10Ni steel. It has been shown in the present work that the liquid

phosphide is extremely fluid and penetrates along several grain boundaries
of the parent metal, as shown in Figure 9. During solidification, HAZ
cracking results. The model proposed by Smith (26) for weld cracking is a
good start but disregards such important parameters as fracture stress and
grain size.

The Saveiko (27) model (3.3.3) assumes that complete coverage of
the grain boundaries takes place and the surface tension is the controlling
factor. This is not possible because according to the Smith model the
surface tension depends upon the contact angle which in this case is always
assumed to be zero. In practice, complete coverage does not take place and
the film thickness and the degree of spreading depend entirely on the
composition of the liquid. The theory once again ignores the relative
effects of grain size, matrix strength, grain boundary strength, the
relative rates of grain boundary sliding and migration. The important
step this theory makes is the relating of stress with a surface energy term
for crack formation.

The liquid filled theories described in section 2.3.4 are useful
because they postulate that a liquid phase at a grain boundary is a notch
and when the grains are completely surrounded with liquid they have nil
strength. This is consistent with practice because the centre of a weld
and the fusion boundary region are particularly crack prone. All the
liquid filled theories are based on the Griffith's crack criterion (28)
and their difference is reflected by the lowering of the surface energy
term by the liquid phase. Even though the liquid filled theories are an
improvement on the pictorial models, they still ignore many important
variables outlined in section 2.2. For the Prokhorov (35) model (2.3.5)

to be a possibility there must be an excess of liquid to allow complete grain boundary coverage and grain boundary rotation. During welding this is most unlikely because there is insufficient time at temperature.

## 2.5 Group 2 - Solid State Cracking Theories (14,37,38)

All the solid state theories are of a creep origin and the morphology of the cracks apply to the type 2 cracking. In general, solid state cracking theories indicate the formation of two main types of crack, wedge shaped cracks (w-type) and cavities due to grain boundary sliding because there is insufficient time for the vacancy condensation mechanism (38) to take place. In general, relationships between temperature, strain rate and type of fracture are very difficult to predict. The change from transgranular cracking to intergranular cracking depends upon several factors such as composition, microstructure, grain size and the relative degrees of grain boundary migration and sliding. Theories to explain how wedge shaped cracks and cavities form during welding can only be descriptive.

The plot of elongation against temperature for various alloys shows a ductility trough or dip at an intermediate temperature as shown in Figure 3. At this intermediate temperature grain boundary sliding is prevalent and both wedge shaped cracking and cavitation are believed (38) to occur. Intergranular fracture is favoured by low strain rates, such as tensile testing. From practice, clean grain boundaries are found to increase the rupture life and elongation and therefore decrease the tendency to intergranular fracture. Inclusions of the non-welding type are believed (38) to be particularly effective in promoting intergranular cracking.

Relationships from creep theory all relate stress with the interfacial energy of the crack surface. The Stroh-McLean (33,34) equation is

perhaps the most well known relationship of this type for wedge shaped cracking.

$$\sigma_f^2 = \frac{12.\,\gamma b.G}{\pi L} \qquad \left(\frac{\sigma f}{2} = \tau\right)$$

$\sigma_f$ is the stress to initiate cracking (dynes per square cm).

$\gamma_b$ is the surface energy per unit area of crack formed along a grain boundary.

G is shear modulus.

L is length of sliding boundary.

$\tau$ is shear stress (dynes per square cm).

According to creep theory the surface energy term $\gamma_b$ must be less than 1000 dynes per square cm for wedge shaped cracking (33,34).

## 2.6 Summary of the solid state theories of cracking.

All the cracks which form in the solid state in weld metals or HAZ's are caused by grain boundary sliding. A schematic representation of the possible mechanism of initiation and growth of cavities is shown in Figure 4. Solid state cracking of a creep type is not the most predominant form of high temperature weld cracking, but cracks which form due to grain boundary liquation (Group 1 theories) act as notches for this second type of cracking. The precise mechanism of cracking is not known, but it is presumed to be similar to creep ruptures (Figure 4) and involves grain boundary sliding.

CHAPTER 3.    CLASSIFICATION OF HIGH TEMPERATURE WELDING CRACKS IN ALLOYS.

## 3.1 Introduction

In chapter 1 the confused state of the terminology regarding hot cracking was described and the various methods of crack classification were presented.  It is obvious there is a need for a clear and unambiguous terminology for cracking and, in this chapter, an attempt is made to present a concise classification of cracking.  The classification is based on the original terminology co-authored with Boniszewski and Eaton (39) but it has been further simplified and modified to include the results of this investigation.

## 3.2 Appraisal of Classification Parameters.

The extensive literature describing high temperature cracking is confused by an ambiguous terminology.  Unfortunately the situation is further confused because each individual stage of metal production has a different term to describe the same intergranular rupture.  Classifications of high temperature weld cracking are usually based upon the temperature of formation, location and size, which only lead to further confusion. Temperature is not applicable because the cooling rates during welding are steep, and it is impossible to attribute cracking to one particular temperature.  Location is unreasonable because weld metal cracking and heat affected zone cracking are thought to be fundamentally related.  Size is unscientific because large cracks will undoubtedly consist of mixed fracture modes (40,47,51,96).  The only reliable criterion on which cracks can be classified is their physical appearance which can be analysed by light microscopy and electron fractography.(39).

### 3.3  General Considerations.

High temperature cracking is assumed to occur above  >0.5 Tm, where Tm is the melting point in $^{O}$K.  In general the cracks are inter-granular in the sense that they propagate along boundaries rather than across boundaries.  During welding the strain rate and temperature at which cracking takes place are difficult to predict, but from creep theory low strain rates and high temperature favour intergranular rupture.  There is no transgranular fracture in the strict sense of cleavage, although there is an isolated report of transgranular cracking taking place in austenite (41).  The report of transgranular high temperature cracking could quite well be a mis-interpretation of cracking along ghost grain boundaries (Figures 10 and 11).  Another form of high temperature, intergranular separation is the cavity which can link up to form cracks in both the weld metal and HAZ.  In the majority of cases, cracking takes place when the metal matrix has a face-centred cubic structure (e.g.) Nickel base alloys (42);  Aluminium base alloys (43), Copper base alloys (44), and ferritic alloys which have an austenitic structure (45) at high temperature.  The formation of intergranular cracking depends on two factors:  the mechanical factor (degree of restraint) and the metallurgical factor (the degree of microsegregation) and the relative influence of these two factors decides whether cracking occurs.

### 3.4  General Description and Definition of Cracking.

The high temperature cracking in ferrous and non-ferrous alloys during welding may be defined as "the boundary separations which propagate with low overall ductility when a metal is subject to deformation by the stresses accompanying welding".  The boundaries are between cells, dendrites,

grains and the so-called "ghost" grain boundaries*  and the loss of ductility

is normally enhanced by the presence of boundary microsegrates in the form

of films, inclusions and precipitates.  There is no transgranular cracking,

but cracks may appear transgranular where they form at ghost boundaries or

where they propagate along newly migrated grain boundaries and thus cut

across the solidification structure.  As well as cracking, cavities are

very often observed along the boundaries.  In some areas the cavities

coalesce to form cracks.  The relative influence of strain rate and temperature

influences cavity formation.  From these various considerations two main

types of intergranular weld cracking can be classified as shown in Table 2

and Figure 5.

## 3.5  Type 1:  Cracking Associated with Microsegregation.

These consist of the boundary separations associated with micro-

segregation which may take the form of films, precipitates and inclusions.

The microsegregation may consist solely of alloying elements or may be

completely impurity elements.  In the majority of cases the microsegregation

is a mixture of impurities and intentional alloying elements (Figure 6).

The morphology of this form of cracking is characterised by a series of dis-

connected, jagged ruptures.  Electron fractography carried out on this form

of cracking may show dendritic films due to liquation and fast cooling,

(Figure 43-46).  Segregation cracking can further be sub-divided into types

1A and 1B dependent on their location in the weld metal or the HAZ.

### 3.5.1  Type 1A:  Solidification Cracking.

This is the most described form of boundary cracking, and it is

now universally known as weld metal solidification cracking (16).  Russian

workers (46) use a similar term, "crystallization cracking" to describe the

* ghost grain boundaries are impurity decorated prior    grain boundaries.

same basic morphological form of cracking. In the past, terms such as hot

cracking and hot tearing have been used, but these have caused much confusion

and the term solidification cracking is preferred. The terms hot tearing

and hot cracking may be used to describe the general phenomena of inter-

granular high temperature cracking, whereas the term super-solidous cracking

(17) should be discontinued because it commits one to assuming that cracking

occurs above the solidus temperature. This need not be the case, and Van

Eegham (24) has evidence to show that solidification cracking occurs in

castings at a temperature at which they are fully solidified. Solidification

cracks are seen to propagate along the impurity enriched prior austenite

grain boundaries, and they appear in three basic morphological forms which

depend on the $R/_G$ ratio (48), where G is the temperature gradient and R is

the growth rate as shown in Figures 6 and 7. The more common crack

morphologies encountered in this investigation are shown in Figure 8u-8z.

### 3.5.2 Type 1B: Liquation Cracking.

Liquation of low melting point constituents in the HAZ of alloys

takes place during welding, and this can promote grain boundary embrittlement.

The term 'liquation cracking' is proposed to describe this form of

cracking because it infers the association of liquated films with the

cracking even though the actual grain boundary separations may take place in

the solid state. In the Welding Institute literature, (15,16), the term hot

tearing is often used but, because of the confusion with foundry terminology,

this term should be discontinued. Liquation cracks have a similar morphology

to solidification cracks because they have jagged edges and contain irregular

openings. One of the major causes of liquation cracking can be retracted to

the original solidification structure of the parent metal. Even after severe

mechanical deformation at high temperatures the as-cast structure may still persist. During welding any interdendritic low melting point microsegregates in the parent metal can re-liquate and HAZ cracking can result. Numerous phases can liquate based on the elements which extend the liquidus-solidus range of temperature (e.g., C, S, P, O, N, B). Phosphorus rich liquids such as Ledeburite $Fe_3P$ easily wet the grain boundaries and are especially embrittling, (Figure 9). A special form of liquation cracking is the separations which can occur along ghost grain boundaries in steels which readily recrystallise during welding, (Figures 10 and 11).

### 3.6 Type 2: Ductility-Dip Cracking.

This type of cracking occurs along boundaries which are relatively "clean" in as much as they are free from liquated films. Cracking is assumed to occur at a temperature low enough to exclude liquid film formation. The operative mechanism involved in this type of cracking are the relative amounts of grain boundary sliding and grain boundary migration. Grain boundary sliding initiates cracking whereas grain boundary migration avoids crack propagation by blunting any cracks which form by leaving them stranded in the metal matrix. In many respects the intergranular separations resemble Stroh-McLean wedge cracks (33,34) and the cavities are similar to those encountered in creep rupture. The cracks usually form normal to the principal stress and appear smooth edged and reflect the effect of tensile displacement by grain boundary sliding. Electron fractography carried out on this form of cracking shows a thermally faceted structure sometimes decorated with a small dispersion of carbides as shown in Figure 63. Detailed electron fractography is an ideal method of discriminating between types 1 and 2 cracking. The fracture surfaces show an absence of film formation due to liquation. Type 2

cracking is believed to be associated with a ductility trough (Figure 3) at an intermediate temperature of approximately $1050^\circ$C for austenitic steels. Bengough (49) has shown that this ductility dip is accentuated by a coarse grained steel. The probability of ductility dip cracking is also increased by a high intragranular strength compared with the intergranular strength which promotes grain boundary sliding. Ductility dip cracks can be sub-divided into two main types depending on their location in the weld metal or HAZ.

### 3.6.1 Type 2A: HAZ Ductility Dip-Cracking.

In the literature HAZ ductility dip cracks have been referred to by numerous terms. The morphology of cracking is not unlike the wedge shaped cracks and cavities observed during creep rupture. Typical illustrations of these two types of ductility dip separation are shown in Figures 11, 12 and 25. In Figure 11 HAZ ductility dip cracking cannot be confused with liquation cracking because it occurs along the recrystallised grain boundaries and ignores the ghost grain boundaries.

### 3.6.2 Type 3B: Weld Metal Ductility Dip-Cracking.

Similar shaped cracks have been observed in austenitic steel weld metals. The cracks are observed to ignore the solidification structure of the weld metal and they propagate along the migrated grain boundaries. Observations of this type of cracking have been reported (47,50-52) in AISI 310 (25Cr20Ni steel) and it occurs in other austenitic steels. The reason for the apparent ignorance of this form of cracking are the difficulties of etching the solidification structure and the newly formed recrystallised grains simultaneously. Russian literature (46) refers to this form of cracking as "Polygonisation cracking" and a dislocation model has been

proposed. Typical illustrations of the wedge shaped nature of this form
of cracking and the cavities are shown in Figure 12. Electron fractography
carried out on the surfaces of such cracks reveal slip lines, thermal facets
and carbides but no liquation films (Figures 61-66).

3.7 <u>Interaction of Types 1 and 2 Cracking.</u>

It would be quite unreasonable to suppose that the two main forms
of cracking do not interact. Careful optical microscopy can often reveal
mixed cracking modes, (Figure 5) (40). Typical examples of the two main
types of crack interacting are as follows:-

(a)    Solidification cracks (1A) propagating as ductility dip cracking
       (2B) (40) (Figure 5). This form of cracking often occurs in multi-
       run welds. Fracture surfaces examined from this type of cracking
       show both liquated films, slip lines thermal facets decorated with
       inclusions.

(b)    Solidification cracks (1A) and weld metal ductility dip cracks (2B)
       often straddle the fusion boundary to propagate as HAZ liquation
       cracks (1B) and HAZ ductility dip cracks (2A) (Figures, 9, 13).

(c)    In A286 steel initiation of cracking can occur by a liquation of
       mechanism (1B) and propagation by a ductility dip along "clean"
       grain boundaries (2A). Cracks having this morphology are quite
       common in the HAZ of creep resistant alloys, Figure 5.

(d)    Ghost grain boundaries have been reported to produce mixed modes
       of fracture. Crack initiation can occur in the ghost grain boundary
       and propagation along the "clean" recrystallised boundaries (see
       Figure 11).

3.8 <u>Summary of the Classification.</u>

It is not claimed that the proposed classification is ideal, but it
does allow discrimination between the two main types of cracking. The

classification can often be decided by careful light microscopy but where there is doubt electron fractography should be carried out. If liquated films are observed on the replicas, cracking is of the type 1, solidification cracking (1A) in the weld metal and liquation cracking (1B) in the HAZ. Should the replicas exhibit an absence of films and relatively clean fracture surface, showing thermal facets, a fine dispersion of carbides and possibly slip lines then the cracking is of the type 2. It is obvious that types 1 and 2 forms of cracking will often merge and replicas may show both thermal facets and liquated films. The term "ductility dip" used to describe type 2 cracking is not entirely satisfactory because of the complication of wedge shaped cracks, cavities, and the conditions by which they form. However, they are similar to creep cracks and are broadly associated with the ductility dip which occurs at intermediate temperatures in ductile alloys. The exact position of the fusion boundary and HAZ are still subjects of conjecture (42). An example of such a complication is shown in Figure 8z where cracking occurred in the epitaxial growth region. This form of cracking can be safely classified as type 1 but whether it occurs in the weld metal or HAZ may be arguable.

3.9  Conclusions.

On the basis of microscopic evidence two main types of cracking can be classified which can be sub-divided into four specific types.

Type 1:  Boundary cracks associated with microsegregation.

Type 1A:  Weld metal solidification cracking.

Type 1B:  HAZ liquation cracking.

Type 2:  Boundary cracks propagating along relatively "clean" grain-boundaries and associated with the ductility dip which occurs below the recrystallisation temperature.

Type 2A:.    HAZ ductility dip cracking.

Type 2B:     Weld metal ductility dip cracking.

CHAPTER 4.  STRUCTURE AND PROPERTIES OF A286.  (A 25N115Cr intermetallic

strengthened austenitic steel).

## 4.1  Introduction.

During World War II an age hardening austenitic steel with excellent

creep ductility was developed by Krupp in Germany.  The steel was to be used

in the aircraft industry for elevated temperature application, and was named

'Tinidur'.  In 1960 Allegheny Ludlum, U.S.A., patented (53) a steel of

similar composition named A286 which was also strengthened by titanium rich

intermetallic compounds.  Today this steel is known by numerous codes, some

of which are as follows:-

AISI 616, (U.S.A.)., A286 (U.S.A.)., F.V.559 (Firth

Vickers, U.K.)., G.68 (Jessop-Saville, U.K.)., (54).

Unfortunately, the application of A286 has been limited because it

is not readily fusion welded without the formation of HAZ cracks.  The

incidence of HAZ cracking has been found to be more pronounced in thick

sections rather than in fine grained thin sheet.  The application of A286

has, therefore, been limited to thin sheet which is relatively easily T.I.G.

fusion welded.

## 4.2  Chemical Composition.

A286 is made under licence in the U.K. by Jessop-Saville and is

known as G68.  In the literature numerous chemical compositions are quoted

and the data sheet (54) for G68 gives the following specification in weight

percent.

| | |
|---|---|
| Carbon | 0.08 |
| Manganese | 1.35 |
| Silicon | 0.95 |
| Chromium | 15.5 |
| Nickel | 26.0 |

| | |
|---|---|
| Molybdenum | 1.25 |
| Titanium | 1.9 |
| Vanadium | 0.32 |
| Aluminium | 0.20 |
| Iron | balance |

The steel can be described as an austenitic iron, nickel, chromium alloy strengthened by additions of molybdenum, vanadium, titanium and aluminium. The ratio of titanium to aluminium may vary depending on the ageing characteristics required. Titanium and aluminium combine during ageing to form a coherent gamma prime ( $\gamma'$ ) precipitate which imparts the creep strength. The manganese level is always maintained below 1.35 wt% because titanium is a stronger desulphurizer and there is no advantage having larger amounts. Boron is also added in small amounts (0.003 - 0.015 wt%) to further improve the creep ductility but it can be argued that such low levels are always present as trace elements.

4.3 Steelmaking.

A286 cannot be made by air melting because the titanium reacts with the oxygen and nitrogen in the atmosphere to produce a dirty steel. Some form of vacuum melting is required and the CEVAM process (consumable electrode vacuum arc) has been successfully used by Jessop-Saville Limited (55). In the CEVAM process an air melted or powder metallurgy ingot serves as an electrode which is consumably melted under vacuum in the furnace. Air melted ingots are hot short and they have a low transverse ductility (56). The formation of titanium oxides and nitrides render the steel unworkable. Vacuum melted A286 is also difficult to hot work and this is a useful guide to the steels weldability.

## 4.4 Hot Deformation.

The hot deformation of A286 is understandably more difficult than non-hardenable austenitic steels such as AISI 304. This is because A286 is designed to resist hot deformation and obviously more force is required during forging and hot rolling. Cracking in A286 often occurs because too high a reduction in cross section area is attempted for a particular pass. If too high a forging temperature is used 1300°C, liquation of an inter-metallic compound occurs which is reported (57) as a Laves type phase. Blum and Witt (58) have identified the Fe-Fe$_2$Ti eutectic which forms at 1290°C and solid solution elements will further reduce the liquation temperature. At 1250°C a liquid phase rich in nickel, titanium and silicon (Ni$_{13}$Ti$_9$Si$_6$) has also been reported to form (57) which can lead to cracking. The formation of these small droplets of liquid at the surface of the billets during hot working is known as "freckle formation".

## 4.5 Physical Metallurgy.

The commercial development of intermetallic strengthened nickel-base alloys (59,60) and iron-nickel-chromium base alloys (61,62) has stimulated great interest in the possible precipitation reactions. In all these alloys the hardening mechanism is associated with the precipitation of a face centred cubic phase known as gamma prime ( $\gamma'$ ) of chemical composition (Ni$_3$(A Ti)). This phase is always associated with a peak hardness of 300 H.V. Mihalisin and Decker (63) have reported that the maximum response to hardening can be produced by varying the aluminium to titanium ratio which alters the lattice parameter of gamma prime ( $\gamma'$ ) and therefore changes the degree of lattice misfit. Gamma prime ( $\gamma'$ ) is not necessarily the equilibrium phase and is generally formed at an intermediate stage in the ageing process according to the sequence.

Solid Solution $\rightarrow$ Zones $\rightarrow \gamma'$   Equilibrium precipitate

or

Overaged precipitate.

Similar reactions take place in A286 and these have been described in detail (62). By varying the aluminium to titanium ratio the peak hardness is varied and the ageing rate can be retarded or enhanced. During ageing, hot deformation and welding, numerous phases can form which can be divided into two main groups. Group 1 consists of the phases which impart precipitation hardening or dispersion hardening of the austenitic matrix, and Group 2 are the embrittling phases.

### 4.5.1 Group 1. Strengthening Phases.

#### Gamma Prime $\gamma'$.

This is the principal hardening phase which appears as sub-microscopic spheriods and has the general formula $N_{i3}(Al\ Ti)$. The structure of gamma prime is f.c.c. and the lattice parameter is altered by the Al to Ti ratio. (a = 3.59 kx units). In certain compositions $Ni_3(Al\ Ti)$ can be extremely stable and it is the principal phase during overageing.

#### $Ni_3Al$

This is similar to gamma prime ($\gamma'$) but is ordered, i.e., a superlattice, with the nickel atoms occupying the cube faces and aluminium the cube corners.

#### $Ni_3Ti$ ($\eta$) eta phase

This phase appears after the ageing peak and has a hexagonal structure with lattice spacings a = 2.5454 kx units and c = 2.829 kx units.

#### $NiAl$ and $Ni(Al\ Ti)$

B.C.C. NiAl readily forms in A286 whilst Ni (Al Ti) can also

precipitate when the Al to Ti ratio is over 2.6. Wilson (61) has reported that Ni(Al Ti) rapidly forms during overageing and is unsatisfactory because it does not impart any strengthening.

## $Ni_2$(Al Ti) Heusler Type Phase (62)

With Al to Ti ratios of unity $Ni_2$(Al Ti) can form in the overaged structure. The lattice parameter of this phase is 5.83 $\overset{o}{A}$ which is approximately twice that of bcc NiAl . Like (Ni(Al Ti) this phase grows rapidly and does not impart much strengthening.

### 4.5.2 Group 2. Non-Strengthening Phases.

The non-strengthening elements usually embrittle the grain boundaries.

## G. Phases ($Ni_{13}Ti_8Si_6$ and $Ni_{14}Si_{19}Ti_6$)

This is a complex f.c.c. phase based on the Ni-Si-Ti system. Several compositions have been reported, (57,60).

## Laves Phase $M_2$Ti

The equilibrium diagram for iron titanium suggests that $Fe_2Ti$ can form at 70 wt% iron whereas the compound FeTi forms at 50 wt% iron. According to Blum and Witt (58), A286 is difficult to weld because of the formation of an Fe - $Fe_2$Ti eutectic which wets the grain boundaries in the HAZ and induces cracking. The structure and composition of this phase was carried out by analyses on bulk residues. This technique is inadequate because the presence of other compounds in the residue complicate chemical analysis, while the formation from X-ray powder patterns is not sufficient to establish the structure uniquely. The melting point of the Fe-$Fe_2$Ti eutectic is 1290°C and Gemmill (63) has reported that the iron can be replaced by silicon and chromium to form $M_2$Ti which lowers the melting point to 1273°C. $M_2$Ti is hexagonal and can form in the grains as well as at the grain boundaries.

Titanium Sulphide.

The Fe-Ti-S phase diagram, shown in Figure 14, suggests that both Laves phase ($Fe_2Ti$) and titanium sulphide can form in the HAZ of A286. Manganese sulphide will not form preferentially to titanium sulphide because the free energy diagram for binary sulphides (Figure 15) shows titanium to be more negative.

Numerous compositions of titanium sulphide are possible (67). When the phase contains less than 50 at % sulphur it is a sub-sulphide and with greater than 67 at % sulphur it is referred to as a higher sulphide. Of the many sulphides which are possible tau phase $Ti_2S$ (66) is the most commonly reported in steels.

Metal Phosphides ($M_3P$) M = Ti, Fe, Ni, Cr.

Geiger et al (68) have reported that angular shaped particles in the HAZ of A286 are in fact metal phosphides which can be often confused with Ti(CN), TiMo(C) and $Ti_2S$. During welding the phosphide particles can liquate, wet the grain boundaries and embrittle the steel. Phosphorus at the levels met in commercial alloys is usually in solid solution but can form stable compounds with titanium.

4.6 Ageing Characteristics.

A286 has a peak hardness of 300 H.V. Each individual cast has a slightly different ageing response. A typical hardness plot against the Holloman and Jaffe tempering parameter K is shown in Figure 16, where,

$$K = T(1 + \frac{Log\ t}{20})$$

T = the tempering temperature in $^{\circ}K$

t = the time a temperature in hours.

Solution treatment at $980^{\circ}C$ produces the expected shape of hardness curve after ageing in the temperature range $600^{\circ}C$ - $800^{\circ}C$. Higher, solution treatment temperatures have been found to produce unusual ageing responses. During ageing there is also a change in density of 0.5% (57) and a non-uniform shrinkage.

## 4.7 Mechanical Properties.

The mechanical properties of A286 are reported in great detail in the Jessop-Saville data sheet M969. After solution treatment at $980^{\circ}C$ the alloy can be age hardened to produce the following room temperature properties.

### 4.7.1 Room Temperature Properties.

| | |
|---|---|
| 0.1% Proof Stress | 38 t.s.i. |
| 0.2% Proof Stress | 45 t.s.i. |
| U.T.S. | 65 t.s.i. |

Charpy impact properties    40-60 ft.lbs.

### 4.7.2 Elevated Temperature Properties.

### Hot Tensile Testing.

Tests carried out on $\frac{7}{8}''$ diameter bar material in the solution treated condition ($980^{\circ}C$ water quench).

| Criteria | Temperature | | | | | | | | | |
|---|---|---|---|---|---|---|---|---|---|---|
| °C | 20 | 204 | 371 | 427 | 538 | 593 | 649 | 704 | 760 | 816 |
| °F | 68 | 400 | 700 | 800 | 1000 | 1100 | 1200 | 1300 | 1400 | 1500 |
| 0.2% proof stress tons f /sq.in. | 42.0 | 41.7 | 41.7 | 41.5 | 39.1 | 40.2 | 39.3 | - | -- | |
| | 70.5 | 65.5 | 65.5 | 65.2 | 61.4 | 63.16 | 61.8 | | | |
| UTS tons f./ sq.in [Kg/sq min. | 65.2 | 64.7 | 61.4 | 61.6 | 58.5 | 54.5 | 46.2 | 38.6 | 28.6 | 16.3 |
| | 102.2 | 101.5 | 96.5 | 97.0 | 92.0 | 85.8 | 72.8 | 60.7 | 45.0 | 25.7 |
| Elongation 2 in G.L. (0.505 in. dia). | 25.0 | 21.5 | 22.0 | 18.5 | 18.5 | 21.0 | 13.0 | 11.0 | 18.5 | 68.5 |
| Reduction in area. | 36.8 | 52.8 | - | 35.0 | 31.2 | 23.0 | 14.5 | 9.6 | 23.4 | 37.5 |

## Creep Properties.

The most attractive property of A286 is the elevated temperature creep resistance. In comparison with other commercial alloys, A286 has excellent 10,000 hours stress rupture properties as shown in Figure 17.

### 4.8 Weldability.

The elevated temperature properties of A286 are attractive but the major drawback to the widespread application of this alloy has been the poor weldability. During fusion welding numerous small HAZ cracks form. According to the literature the cause of cracking is the liquation of the $Fe - Fe_2Ti$ eutectic (58) in the HAZ at $1290^\circ C$. This phase wets the grain boundaries and embrittles the alloy. Continuous grain boundary films of titanium carbonitride also form and on cooling gamma prime ($Ni_3AlTi$) may precipitate which restricts plastic deformation in the grains and induces grain boundary

sliding. During ageing there is a contraction of 0.002 in per in (58) which accompanies the precipitation of gamma prime (Ni3AlTi) in the temperature range $590^\circ$C - $870^\circ$C and this further increases the internal stresses to promote solid state cracking. Blum (58) has concluded that the grain size and HAZ width are the two most important parameters with respect to HAZ cracking and showed that:

$$\text{HAZ cracking tendency} \simeq \frac{\text{grain size}}{\text{HAZ width}}$$

Hence it can be concluded that a coarse grain size and a narrow HAZ can promote cracking.

The suggested remedies to eliminate cracking are the removal of the titanium from the composition. Unfortunately this is not possible because titanium imparts the beneficial hardening and the creep resistance of the alloy. Gemmill (69) has suggested that in large sections crack initiation may be in the solid state. Today A286 is only readily weldable in fine grained thin sections of grain size 25 µm.

## 4.9 Effect of Boron on the Properties of Austenitic Steels.

Small additions of boron 0.005 wt% are known (68) to improve the hot workability of austenitic steels. It may be argued that austenitic steels always contain a trace of boron as an impurity. During the welding of steels containing 0.005 wt% boron, HAZ cracking may result due to the formation of low melting point borocarbides at the grain boundaries. Boron is also thought to accelerate the precipitation of $M23\,C_6$ and this phase has an adverse effect on the corrosion resistance of the steel.

Steels which are prone to intergranular cracking during welding can be improved by the introduction of a second phase to the austenite. The advantage of a second phase such as delta ferrite is that it is believed to soaks up any low melting point impurities and refine the grain size.

Unfortunately delta ferrite is metastable and during prolonged service at

temperatures in the range $600^{\circ}C - 900^{\circ}C$ is prone to transform to sigma

phase and carbides. Austenitic steel welds with sigma phase at the grain

boundaries are especially prone to knife line corrosion in service. An

alternative to delta ferrite is required and Medovar (72) has suggested

that the eutectic boride is suitable. Russian workers (72-74) have shown

that boron in additions of 0.2 - 0.5 wt% improve the cracking resistance

of austenitic steels and any cracks which form are healed by the excess

boride eutectic which liquates during welding. Boron has the same

advantages of delta ferrite but does not transform to other phases in

service. German workers (16) have studied the effect of 1 - 2 wt% boron

additions on the properties of austenitic steels. Boron is found to

increase the tensile strength and creep strength, but decreases the elevated

and room temperature toughness of the steel. Although the scaling resistance

of boron containing austenitic steels is improved the corrosion resistance

in reducing and oxidising acids is impaired because of the formation of

$(Cr\ Fe)_2B$. The advantages outlined in the literature of introducing a

second phase to the austenite has been studied in this investigation by

adding 0.39 wt% boron to A286 (a 25Ni15Cr austenitic steel), (Chapter 9).

# CHAPTER 5. EXPERIMENTAL METHOD.

## 5.1 Introduction.

Preparation of specimens for metallographic examination can be extremely difficult. A chapter is therefore required describing the detailed preparation of specimens for light microscopy, electron fractography and electron micro-probe-analysis.

## 5.2 Light Microscopy.

Preparation of metallographic specimens which contain cracks is extremely difficult. In general, stainless steels are difficult to mechanically polish but electropolishing in a solution of 950 ml of glacial acetic acid and 75 ml of perchloric acid for 45 volts at 40 seconds produce an excellent finish. Unfortunately electropolishing produces a bevelled crack surface and local pitting occurs at inclusions and intergranular films. Experimentally the best method of preparing stainless steels specimens containing cracks is by successive grinding on emergy papers, diamond polishing followed by hand linishing with gamma alumina on a selvyt cloth. The need for careful preparation of metallographic specimens in austenitic steels is not a trivial matter because poor preparation very often masks the microstructural detail. After final polishing a thorough ultrasonic cleaning in liquid soap will remove the debris from the crack, and this is followed by rinsing in hot water and final cleaning in methanol followed by drying on a filter pad. The filter pad draws out all the excess liquid from the crack, whereas a hot air dryer tends to produce staining around the edges of the crack.

## 5.3 Conventional Reagents for Etching Stainless Steels.

There are numerous reagents for etching stainless steels, and the relative merits of the more common solutions with respect to AlSl 304 and A286 has been determined. The details of these reagents are given as follows:

### 5.2.1 Acid Chloride Solutions and Electrolytic Etchants.

These are usually based on iron chloride with additions of hydrochloric acid, or cupric chloride with the addition of hydrochloric acid and nitric acid. In general, acid ferric chloride solutions were found unsatisfactory for etching AlSl 304 and A286 because they tended to stain the microstructure. Solutions based on cupric ions instead of ferric ions produced improved results, but once again staining resulted and it was impossible to produce a deep etch without severe pitting.

Etchants based on Ferric Chloride

| (i) | Ferric chloride | 6 grammes |
|---|---|---|
|  | Hydrochloric acid | 50 ml |
|  | Water | 100 ml |
| (ii) | Ferric chloride | 10 grammes |
|  | Hydrochloric acid | 100 ml |
|  | Distilled water | 100 ml |

Etchants based on Cupric Chloride

| (i) | Kallings Reagent |  |
|---|---|---|
|  | Cupric chloride | 5 grammes |
|  | Hydrochloric acid | 100 ml |
|  | Ethyl alcohol | 100 ml |
|  | Water | 100 ml |
| (ii) | Marbles Reagent |  |
|  | Cupric sulphate | 4 grammes |
|  | Hydrochloric acid | 20 ml |
|  | Water | 20 ml |

### 5.2.2 Electrolytic Etchants.

(i) 10% Oxalic Acid (Electrolytic).

An electrolytic oxalic acid etch 6 volts is an excellent reagent for revealing the weld metal solidification structure in austenitic steels.

Unfortunately this reagent does not reveal the grain boundaries in the HAZ.

(ii)  **10% HCl in methanol (Electrolytic).**

This reagent has been successfully used to etch the grain boundaries in AISI 304 and A286. The grain boundaries in the HAZ of these steels are usually difficult to etch but quite good results have been obtained at a potential difference of 8 volts.

(iii) **Metharegia**

Extreme care is required with this reagent which is a mixture of concentrated nitric acid, concentrated hydrochloric acid in methanol. Similar reagents can be prepared in glycerin and the solution is potentially explosive. The composition of this mixed acid reagent which has given best results is as follows:-

50%  concentrated hydrochloric acid

10%  concentrated nitric acid

40%  methanol

## 5.4  Selective Etchants.

In austenitic steels a similar problem to ferritic steels exist when recrystallization takes place and ghost grain boundaries may result, (Figure 11). The ghost boundaries are the prior austenite grain boundaries which are decorated with carbides. Conventional etchants may not show up these prior austenite grains but selective etchants reveal these regions much more clearly. Selective etching in either palladous chloride (77); a sulphide forming reagent (78), or a mixed acid reagent has produced favourable results.

These etchants heighten changes in composition and are invaluable when determining the cracking morphology in the HAZ of austenitic steels. The three selective etchants used to study HAZ cracking in A286 and AISI 304 steels are as follows:

## (i) Chemical Composition of Palladous Chloride Reagent (77).

Palladous chloride (PdCl$_2$)    0.5 gr

Hydrochloric acid 35%    23 ml

Distilled water    100 ml

Non ionic wetting agent (triton x 100) a few drops

The solution should be kept in a dark coloured bottle.

## Metallographic Procedure.

1. The specimen is polished and etched with a mixed mineral acid reagent containing copper ions, e.g. Kallings reagent.

2. This is followed by total immersion in palladous chloride solution until the surface turns black by deposition of "palladium black".

3. The specimen is washed and dried and under the light microscope inclusions and interdendritic films show silvery bright in a dark background. This reagent is ideal for looking at sulphides, carbides and slip lines, but the big drawback is the cracking of the palladous chloride layer. For this reason an alternative reagent was used.

## (ii) Selective Etchant Depositing Adherent Sulphide Film.

Behara (78) has developed a similar reagent to the palladous chloride etchant which produces an adherent sulphide film on the metal surface. The carbides and nitrides are not coated and remain bright.

## Composition of Reagent.

(i) An etching reagent of hydrochloric acid and ammonium bifluoride. (HCl 35% 200 ml; NH$_4$ FHF 24 gr; 1 litre distilled water).

(ii) A film forming reagent of a complex potassium pyrosulphite commonly known as metabisulphite (800 mg).

Just before use 800 mg of potassium metabisulphite (K$_2$S$_2$O$_5$) are added to 100 ml of stock solution and stirred until completely dissolved. The reagents (a) and (b) have an active life of 2 hours after mixing.

Metallographic Procedure.

1.  The specimen is immersed in the reagent for 20 - 90 seconds and the
    solution becomes turbid owing to the precipitation of sulphur.
    Twenty seconds exposure gives a light etch, whereas 90 seconds gives
    a deep etch.

2.  After washing and drying the specimen, bright contrast is observed
    where the carbides are present.

    This reagent is suitable for examining the HAZ of austenitic steels
and shows clearly compositional differences.

(iii)   Selective Etching Mixed Acid Reagents.

    Perhaps the best selective etchant used was found by accident and is
a mixture of methylated spirits, nitric acid and hydrochloric acid in the
proportions 85% ethanol, 10% concentrated nitric acid and 5% concentrated
hydrochloric acid.  The solution may be left made up.  When used electro-
lytically at a potential difference of 8 volts the etchant selectively
stains ghost boundaries and microsegregation.  Excellent results have
been obtained with A286 using this reagent.

5.5  Preparation of Carbon Extraction Replicas.

    Carbon extraction replicas have been prepared in the conventional way
from freshly formed fracture surfaces of HAZ cracks in AISI 304 and A286.
The salient features of the procedure are as follows:

1.  The HAZ was carefully machined out from the weldment so that a small
    slice is produced of thickness 0.12 inch.  A small notch was then
    sawn along the fusion boundary.

2.  The slice was next cooled in liquid nitrogen and this was immediately
    followed by slow bending to fracture.

3. The edges of the fracture and the areas on the fracture of no interest were painted in lacomit.

4. Carbon was next deposited on the fracture surface under vacuum in the shadowing unit. The fracture was rotated at 3,000 r.p.m. during this operation and the carbon was deposited in small bursts. In this way a strong carbon film was formed reproducing faithfully the texture of the fracture.

5. Stripping of the replicas was carried out using a solution 10% bromine in methanol. Holding times up to six minutes were used and, on most occasions, the replicas easily floated off in distilled water. The replicas obtained in this way were very clean.

6. In the case of replicas which were difficult to strip, the specimen was etched for 2-5 minutes in 10% perchloric acid in methanol. The solution was used electrolytically and the voltage was gradually increased to a maximum of 20 volts. Replicas prepared in this way had a tendency to be dirty but this was unavoidable.

## 5.6 Preparation of specimens for Electron-Micro-Probe-Analysis.

For solid specimens, normal mechanical polishing was found suitable followed by ringing the regions of interest with a sharp scriber. For line scanning across regions enhanced or depleted in elements the specimens were etched in a suitable selective mixed acid reagent. An MSL electron micro probe was used for the analysis of the bulk specimens.

For the analysis of particles extracted on the replicas use was made of the electron microscope micro analyser (E.M.M.A) which is attached to the Siemens Elimnskop 1A Microscope. The replicas were placed in a special holder and could be viewed direct at a reduced applied voltage. Replicas were also coated in aluminium and examined in the M.S.L. probe so as to obtain characteristic X-ray radiation images. The replicas were aluminium

coated so as to assist the dissipation of heat during the bombardment with electrons when analysing.

# CHAPTER 6. THE DEVELOPMENT OF A HORIZONTALLY OPPOSED TENSILE MACHINE

## FOR HIGH TEMPERATURE WELD CRACKING STUDIES.

### 6.1 Introduction.

In the literature, (79-84) reviewing what are popularly termed hot cracking tests, no single method of assessing crack susceptibility has received universal acclaim. The high temperature crack resistance of a weld metal and HAZ has been estimated by measurements of crack length (79-93), applied load, (85), strain rate (87-89) applied strain (89) empirical equation based on chemical composition (92-93) the determination of the high temperature ductility and the plastic brittleness range (92,93). Unfortunately, none of these tests give a reliable quantitative means of determining the conditions necessary to initiate cracking during welding. In the majority of tests, cracks several inches in length are produced. This situation is scientifically unsatisfactory because two main types of cracking have been classified which are physically different. The detailed classification was presented in chapter 3.

In some areas these two main types of crack merge, and measurements of crack length in the weld metal and HAZ incorporate mixed regions of cracking. Microsegregation of low melting point constituents are known to have an important effect on the formation of type 1 cracking and empirical equations based on chemical composition are claimed (92) to give reasonable correlation with crack length, although this is doubtful. In areas where the two main types of cracking interact the validity of equations based on chemical composition is questionable. A test procedure is therefore required which can discriminate between these two main types of cracking and can also compare the high temperature crack resistances of various weld

metals and parent metals. In an attempt to fulfil this need a

Horizontally Opposed Tensile Machine of original design was developed,

the details of which are described in the following chapter.

## 6.2 General Considerations.

High temperature welding cracks are difficult to produce

experimentally with any degree of accuracy. In order to produce inter-

granular cracks during welding, the mechanical restraint has to be

increased to a critical level. The "High Temperature Weld Cracking

Resistance" of an alloy can thus be estimated by measuring the stresses

required to initiate cracking and the overall extension of the test plate

during welding. The overall extension is assumed to give an estimate of

the high temperature ductility of the weld and HAZ. In essence the idea

of the test is to gradually apply an external load which induces additional

strains to the welding thermal strains to such a level that residual

ductility in the weld and HAZ is exhausted and cracking results.

## 6.3 Description of the Machine.

The main body of the machine consists of a simple fabricated structure

(A) which incorporates all the equipment in a self contained unit, (Figure

18). A test piece in the form of a flat plate of cross section area up to

4" x ½" is held in the two wedge boxes (B) and (C). Each wedge box is

provided with spring loading to hold the internal wedge grips in the enclosed

position and a level (D) for opening them to facilitate insertion of the

test piece. The stationary wedge box (B) is screwed into the main structure

in one of four positions (E) which are spaced at 3 inch intervals. This

gives an adjustment of 12 inches for various sized test specimens. The

moving wedge box (C) is restrained by a tee-piece passing through a slot

(F) in the structure which allows 4 inches of complementary movement to the

load cylinder stroke.

The cylinder (G) comprises a casing within which slides a one piece piston/rod unit (H), and the piston is fitted with special bronze piston rings to reduce the friction, so making the pressure gauge reading a fairly true indication of the load at the moving wedge box. A cross head (I) is attached to the piston and two tie rods (J) couple the cross head to the moving wedge box, so transmitting the load. A support (K) is provided at the end of the piston rod to minimise any tendency there may be for it to bend.

The hydraulic supply takes the form of a pre-coupled pump motor unit (L). This unit is positioned by the side of the hydraulic resevoir tank (M) which is fitted into the base of the main structure. The rate of pumping which alters the crosshead speed can be varied by adjusting a calibrated lever switch (N). A directional valve (O) is incorporated in the circuit so that the moving wedge box (C) can traverse in either direction. The pressure supplied to the cylinder determines the tensile load applied to the test piece, and is adjusted by varying the pressure relief valve (P). The pressure in the cylinder is displayed by a pressure gauge (Q) which is calibrated in tons load. Controls, (O), (P) and (Q) are housed in a panel at the front of the rig. A detailed illustration of the apparatus describing the various components is given in Figure 18 and the abridged details of the machine are given in Table 3.

## 6.4 Instrumentation.

The important parameters, applied load (stress), extension and strain rate can be determined with tolerable accuracy without the use of expensive equipment. In the apparatus the pressure in the cylinder (load) can be read directly from the pressure gauge (Q), the range of strain rates being obtained by measuring the various crosshead speeds. The calibration

curve for the range of travel speeds is shown in Figure 19. Extension

measurements can be determined by a simple extensometer and transducer

arrangements shown in Figures 20, 21. By a simple electrical circuit

shown in Figure 22 stress measurements are read direct from the strain

gauges attached to the tie rods of the tensile machine. The stress

measurements are accurate to $\pm$ 3% and the calibration was carried out by

means of a mild steel test bar in the Instron tensile machine. By this

simple circuit, readings of applied stress and overall extension can be

monitored to an X-Y recorder and a plot of stress against strain can be

obtained as shown in Figure 23. The machine is also designed so that

there is adequate space available for preheating the test piece and preheat

temperature can easily be recorded.

## 6.5 Application of the Machine.

### 6.5.1 Evaluation of Parent Metal.

The procedure which has been used to evaluate the resistance of

various steels to weld and HAZ cracking is shown in Figures 20 and 23.

A flat plate of the alloy steel is loaded to a constant level of applied

stress, and a stationary weld pool is formed on the surface of the plate

by the T.I.G. process at a set level of current, voltage and time. The

tensile stress is gradually increased and a direct plot of applied stress

against overall extension is obtained on an X-Y recorder. Once crack

initiation occurs, the propagation of the cracks is reflected by a marked

increase in the overall extension of the plate. A simple extensometer

and transducer arrangement is used to measure extension as shown in Figure

20. Examination of the series of small spot welds reveals the start of

cracking.

### 6.5.2 Evaluation of Manual Arc Electrodes.

A valuable application of the machine is to evaluate the hot cracking susceptibility of various manual arc electrodes. It is essential to use run on and run off plates which are welded to the test plate so as to remove the problem of having a start and finish in the stressed region of the weld. The bead is deposited normal to the applied stress, and a schematic representation of the set up is shown in Figure 24. As with the evaluation of the parent metal the applied load is increased in steps and the overall extension is successively measured until a threshold level of load is reached at which crack initiation occurs. Unlike other tests at least six weld beads have to be deposited at increasing levels of applied stress and this makes the test procedure more time consuming because each bead has to be allowed to cool. However, the results obtained are readily reproducible and crack length measurements are unnecessary.

Manual arc electrodes produced by different manufactures will give different depths of penetration even though the composition of the weld metal is nominally the same and the welding parameters are constant. This is presumably because of the variable arc lengths and because different electrode coatings produce varying arc efficiencies. The variable arc length is a human error and ideally an automated apparatus (89) using a fixed arc length is required to deposit the beads. Weld beads of different geometry (89) will also have different cracking resistances and the discrepancy will be exaggerated when a tensile load of increasing severity is applied. The test is not exclusive to single weld beads because the crack resistance of multi-run welds can be determined.

## 6.6 Summary.

A practical method of assessing the high temperature crack resistance of alloys during welding in terms of applied stress and extension has been developed. The procedure is a logical development of the simple bead on plate test. In the present test an applied load is raised in steps to a threshold level above which cracking occurs, and this is reflected by a marked increase in the overall extension of a flat plate specimen. The extension of the test plate is a measure of the overall high temperature ductility of the weld. A test of this nature brings weldability studies into line with other mechanical tests since the tensile test is an accepted method of measuring the hot ductility of alloys (forgeability studies) and maintaining the load constant and measuring the extension is a similar procedure to creep testing.

At least six tests at increasing applied load have to be carried out before a fair assessment of the relative crack resistances of various weld and parent metals can be determined. This can be time consuming when compared with the Murex Hot Cracking Test (86) in which a single manual arc bead is deposited. However, once the applied threshold stress and overall extension necessary to initiate cracking for a given weld metal and parent metal are known, a fairly reliable and reproducible estimate of their crack resistance is obtained. There is no need for the often difficult, and questionable measurements of crack length to be made, because the crack resistance of the alloy is expressed in terms of the applied stress and overall extension necessary to initiate cracking for a standard sized specimen. After testing, optical microscopy can be carried out to classify the types of cracking most likely for given combinations of parent metal and filler metal.

Once cracking occurs, the test plate can be loaded to rupture and
the resultant fracture faces examined in detail. On the other hand, further
tests under conditions which simulate the stresses, strains and temperature
cycles met in service can be carried out. The test procedure is not
restricted to a single bead because multi-run welds can easily be deposited.

From the fundamental view-point, uniaxial loading of a rectangular
cross-section test specimen is far from ideal because the applied stress is
not distributed uniformly over its area when plastic flow begins. The
situation is further complicated when a weld bead is deposited because local
hot deformation takes place in the weld metal and HAZ. Steep gradients of
temperature, stress and strain make absolute measurements difficult, but
these are the conditions under which high temperature welding cracks form
in practice. In the author's opinion, the applied stress and overall
extension at which crack initiation starts is a more reliable index of the
high temperature weld crack resistance of an alloy than the measuring of
propagated lengths of cracks which may consist of several mixed modes of
fracture.

Perhaps the most important factor when constructing any mechanical
testing procedure is the total cost and the reliability of the information
obtained. The Horizontally Opposed Tensile Machine has been found to be
no more expensive than other comparable tests. In general, the test specimens
are not expensive to produce, and the versatility of the machine means that
high temperature cracking resistance of both the weld metal and parent metal
can be assessed. It is appreciated that the applied stress and the extension
measurements are only comparative for a given sized test piece, but the
results are readily reproducible.

CHAPTER 7.   EFFECT OF GRAIN SIZE ON THE HEAT AFFECTED ZONE (HAZ)

CRACKING OF AN 18Cr10Ni STEEL (AISI 304).

7.1  Introduction.

The cracking theories described in chapter 2 show that grain size

has a great influence on the onset of cracking.  In steels such as A286

described in chapter 4, liquated films readily form in the HAZ during welding

and it is therefore difficult to separate the effect of grain size and

liquated films on the onset of cracking.  In AISI 304, an 18Cr10Ni non-

hardenable austenitic steels,liquation phases do not normally form in the

HAZ during welding, and any cracks which do form are of the type 2.  During

fusion welding,AISI 304 is extremely crack resistant because the grain

boundaries can easily migrate.  However, coarse grained forgings in this

steel have been reported (70,71) to be crack prone during tungsten inert

gas (T.I.G) welding.  In order to study the effect of grain size on HAZ

cracking, flat plates of AISI 304 steel were heat treated for various times

at $1200^{\circ}$C to produce a wide range of grain sizes.  The plates were then

stressed to fracture in the experimental horizontal opposed tensile machine,

and the results of this work are described in the following chapter.

7.2  Material for Investigation.

The steel under investigation is AISI 304 an 18Cr10Ni alloy which

contains a small trace of boron 0.004 wt% to improve the forgeability.

Drillings taken from the steel were analysed, and the results are shown

below.

| | | | | Element wt% | | | |
|---|---|---|---|---|---|---|---|
| CAST No. | C | Mn | Si | Ni | Cr | Mo | B |
| A.1.S.1.304 B Lateral Steel | 0.053 | 1.52 | 0.4 | 9.62 | 19.07 | 0.12 | 0.004 |

Flat plate sections 18" x 2" x ½" were sawn from a large forging and heat treated to produce a range of grain sizes.

## 7.3 Experimental Method.

### 7.3.1 Heat Treatment.

The grain coarsening heat treatments were carried out at $1200^{\circ}C$ in a platinum wound furnace under an argon atmosphere for various times up to 100 hours followed by water quenching. This heat treatment produced a range of grain sizes from 25 $\mu$m to 300 $\mu$m as shown in table 4. The plates were next machined into test plates of dimensions 18" x 1.5" x 0.375".

### 7.3.2 Grain Size Determinations.

Grain size measurements were determined by the mean linear method (97). The length of traverse of 100 grains was made and the number of millimetres per grain width 'd' (mean linear intercept) was determined. This was repeated six times and, by multiplying the average grain width 'd', the average spherical grain diameter L was found.

$$L = 1.6485 \quad d......  \quad\quad (97)$$

L - average spherical grain diameter

d - mean linear intercept

The value of 'L' obtained by this method has a relative error of $\frac{0.65}{\sqrt{n}}$ (98) where n is the number of grains intersected. The results of the grain size measurements are given in table 4.

### 7.3.3 High Temperature Weld Cracking Tests.

Use was made of the experimental tensile machine described in chapter 6. Flat plate test specimens were placed in the jaws of the machine, and a small stationary weld pool was formed by using a TIG welding torch at 100 amps, 10 volts for 30 seconds (Figure 20). The stress was increased in steps as shown in table 5 and, at a critical level, HAZ cracking occurred.

All the seven test plates were tested in this way and the applied stress
and overall extension necessary to initiate cracking was determined.

### 7.3.4 Metallographic Examination.

Small micro-sections containing the HAZ cracks were polished as
described in chapter 5. This was followed by etching in 10% hydrochloric
acid in methanol at 8 volts. Light microscopy revealed the cracks in test
plates 1-6 to be of the type 2 (Figure 25) of the proposed classification
chapter 3. Test plate 7 produced both type 1 and type 2 cracking because
the parent metal grain boundaries were heat treated so as to decorate them
with boro-carbides. $M_{23}(BC)$. Light microscopy revealed ghost boundaries
along which liquation cracks and cavitation occurred, and also ductility dip
cracking along the newly recrystallized grain boundaries (Figure 11).

### 7.4 Experimental Results.

The grain size measurements, critical stress and overall extension
to initiate cracking have been summarised in tables 4, 5 and 6. As expected
the finer grain size steel was able to withstand a greater applied stress
than the coarser grained steel. The extension of the finest grained steel
was also much greater than coarsest grained steel. Graphs of applied stress
and overall extension were plotted against the reciprocal of the square
root of the grain size and a direct correlation was found as shown in
Figures 26 and 27. This is consistent with fracture theory (28-34).

### 7.5 Summary of Results.

Grain size has a marked effect on the HAZ cracking in austenitic
steels. With age hardening alloys, such as A286, an external applied stress
is not required to produce HAZ cracks because the grains are extremely rigid
and liquation phases readily form during welding. In a non-hardenable
austenitic steel such as AISI 304, an applied stress is required to initiate

cracking during welding. A coarse grained steel (280 $\mu$m) requires an applied stress of 7 tons per square inch to initiate cracking where a fine grained steel (30 $\mu$m) required over twice the applied stress. The reason for this trend can be found by a simple analysis of the wedge shaped cracking proposed by Stroh and McLean, (33,34) (Figure 25). This relationship (section 2.5) proposes that the shear stress necessary to initiate cracking is proportional to the reciprocal of the length of sliding boundary. A coarse grained steel will have a larger length of sliding grain boundary than a fine grained steel. This trend has been verified (49) in 18Cr8Ni steel which shows a much greater ductility dip at 1050°C in a coarse grained steel. A complication to this simple picture of wedge cracking (Type 2) was found when the steel was heat treated at 750°C to precipitate $M_{23}(BC)$ at the grain boundaries. During welding, the $M_{23}(BC)$ liquates and cracks initiate, but subsequent recrystallization during cooling strands the cracks at ghost boundaries, the liquation cracks (Type 1) have a blunted appearance as shown in Figure 11W. Type 2, HAZ ductility dip cracking and cavitation along the ghost grain boundaries can also occur as shown in Figure 11.

CHAPTER 8. A DETAILED STUDY OF HAZ CRACKING IN A286 (A 25Ni 15Cr INTER-
              METALLIC AUSTENITIC STEEL).

## 8.1 Introduction.

A286 is a 25Ni, 15Cr, intermetallic strengthened austenitic steel
which is extremely difficult to weld without the formation of HAZ cracks.
Grain boundary migration is extremely difficult in A286 because the grains
are extremely rigid with respect to the grain boundaries. This is in sharp
contrast to AISI 304, an 18Cr, 10Ni, non-hardenable, austenitic steel, in
which the relatively soft grains permit grain boundary migration to occur.
The purpose of this investigation was two-fold:

(i)   Investigate the effect of welding variables on the HAZ cracking of
      A286.

(ii)  A detailed microstructural and fractographic analysis of the nature
      of HAZ cracking.

## 8.2 Material for Investigation.

The A286 used in this investigation was obtained from a commercial,
as-forged gothic billet of width 12 inches across the flat faces. Drillings
were taken from the billet, and the chemical analysis revealed the steel to
have a lower titanium and aluminium level than expected.

| CAST No. | wt% Element | | | | | | | | | | | |
|---|---|---|---|---|---|---|---|---|---|---|---|---|
| | C | Mn | Si | S | P | Ni | Cr | Mo | C | Al | Ti | B |
| A286 | 0.05 | 1.82 | 0.76 | 0.008 | 0.012 | 24.96 | 14.76 | 1.02 | 0.39 | 0.145 | 1.55 | S0.007 10.005 |

### 8.2.1 Ageing Characteristics.

Small microsections of A286 were solution treated 980°C water quenched followed by ageing in the range 600°C to 800°C. Vicker hardness measurements were carried out on the steels and the results of this work are shown graphically in Figure 28. The peak hardness for A286 is 270 HV instead of 300 HV, and this can be accounted for by the lower level of titanium.

### 8.2.2 Creep Testing.

Creep specimens 0.252 inches diameter, 12 mm thread, 1.75 mm pitch and $1\frac{1}{4}$ in. parallel length were machined from A286 in the 980°C water quenched, solution treated condition. The test pieces were loaded at 700°C and 750°C respectively and the time to rupture was determined as given in table 7.

### 8.3 To Investigate the effect of welding variables on the HAZ cracking of A286

#### 8.3.1 Material

Plates of approximate dimensions 10 in x 9 in x 1 in were sawn from a gothic billet of A286 and solution treated for 2 hours at three separate temperatures, 980°C, 1050°C and 1150°C followed by water quenching. Grain size measurements were determined by the mean linear intercept technique as outlined in the previous chapter. The effect of solution treatment temperature on the grain size is summarised in table 8.

#### 8.3.2 Consumables.

Three manual metal arc electrodes are recommended for welding A286. The first is the Bohler Fox CN 20 Co 50 which contains 50% cobalt. On the basis of cost alone this electrode is not a commercial proposition irrespective of the claims which are made by the manufacturers. Nicrex 326F which was recommended by Murex Limited was also tried, but produced HAZ

cracking and the elevated temperature properties of the weld deposit were inferior to A286. The only manual metal arc electrode of commercial significance for welding A286 was the WRKS10 experimental electrode developed by Welding Rods Ltd., Sheffield, for Jessop-Saville Limited. Drillings were taken from the coating, filler metal and the weld metals deposited by 10 SWG, 8 SWG and 6 SWG electrodes and their analyses are shown in table 9.

### 8.3.3 Bead on Plate Testing.

Bead on plate tests were carried out on the various solution treated plates using 10 SWG, 8 SWG and 6 SWG manual metal arc electrodes at a range of heat inputs. All the electrodes were deposited DC + ve so that approximately 66% of the heat input is at the electrode tip. The schematic arrangement for depositing the electrodes on the plates is shown in Figure 29. Three testing temperatures were used - $20^{\circ}$C, room temperature, and + $200^{\circ}$C and after welding the plates were dye penetrant tested for HAZ cracking.

### 8.3.4 Assessment of HAZ cracking tendency.

Any estimates of the degree of cracking in the HAZ of A286 can be at best semi-quantitative. The crudest form of measurement is dye penetrant testing after welding. This method gives the general trend that 10 S.W.G. lower heat input electrodes produce a greater amount of cracking than 6 SWG higher heat input electrodes, Table 10. A more sensitive method of measuring the incidence of HAZ cracking was required, to reflect the relative effects of solution treatment temperature, preheat temperature as well as heat input. The most reliable technique was found by determining the number of cracks encountered along a line drawn parallel to the fusion boundary in the HAZ. The incidence of HAZ cracking is expressed as the number of cracks per centimetre of line scan in the HAZ. (Table 11).

### 8.3.5  Grain Size Measurements.

The mean linear intercept method outlined in chapter 7.3.2 was again used to measure the grain size in the HAZ. Substantial grain coarsening was found to take place in the HAZ as shown in table 12.

## 8.4  A Detailed Microstructural and Fractographical Analysis of the Nature of HAZ Cracking in A286.

### 8.4.1  Light Microscopy.

#### (A)  Examination as-polished.

Micro-specimens were prepared as outlined in chapter 5, the final polish being carried out with gamma alumina on a selvyt cloth. In the unetched condition several interesting microstructural features were observed.

(i)   In the fusion boundary region, rosette shaped cracks were observed associated with Chinese script shaped particles (Figure 30).

(ii)  From these rosette shaped cracked regions straighter edged cracks are observed to propagate into the parent metal normal to the fusion boundary (Figure 31,33).

(iii) Film like arrays of non-metallic inclusions were also observed (Figure 32).

#### (B)  Examination of Etched Structure.

Etching was carried out in a conventional reagent metharegia followed by a thorough washing in distilled water, and a final drying on a filter pad. Examination of the HAZ at low magnification revealed an apparently chemically homogeneous microstructure containing grain coarsening in the HAZ. In the regions where the cracking had occurred, the cracks were seen to propagate in a direction normal to the fusion boundary. The reason

for this is simple, the cracks propagate along temperature and strain
gradients in the HAZ. A typical example of HAZ cracking is shown in
Figure 34. In the hottest region of the HAZ, near the fusion boundary,
the cracks have a jagged morphology due to liquation (Figure 30, 33, 34),
whereas in the colder regions, the cracks have a more straight edged, wedge
shaped appearance (Figure 33). The cracks are similar to the type 2
separation which form in the HAZ of AlSl 304 steel in chapter 8.

(C) Selective Etching.

Selective etching with the mixed acid reagent revealed the heavily
microsegregated structure of A286. The etching reagent had the chemical
composition 10% nitric acid, 5% hydrochloric acid in methanol, and was used
electrolytically at 6 volts. In some regions the pronounced as-cast
dendritic structure of the original casting appears well preserved. Under
normal white light the dendrites appear blue-red and the deleterious inter-
dendritic microsegregates appear as a white etching constituent (Figures
35,36). In these white etching regions of the HAZ, liquation cracks can be
seen to form as shown in Figures 37,38. During welding, the white etching
low melting point constituent re-liquates and the rosette shaped cavities
or cracks can result (Figure 30).

8.4.2 Electron-Micro-Probe-Analysis.

Detailed light microscopy revealed several interesting features
which have been qualitatively analysed.

(i)   Rosette shaped liquation cracks associated with Chinese script.

These regions were found to be rich in titanium and presumably a
titanium rich phase has re-liquated during welding in the HAZ (Figure
39).

(ii)  Regions of Straight Edged cracking.

In the vicinity of these cracks titanium and molybdenum rich phases
can be seen to liquate (Figure 40).

(iii) Film like arrays of inclusions.

Electron-micro-probe-analysis was unable to detect these films but localised titanium rich liquated pockets were detected (Figure 41). Selective etching of A286 reveals the prior austenite interdendritic grain boundaries to be a white etching constituent. This region re-liquates during welding and HAZ cracking can result. A qualitative line scan by electron-micro-probe-analysis revealed the white etching region to be greatly enhanced in Ti,Ni, possibly enhanced in V,S,C and depleted in Fe, Cr. The white etching liquid in which HAZ crack initiation takes place is presumably a Ti,Ni, V, S, C, P, alloy. (Figure 42).

8.5 Detailed Electron Fractography and Electron-Micro-Probe-Analysis.

Light microscopy has revealed HAZ cracking in A286 to consist of two possible modes of fracture. The initiation stage occurs in the fusion boundary region due to liquation of a titanium rich constituent. Initiation of cracking always occurs in the white etching Ti, Ni, S, V, C constituent which is the last liquid to solidify in the original A286 casting. Propagation of the cracks would appear to be by a ductility dip mechanism because the cracks have a straight edged morphology. Electron fractography complemented by electron-micro-probe-analysis was carried out on the various liquated phases to verify the light microscopy observations.

Electron fractographic studies of the HAZ cracking in A286 were extremely difficult to carry out. This is because the cracked region of interest is extremely small (<1 mm). Carbon extraction replicas were prepared as previously outlined in chapter 5 and examined in the Siemens Elimnskop 1A electron microscope. By careful painting with lacomit, the hottest regions of the HAZ containing the liquated products were isolated,

and replicas containing such particles were extracted. Replicas were also selectively extracted from the colder regions of the HAZ to coincide with the cracked regions which appear as ductility dip cracking. For simplicity the HAZ has been split into 2 zones. Zone I is the hot region containing all the liquated constituents which promote crack initiation. Zone II is the colder region in which the straight edged ductility dip cracks propagate large distances into the parent metal. The following section describes in detail the salient observations of this work.

### 8.5.1 Replicas Extracted from Zone I.

#### (A) Fern Shaped Particle of Titanium Sulphide.

In the hottest region of the HAZ, near the fusion boundary the fracture surface contains liquated films. This region corresponds to the initiation of HAZ liquation cracks. Typical areas containing fern shaped or dendritic particles can be seen in Figures 43 to 46. Selected area electron diffraction carried out on such particles when indexed have 'd' spacings corresponding to $Ti_5S_4$. The prominent 'd' spacings were found to be 2.7, 2.0, 1.86 and 1.5 which corresponds to $Ti_5S_4$ which is presumably the liquated form of $Ti_2S$ containing more sulphur. (Sheets 1, 2 Appendix 1) Electron-Microscope-Micro-Analysis of the particles was also carried out as a complementary investigation, and both titanium and sulphur were unambiguously identified (Figure 45).

#### (B) Liquated Carbides.

In addition to the fern shaped titanium sulphides liquated particles of a different dendritic morphology were observed (Figures, 47, 48). The selected area electron diffraction patterns from Figure 49 consisted of a series of closely spaced spots in a cubic array. Analysis of the 'd' spacings from this pattern indicate the particle to be $M_6C$ (Sheet 3, Appendix 1).

It was also possible to fully index this diffraction pattern as an $\begin{bmatrix}001\end{bmatrix}$ zone of the face centred cubic structure as shown in Figure 49. The dendritic carbides are believed to grow preferentially along the $\begin{bmatrix}001\end{bmatrix}$ zone and this is why they are extremely thin and embrittle the grain boundaries.

## (C) Iron-Titanium Phase.

In addition to the liquated sulphides and carbides an iron-titanium phase having a dendritic morphology was observed to liquate in the HAZ of A286 as shown in Figure 50 and 52-54. Selected area electron diffraction was carried out on this phase, but the 'd' spacings did not correlate with either Laves phase $Fe_2Ti$ or $M_{23}C_6$. (Appendix 1, Sheet 7). The unsolved diffraction pattern of this iron-titanium phase is shown in Figure 51, and it is probably a $\begin{bmatrix}123\end{bmatrix}$ zone of a f.c.c. crystal.

## (D) Shattered films, $(TiV)_2CS,Y$-Phase, (66,99).

By far the largest particles on the fracture surfaces examined were thin films, sometimes in excess of 30 $\mu$m in length which were extremely brittle and had a shattered film appearance. The shattered films are not found on the crack surfaces, but form in the white etching regions of the HAZ and appear as ductile rupture along the intergranular rupture (Figure 55). This phase was mainly found in the HAZ, but it is believed to be distributed throughout the parent metal (Figure 56). Selected area electron diffraction has been carried out on several of these particles, and the pattern is always of the same type, probably corresponding to $\begin{bmatrix}0001\end{bmatrix}$ basal plane of the hexagonal close packed crystal, (Figure 57). The most prominent 'd' spacing are 2.77, 2.22, 1.60 and 1.38 which correspond to Y-phase (66,99) a titanium carbosulphide which is hexagonal close packed (Appendix 1, Sheets 4-6).

Electron-Microscope-Micro-Analysis of the shattered films showed that they contained titanium, vanadium and sulphur. In order to check carefully that the films contained sulphur and not molybdenum, the probe spectrometer was rotated at a slow speed of $\frac{1}{4}$ degree per minute and the angles at which the radiation peaks occurred were measured accurately. In this way vanadium and sulphur were unambiguously detected as shown in Figures 58,59. As a final check replicas containing the shattered films were coated in aluminium and the characteristic X-ray images were photographed. The same results were obtained (Figure 60) and the shattered films were, therefore, concluded to consist of Ti,V, and S. In the light of recent work, (99), it is believed that Y-phase is a carbosulphide and the shattered films can be assumed to have the general formula $M_2(C,S)$.

### 8.5.2 Replicas Extracted from Zone II.

Zone II is the colder region of the HAZ in which the straight edged type 2 cracking occurs. The temperature of this region of the HAZ is insufficient for liquation constituents to form, although there is a gradual merging rather than a sharp demarcation line between the two zones. In order to produce replicas from the ductility dip cracking region the carbon coated HAZ fracture surface was carefully painted with lacomit so as to leave only the colder regions of the HAZ. The extraction replicas are then stripped from the fracture surface and collected in copper grids as outlined in chapter 5. The basic features of cracking in Zone II of the HAZ are as follows:-

(A) Transition from Zone I to Zone II.

At low magnification the structure may still have a "burnt" and "overheated" appearance (Figure 61) (cf with Figure 70) because there is a

gradual transition from liquation cracking to solid state cracking. The detail of the cracked region in Figure 61 is characterised by thermal facets, slip lines and small precipitates which decorate the crack surface, (Figure 62).

### (B) Thermal Faceting.

On increasing the magnification, the thermal facets cannot be mistaken because they appear as a series of steps or corrugations on the fracture surface. Thermal facets occur when a newly formed crack face is exposed at high temperature, and the only means of surface energy reduction is by an increase in the surface area. Thermal rippling of the fracture face takes place to produce the faceted appearance in Figure 63.

### (C) Slip Lines.

In some areas superimposed on the thermal facets are slip lines. Such slip lines could be produced during the fracture of the specimens for electron fractography, although there is a possibility they may be caused by the considerable grain boundary sliding in the HAZ. Typical illustrations of slip line formation are shown in Figure 64 and 65.

### (D) Carbides.

Along with the thermally faceted crack surface, arrays of carbides are observed. The carbides have a plate like morphology and a streaky selected area electron diffraction has been indexed, and the 'd' spacings correspond to Ti(CN), (Sheets 8, 9, Appendix 1). Typical examples of these arrays of titanium carbonitrides are shown in Figure 66. Under the electron beam the carbides show differential thermal contrast.

## 8.6 Mechanism of HAZ Cracking in A286.

A286 is extremely resistant to hot deformation because it is solution strengthened by Mo, V, B and precipitation hardened by gamma prime ($Ni_3$,Al,Ti). Even in the solution treated condition the grains of A286 are extremely rigid and grain boundary migration is extremely difficult. This results in grain boundary sliding being highly probable at high temperature. Since A286 is difficult to hot work the brittle as cast structure is difficult to break down, and the last remaining low melting point liquid to solidify may re-liquate during welding. In A286 there is the worst possible mechanical factor (rigid grains which do not readily deform and promote grain boundary sliding) coupled with the worst possible metallurgical factor (interdendritic solidification products which re-liquate during welding). During fusion welding HAZ cracking occurs. The microstructural nature of the cracking indicates a two stage cracking mechanism.

### 8.6.1 Stage 1 - Initiation of HAZ Crack.

Even after severe hot working the remnants of the cored as cast structure remain. Selective etching reveals this structure. The initiation stage of cracking in A286 is located near the fusion boundary in the former interdendritic interstices of the cored parent metal. Such regions appear white when etched in the selective reagent (Figure 36). Electron-micro-probe-analysis has shown this region to be locally enhanced in Ti, V, Ni, C and S, and depleted in Cr and Fe (Figure 42). The liquation cracks which form in the white etching regions have been found by electron-micro-probe-analysis to be enhanced in Ti and S. Electron fractography revealed the morphology of the liquation products. Numerous phases were determined of which titanium sulphide, titanium vanadium sulphide, carbosulphide complexes and carbides $M_6C$ type were predominant. The liquation stage reduces the

surface energy of the grain boundaries and any localised liquid pools corresponding to a grain boundary will initiate cracking. Microstructurally, the liquation cracks which correspond to the initiation stage appear as irregular, jagged separations which are often associated with "Chinese script", shaped solidification products. Stage I, the initiation of cracking, is the most important step and, if it is avoided, the stage II will not be possible.

### 8.6.2 Stage II. Propagation of HAZ Cracks.

The second stage of cracking is the propagation of the cracks into the parent metal along relatively clean recrystallised grain boundaries. This corresponds to type 2 cracking in the classification. Crack propagation need not necessarily occur along the recrystallised grains but can occur along the white etching regions where they are superimposed. The electron fractographic detail of such cracks show inclusions, thermal facets, which appear to be decorated with Ti (CN). Microstructurally this stage appears as straight edge cracks and cannot be confused with the initiation liquation stage.

## CHAPTER 9. EFFECT OF BORON ON THE HIGH TEMPERATURE WELD CRACKING OF A286.

### 9.1 Introduction

According to the Russian literature (72-74) the addition of boron in amounts from 0.2 - 0.4 wt% improves the weld cracking resistance of austenitic steels. The advantages of producing a duplex austenite plus eutectic boride structure have been outlined previously in section 5.9 of this dissertation. A 0.39 wt% addition of boron was made to the basic composition of A286 and the effect on the weldability has been studied in the following chapter.

### 9.2 Material for Investigation.

The material for investigation was in the form of a flat plate 10 in. x 10 in. x 1 in. and was solution treated $980^{\circ}C$ 2 hours water quench. Drillings were taken from the plate and the chemical composition is given below.

| Cast No. | Element wt % | | | | | | | | | | | |
|---|---|---|---|---|---|---|---|---|---|---|---|---|
| | C | Si | Mn | S | P | Ni | Cr | Mo | V | Al | Ti | B |
| A286 B | 0.025 | 1.03 | 1.65 | 0.007 | 0.006 | 25.52 | 14.92 | 1.08 | 0.38 | 0.3 | 2.17 | 0.39 |

### 9.3 Mechanical Properties.

#### 9.3.1 Ageing Characteristics.

Small microsections of A286 B were solution treated $980^{\circ}C$ water quench followed by ageing in the temperature range $600^{\circ}C$ - $800^{\circ}C$. A peak hardness 300 HV 30 was obtained which is markedly higher than the steel without boron (Figure 67). However, this can be explained in terms of the relative levels of titanium and aluminium which are the hardening elements.

The A286 B contains 2.17 wt% titanium, whereas the A286 contains only 1.5 wt% titanium.

### 9.3.2 Charpy Impact Properties.

As a comparison, the impact properties of aged A286 with and without a boron addition were compared. In general the room temperature impact properties of A286 with 0.39 wt% boron were $\approx$ 10 ft.lbs. lower than conventional A286 as shown in Table 13.

### 9.4 Bead on Plate Tests.

Bead on plate tests were carried out on one inch thick plate at a range of preheat temperatures and heat inputs as summarised in Table 14. After welding, the beads were examined by dye penetrant testing, and only 10 s.w.g. electrodes produced HAZ cracking.

### 9.5 Light Microscopy.

The microstructure in the HAZ of boron treated A286 consists at a duplex austenite plus eutectic boride, (Figure 68). At high magnification, the eutectic boride can be seen to have a brittle dendritic morphology, (Figure 69). Any HAZ cracking which occurs in the boron treated A286 is seen to cut across the eutectic boride (Figure 70). Electron-micro-probe-analysis of the eutectic boride in the cracked region revealed a local enrichment in Ti,Mo,Cr and V as shown in Figure 71.

### 9.6 Grain Size Measurements.

The grain size measurements in the HAZ of A286 plus 0.39 wt% boron were determined by the mean linear intercept method. Six hundred grains were counted and, in general, the parent metal and HAZ grain sizes were much finer than conventional A286. As a direct comparison, the HAZ grain size of boron treated A286 (Table 15) is half the HAZ grain size for conventional A286 (Table 12).

## 9.7  Electron Fractography.

Detailed electron fractography confirmed the light microscopy
observations by revealing dendritic borides due to liquation, (Figure 72).
Electron-micro-scope-micro-analysis revealed the major chemical constituents
which form with the boron to be Ni,Ti,Cr and Fe.  Examination of the cracked
regions in the HAZ showed the fracture surface to be brittle (Figure 73)
and verifies the light microscopy observations which showed the cracking to
cut across the eutectic borides.

## 9.8  Simulative Welding Trials.

### 9.8.1  Introduction.

The approximate temperature at which grain boundary liquation
takes place in the A286 and the A286plus boron was indicated by carrying
out various heat treatments in the $1200^{o}C$ - $1400^{o}C$ temperature range.  From
this work a direct comparison of the grain coarsening tendencies of the two
steels could be made.  Examination of the fracture surfaces of specimens
which have been overheated and burnt will aid the interpretation of the
electron fractographs obtained from HAZ's in the bead on plate tests.

### 9.8.2  Material for Investigation.

The A286 and A286 plus 0.39 wt% boron had the same chemical
composition as the steel used for the bead on plate tests.  Rectangular
samples 0.75 in. x 0.75 in. x 1 in. were used for the simulative trial welds
and they were machined from plate material used for the bead on plate tests.

### 9.8.3  Simulative Welding Heat Treatments.

The steel blocks were sealed under vacuum in a 1 inch outside
diameter silica tube and rapidly heated to the various testing temperatures
in a platinum wound furnace.  The standard time of 1 hour was selected at
the temperatures of $1200^{o}C$, $1250^{o}C$, $1300^{o}C$, $1325^{o}C$, $1350^{o}C$, $1400^{o}C$

respectively, followed by water quenching. Duplicate samples of A286 with and without boron which had previously received heat treatments at $1300^{\circ}$C, $1325^{\circ}$C, $1350^{\circ}$C were re-solution treated at 950$^{\circ}$C for 1 hour to determine whether the eutectic liquid would go back into solution, i.e. reclamation of a burnt steel.

### 9.8.4 Light Microscopy.

After 1 hour at $1200^{\circ}$C, there were no signs of grain boundary liquation in either the A286 or the A286 plus boron steel. At $1250^{\circ}$C the steel containing boron showed signs of eutectic liquation. At $1300^{\circ}$C the eutectic boride had increased in quantity and the A286 steel had also commenced to liquate. As the heat treatment temperature was increased, the amount of second phase increased until at $1400^{\circ}$C the sample took the shape of the silica tube, (Tables 16, 17). The 950$^{\circ}$C 1 hour water quench re-solution heat treatment was found to reduce the amount of eutectic second phase, but the degree of intergranular cracking was increased. The faces of the cracks (Figure 75) were wide apart, straight edged and uncharacteristic of high temperature weld cracking.

### 9.8.5 Grain Size Determinations.

Both A286 and A286 B were solution treated for 2 hours at 980$^{\circ}$C and their average spherical grain diameters were 28 $\mu$m and 22 $\mu$m respectively. After 1 hour at $1300^{\circ}$C the A286 had a grain size in excess of 100 $\mu$m, whereas the A286 B had a grain size of 65 $\mu$m, Tables 18,19. In all the heat treatments, the grain coarsening tendencies of A286 were greater than the boron treated A286 (Tables 18, 19). Figures 74 and 75 shows the relative grain coarsening tendencies of the two steels after heat treatment at $1350^{\circ}$C.

### 9.8.6  Electron Fractography and Electron-Micro-Probe-Analysis.

**(1)  Conventional A286**

Detailed electron fractography was carried out on extraction replicas prepared in the way described in chapter 5.  On examining the replicas obtained from the 1350°C heat treatment, similar, but not identical, fractographic features were observed.  The basic similarities are as follows:

(i)  The fracture surface after the 1350°C 1 hour water quench heat treatment showed a burnt structure as shown in Figure 76.  Similar structures were observed in the hotter regions of the HAZ from the bead on plate tests.

(ii)  Numerous dendritic phases were observed which had been liquated at 1350°C, (Figures 76,77).

(iii)  In regions where cracking had taken place on cooling the thermal facets were observed and these were decorated with numerous small particles.

(iv)  Unlike the HAZ cracking in A286, there was very little change in fractographic detail since there was not the same severe temperature gradient and there was no sign of ductile rupture.

Light microscopy (Figure 75) revealed the A286 to contain numerous intergranular cracks which have different morphology to the HAZ cracks. The cracks formed during heat treatment at 1350°C had a straight edged morphology and they were extremely wide.  Electron fractography revealed their crack morphology to be not unlike type 2 ductility dip cracks.  The crack surface was heavily decorated with small titanium carbonitrides and appeared as a series of smooth thermally faceted contours, Figures 78, 79.

## Electron-Micro-Probe-Analysis.

In order to identify the composition of these phases detailed electron-micro-probe-analysis was carried out. From the diffraction patterns, the liquated phases were mainly carbides, but the probe work indicated their chemical constitution. Figures 80 - 83 show that the liquated phases were complex Ti, V, Mo, S compounds and they also contained carbon. Similar, but not identical, phased were found in the HAZ of A286.

### (2) Boron Containing A286.

Electron fractography was carried out on the steel subjected to 1 hour at 1350°C. Dendritic borides were observed, (Figure 84). Electron-microscope-micro-analysis was carried out on this phase which was found to be enriched in Ni, Ti, Cr, Fe and S (Figure 79).

# CHAPTER 10.   DISCUSSION OF RESULTS.

The confusing terminology mentioned in chapter 1 has previously tended to mask the basic concepts of high temperature intergranular cracking. At present no theory of crack initiation and propagation can be applied to weldment cracking with any degree of certainty.  From basic fracture theory, the stress to initiate cracking is assumed to be directly proportional to a surface energy term and indirectly proportional to a grain size term.  Any comprehensive theory of high temperature weld cracking must include terms of this type.  From the results of this investigation, there is evidence to suggest that fracture stress can be related to a grain size term and a surface energy term.  The grain size term will depend on the degree of grain coarsening or recrystallization in the HAZ, whereas the surface energy term is dependent on the cleanliness of the grain boundaries.  A fundamental understanding of the formation of high temperature weld cracking will also depend on a clear and concise appreciation of the possible types of cracking.  In chapter 3, a detailed classification of high temperature weld cracking is proposed.  For the sake of logical continuity of the dissertation, the classification is placed in chapter 3, even though it is based on experimental observations in this investigation.  Two main types of cracking have been classified.  Type 1 which are associated with microsegregated grain boundaries, and type 2 which are associated with relatively "clean" grain boundaries.

The type 1 cracking is due to liquid or solid films which embrittle the grain boundaries.  In the weld metal this form of separation is termed "solidification cracking" (Figure 8) and, in the HAZ, they are termed "liquation cracks" (Figures 5 and 9).  Type 1 cracks have a jagged, irregular morphology and often consist of a series of unconnected ruptures.

Solidification cracks appear in a number of forms dependent on the solidification pattern of the alloy. Solidification and liquation cracks need not form when the alloy contains an intergranular liquid phase because there is evidence (40, 47) to suggest a solid state mechanism. Providing there is sufficient strain, solidified microsegregates can reduce the surface energy to such a level that type 1 cracks can propagate in the solid state along the impurity enriched prior austenite grain boundaries, (Figures 6 and 9). The composition of the last liquid to solidify is extremely important. In a $2\frac{1}{2}$Cr-1Mo ferritic steel electroslag weld metal, the interdendritic liquid is found to be rich in C, S, P, Mn, Mo, as shown in Figure 6. This is the impurity enriched last liquid to solidify, and it is the cause of the hot shortness in this particular weld metal. The presence of phosphorus in solid solution is believed to improve the fluidity or spreading potential in between the dendrites long after normal solidification is thought to be completed. Hot working does not always remove these deleterious intergranular liquids which are responsible for temper brittleness and liquation cracking during welding. Re-liquation of these regions of the interdendritic liquid is responsible for much of the HAZ cracking in steels. As a general rule, steels which are difficult to hot work will almost certainly be difficult to weld. Electron fractography carried out on the type 1 cracking always show liquated films which sometimes have a dendritic morphology (Figure 43-46). This is the only unambiguous method of discriminating the type 1 (Segregation Cracking) from other fracture modes which do not show liquation phases.

At temperatures which exclude the possibility of a liquid phase a second type of cracking can occur which has a different morphology to

type 1. Such cracks are referred to in the classification (Table 2, Figure 5) as type 2 ductility dip and in microstructural nature, they are not unlike the separations which occur during creep rupture. The name ductility dip cracking is selected because the cracking is believed to be associated with a fall in ductility at some intermediate temperature ($\approx 1050^{\circ}C$ for austenite). A coarse grain size is found to produce a much larger ductility trough than a fine grained steel. Type 2 cracks are characterised by their straight edged, regular features, reflecting uniform tensile displacement of the grain boundaries by sliding. They may also occur as cavities because of the variable temperature and strain gradients in the weld metal and HAZ. The cavities very often coalesce to form a crack in weld metals and HAZ's (Figure 12).

An interesting microstructural detail is the merging of the two main types of crack, a fact which has not been previously recognised. Initiation of cracking nearly always takes place due to liquation and propagation can take place by a creep deformation mechanism (Type 2) in the solid state. The more common combinations of crack interaction are as follows:

(i) Weld metal solidification cracking propagating as ductility dip cracking (Figure 5).

(ii) HAZ liquation cracks interacting with HAZ ductility dip cracks (Figure 5).

(iii) Weld metal cracks straddling the fusion boundary and propagating in the HAZ. (Figure 13).

(iv) HAZ ductility dip cracks associated with cavitation (Figure 11).

The relative influence of the metallurgical factor and the mechanical factor can be considered from the classification shown in table 2. The

metallurgical factor is the effect of intergranular liquids, grain size etc. and the mechanical factor is the degree of restraint in the weldment. For a given set of welding conditions each individual alloy has a metallurgical and mechanical rating with respect to cracking. An alloy having a low metallurgical rating would have a coarse grain size and low melting point intergranular films would be produced during welding. A low mechanical rating would be consistent with a heavily restrained weldment possessing very little residual ductility. Steels which have a history of hot shortness during casting and hot working will almost certainly cause trouble during welding. The relative effects of the metallurgical and mechanical factors are reflected by the ratio of the grain boundary strength ( $\sigma$g.b) to the grain strength ( $\sigma$trans). For age hardening alloys such as A286 which readily forms a liquation phase in the HAZ during welding, the grains are extremely resistant to hot deformation and the ratio of grain boundary strength to grain strength will be extremely low and cracking will result.

In order to produce the two main types of high temperature cracking with a reasonable degree of reproducibility in steels which are resistant to cracking (e.g. AISI 304), the experimental tensile machine described in chapter 6 was developed. The apparatus takes the form of a horizontally opposed tensile which is hydraulically loaded and is specifically designed for weldability studies. The crack resistances of both parent metal and weld metal can be determined and welding variables such as preheating of the test plate can be easily incorporated into the test procedure. In the test, flat plate specimens have single or multi-run beads deposited normal to the applied stress which is increased in steps until cracking occurs, (Figures 23,24). The idea of the test is to increase the restraint to such a level that the residual ductility in the weld metal and HAZ is exhausted and

cracking results in the most susceptible region. Once cracking occurs, there is a significant increase in the overall extension as shown in table 5. The cracking resistance is then expressed in terms of the applied stress and overall extension necessary to initiate cracking. Although the applied stress and overall extension to initiate cracking are only comparative assessments, they are more reliable than the questionable measurements of crack length. The applied stress is a more scientific measurement, and can be qualitatively related to the grain size and the surface energy of the cracked grain boundary. Other test procedures have related bulk chemical composition (93) with crack length which often consists of mixed modes of fracture and results in a wide scatter band.

Using the horizontally opposed tensile machine the effect of grain size on the applied stress at which type 2 cracks form have been studied. From this work, the basic relationship of fracture stress being directly proportional to the reciprocal of grain size has been found which is predicted by the Stroh-McLean equation (33,34) (section 2.6). The plot of applied fracture stress against the reciprocal of the root of the grain size (Figure 26) showed a direct correlation with very little scatter. This would suggest that the applied stress at which cracking occurs is directly proportional to the reciprocal of the root of the grain size over the high temperature range. The plot of overall extension versus grain size also showed a direct correlation but with a higher degree of scatter. This was presumably because the overall extension was difficult to measure accurately. In general a coarse grained steel (300 μm) required only half the applied stress and was able to extend much less than finer grained steel (25 μm) before cracking occurred. This is consistent with theory which postulates a fine grained steel having a high fracture strain.

In order to introduce a metallurgical factor into the HAZ cracking of AlSl 304 a small amount of ledeburite ($Fe_3P$) was added to the weld pool of a melt run in a coarse grained specimen (280 µm). Light microscopy revealed both solidification cracking and HAZ liquation cracking in the steel (Figure 9). The effect of phosphorus was to wet the grain boundaries by liquid penetration and sufficiently embrittle the steel so that no applied stress was required. Another method of varying the metallurgical factor was to heat treat the steel at $750^{\circ}C$ for 8 hours which delineates the grain boundaries with boro-carbides ($M_{23}BC$). On subjecting this structure a welding thermal cycle and an increasing applied stress (table 5), liquation cracks, ductility dip cracks and cavitation along the ghost grain boundaries occurred as shown in Figure 11. The steel containing the boro-carbides (test plate 7, table 5) has a similar grain size to test plate 1, which has clean grain boundaries and the effect of the boro-carbides was to reduce the fracture stress by 2 tons per square inch. This can be interpreted as the second phase of boro-carbides reducing the surface energy of the grain boundaries. A relationship of the type

$$\text{Applied fracture stress} \simeq \frac{\text{grain boundary surface energy term } \gamma'}{\text{square root of grain size} \quad \sqrt{d}}$$

would therefore apply.

From the work on the welding of AlSl 304 (a non-hardenable 18Cr10Ni steel) the relative effects of grain size, surface energy of crack and applied fracture stress were established. With A286 (a 25Ni15Cr intermetallic strengthened steel) HAZ cracking readily occurs during fusion welding because the grains are much more rigid and low melting point liquation phases readily form in the HAZ during welding. It is, therefore, more difficult to relate grain size with a fracture stress in the case of A286. However, grain size

can be shown to have a great influence on cracking in A286. The initial

grain size of the steel can be seen to be markedly altered by the temperature

of solution treatment (table 7). A steel solution treated at 1150°C has an

average spherical grain diameter of 65 μm, whereas a 980°C solution treatment

produces a grain size of 51 μm. In the light of the above relationship a

high solution treatment temperature would reduce the crack initiation stress.

The bead on plate tests carried out on the 1inch thick plates (Tables 8,9)

reflect the marked effect grain has on HAZ cracking. Under all the conditions

of preheat the coarsest grain size was found to produce the greatest amount

of HAZ cracking. The degree of cracking is given as the number of cracks

per cm of HAZ as shown in table 11. Another significant result is the

effect of heat input on the incidence of HAZ cracking. A low heat input

using 10 S.W.G. electrodes produced a greater amount of cracking than a

higher heat input using 6 S.W.G. electrodes (table 11). This can be

explained in terms of the low heat input producing the highest amount of

mechanical restraint. It is assumed that liquation occurs in the HAZ

during fusion welding with both 10 S.W.G. and 6 S.W.G. electrodes. Preheat

was found to reduce the incidence of HAZ cracking. The effect of a low

heat input producing the greatest amount of cracking is a surprising result

because the highest heat input produced the coarsest grain size (table 12).

From the light microscopy the HAZ cracks were observed to be

normal to the fusion boundary (Figure 33). The two basic types of crack

classified in chapter 3 were observed in the HAZ and they were observed to

merge. In the hottest region near the fusion boundary the type 1 liquation

cracks were found to have a jagged, rosette shaped morpholoy, and they were

sometimes associated with "Chinese script" shaped inclusions, (Figure 30).

Selective etching in a mixed acid reagent (section 5.3) revealed the rosette

shaped cracks to be coincident with white boundaries. The white etching

boundaries are the interdendritic microsegregation which are the remnants

of the original as-cast structure (Figures 37 and 38). Electron-micro-probe-

analysis showed the white etching regions to be enhanced in Ni, Ti, V, S

and C and depleted in Fe and Cr. The microsegregation is consistent with

the findings of Hume-Rothery (100-102) who has shown that Ti and Ni depress

the liquidus-solidus temperature. The original solidification sequence of

the A286 casting was Fe and Cr rich dendrites with the white etching regions

corresponding to the low melting point nickel rich liquid which easily

re-liquates during welding. Subsequent hot deformation and solution

treatment has been insufficient to break down the microsegregation in A286

because the alloy is designed to resist hot deformation. The comparatively

low concentration of S and C which probably combined with Ti and V in a

white etching nickel rich liquid is a boundary of weakness in the alloy.

Titanium as well as being a strong carbide former also readily forms

sulphides and complex carbosulphides (99). HAZ liquation cracks showed

titanium enrichment as shown in Figures 39-41. Light microscopy complemented

by electron-micro-probe-analysis has indicated that the problem of fusion

welding A286 is caused by the heavy microsegregation which is not removed by

hot working and solution heat treatment. During welding the white etching

regions liquate and HAZ cracking results. This is the initiation stage.

Examination of the colder regions of the HAZ, several grains into the parent

metal, show the crack morphology to alter from a jagged, irregular shape,

characteristic of liquation cracking, to a wedge shape characteristic of

ductility dip cracking, (Figure 33).

Detailed electron fractography carried out in the HAZ of A286

verified the light microscopy indications. Room temperature fracture

specimens in the HAZ were always intergranular in texture. The most predominant phase on the fracture surface had a shattered film appearance and was extremely brittle, (Figure 56). Selected area electron diffraction revealed the 'd' spacing of this phase to coincide with tau phase (66) or Y-phase (66). Originally this phase was believed to be a nitride (66) but recent workers (99) have indicated that the Y-phase is a titanium-carbo-sulphide. Electron-Microscope-Micro-Analysis of this phase showed Ti, V and S enrichment (Figures 55-60) and it is therefore assumed to be $(Ti\ V)_2$ CS or $M_2CS$. It is important to note that Y-phase also occurs in the parent metal, but the greatest amounts were detected in the HAZ. A286 would therefore appear to contain Y-phase which forms in the interdendritic white etching boundaries and presumably coarsens in the HAZ during welding. In morphology the shattered films (Y-phase) are not unlike the titanium carbon-itrides which often decorate the fracture surfaces (Figure 66). It is probable that the smaller titanium carbo-nitrides particles nucleate the much larger Y-phase particles because titanium has a strong affinity for both sulphur and carbon. The titanium carbo-nitrides can also have a dendrite morphology as shown in Figure 76, and the Y-phase may also show a dendritic morphology and internal thermal contrast as shown in Figure 80.

The fracture surfaces of the cracks which form in the HAZ of A286 have been investigated in detail. Two distinct zones have been found: Zone I corresponding to type 1 liquation cracking and shows liquated films; Zone II which corresponds to HAZ ductility dip cracking and shows a thermally faceted fracture surface. The liquated phases which spread along the grain boundaries in A286 are all titanium rich. Sulphides of titanium are easily identifiable by their fern like appearance. In addition to the sulphides an

Fe-Ti phase forms of 'd' spacings which could not be matched with the more likely phases such as carbides, sulphides and Laves phases. According to Blum (58) an $Fe_2$ Ti phase was the main liquation constituent, but this was not detected in this investigation. The method used (58) to detect Laves phase was by bulk extraction of the precipitates followed by X-ray crystallography using the powder technique. This method of analysing bulk residues has since been superseded by selected area electron diffraction of the actual liquated phase on the crack surface in the electron microscope. Carbides were also found to form in dendritic arrays in the HAZ of A286 and Figure 48 shows a typical $M_6C$ fern which has grown preferentially along the $\begin{bmatrix} 001 \end{bmatrix}$ zone.

In the colder regions of the HAZ corresponding to Zone II, the structure along the grain boundaries have still a burnt and overheated appearance, and the crack surfaces are decorated with thermal facets and slip lines, (Figures 51-65). In this zone there is a complete absence of liquated phases. It is unreasonable to assume that the two zones do not merge and, in some regions, both films and thermal facets are observed as shown in Figure 53. Decorating the thermal facets are a fine dispersion of titanium carbonitrides which show differential contrast at high magnification (Figure 66).

Numerous liquated phases can be found in the HAZ of A286, their shape and composition depends entirely on the welding thermal cycle. During a short, steep welding thermal cycle, as is the case with the manual metal arc process, there is only sufficient time for titanium sulphide $Ti_5S_4$, $M_6C$ and an iron titanium liquid to form which wet the grain boundaries and initiate cracking. A prolonged heat treatment in the range 1200 - 1400°C produced a form of intergranular cracking which is not encountered during welding. The cracks which form have widely separated fracture faces and they are parallel

sided as shown in Figure 75. As the temperature was increased the amount of liquated second phase was observed to increase (tables 16, 17). The boron containing steel was found to liquate first at 1250°C. A further solution treatment at 950°C for 1 hour followed by water quenching was found to greatly reduce the amount of second phase, but the incidence of intergranular cracking in A286 was increased. However, a re-solution heat treatment after welding may be beneficial to remove any liquated films that form which are deleterious to the service properties of the weldment, i.e. corrosion resistance. Electron fractography carried out on the burnt specimens of A286 revealed a dendritic liquation phase of Ti, Mo, V and S which is probably a complex carbosulphide. This phase is obviously formed in the white etching Nickel rich liquid in A286. During welding there is presumably insufficient time for the dendritic carbosulphides to form. Examination of the fracture faces of cracks formed during heat treatment show them to have a different fractographic appearance to cracks formed during welding. In general the crack surfaces are decorated with small carbides, and they are thermally faceted to lower the surface energy of the free surface at the high temperature. Otherwise, the fracture surfaces of the cracks are featureless (Figures 78,79) and any liquid phase which forms has fallen from the fracture face since the cracks are extremely wide.

Boron, as reported by Medovar (72) in amounts up to 0.4 wt% has a significant effect on the resistance to high temperature cracking of A286. The parent metal of A286 with a 0.39 wt% addition was refined compared with commercial A286 (tables 12, 15) and the bead on plate tests on one inch thick plate showed the steel to be more resistant to HAZ cracking. Any HAZ cracks which did occur appeared to propagate across the brittle eutectic boride, and

are presumed to occur in the solid state (Figures 70, 73). No signs of
the reported (72) liquid healing were encountered. The beneficial effects
of boron in A286 can be attributed to, (i) a refinement of the parent metal
grain size (table 15), (ii) an increase in the resistance to grain
coarsening, (iii) a modification of the elemental partitioning during
solidification. The deleterious white etching interdendritic nickel rich
liquid is replaced by a predominantly iron, chromium boride, as shown in
Figure 84. In commercial A286 the interdendritic white etching liquid is
depleted in iron and chromium as shown in Figure 42.

The poor weldability of intermetallic strengthened, austenitic
steels, such as A286 alloy has been limited because they are prone to high
temperature weld cracking. From the work carried out in this investigation,
there would appear to be two alternatives to producing a more weldable alloy.
The most direct method of improving the high temperature weld cracking
resistance is to heavily hot work the alloy to reduce the interdendritic
microsegregation to a minimum, and refine the grain size. Perhaps the only
other alternative is a change in the chemical composition of the alloy
without reducing the other mechanical properties. A controlled addition
of boron has been found to improve the high temperature weld cracking
resistance, but the impact resistance is impaired and this may offset the
weldability advantages.

# CHAPTER 11.  CONCLUSIONS.

From this investigation, a number of important conclusions can be made.

(1)    A classification of high temperature weld cracking has been proposed based on the microstructural nature of cracking which is consistent with the cracking theories.  Two basic types of cracking are classified:  Type 1, associated with microsegregation and liquation phases:  Type 2, associated with relatively clean grain boundaries which, in appearance, are similar to the cavities and wedge shaped cracks appearing during creep deformation.

(2)    Electron fractography is a reliable method of discriminating between the two main types of cracking.  Type 1 cracks show liquation phases on the fracture surfaces, and type 2 cracks are very often thermally faceted and there is a complete absence of liquid films.

(3)    A basic relationship exists throughout the high temperature range of the type, fracture stress is proportional to surface energy of crack and grain size.

$$\text{fracture stress} \simeq \frac{\text{surface energy of crack}}{\text{grain size}} \frac{(\gamma g.b)}{(d^{\frac{1}{2}})}$$

Plots of external applied stress and overall extension to initiate cracking against grain size (Figures 26,27) show this relationship to be valid for AISI 304 stainless steel.

(4)    A method of estimating an alloy high temperature weld cracking resistance using a horizontally opposed tensile machine of original design has been developed.  Cracking resistance is expressed in terms of the external applied stress and overall extension necessary to initiate cracking which is consistent with the fracture theories.

The questionable and laborious measurements of crack length are
unnecessary with this test procedure.

(5)  Grain size has a great influence on the HAZ cracking of A286
(a 25Ni 15Cr intermetallic strengthened austenite steel). A high
solution treatment temperature coarsens the parent metal and the
steel is more suceptible to HAZ cracking.

(6)  A low heat input used to deposit 10 S.W.G. manual metal arc
electrodes produced the greater degree of HAZ cracking on a 1 inch
thick plate than the higher heat input 6 S.W.G. electrodes (tables
10, 11). This is because of the higher thermal restraint imposed
by the 10 S.W.G. electrodes. A preheat of $200^{\circ}C$ was found to
reduce the incidence of HAZ cracking (tables 10,11).

(7)  A mixed acid selective etchant (section 6.3) has been used to detect
the interdendritic microsegregation in A286 which is not removed by
hot working. This is the root cause of the hot shortness in the
steel. Electron-micro-probe-analysis has shown the white etching
interdendritic liquid to be locally enhanced in Nickel, titanium,
vanadium, sulphur, carbon and depleted in iron, chromium (Figure 42).

(8)  During welding, the white etching low melting point regions re-liquate
and where they coincide with grain boundaries, intergranular
embrittlement and the resultant crack initiation takes place, (Figures
36-38). This is consistent with type 1 in the proposed classification
chapter 3. Electron fractography complemented by electron microscope-
micro-analysis has revealed the liquated phases in zone I of the HAZ
to be titanium sulphide $(Ti_5S_4)$. dendritic carbides $(M_6C)$ and an iron-
titanium phase (Figures 45-53).

(9) The propagation of these cracks into the colder regions of the HAZ (Zone II) is along clean grain boundaries, which are thermally faceted and decorated with a fine dispersion of titanium carbonitrides (Figures 61-66). This is consistent with type 2 cracking in the proposed classification in chapter 3.

(10) In addition to the liquation phases, Y-phase $M_2(CS)$ grows in the white etching regions of the HAZ, and further embrittles the steel. Y-phase has a shattered film appearance (Figure 55-60), and it has a chemical composition of titanium, vanadium, sulphur and carbon. Ductile rupture along the white etching regions is observed by electron fractography (Figures 55-60).

(11) A 0.39 wt% boron addition improves the weld cracking resistance of A286 by refining the grain size of the parent metal and the steel is also more resistant to grain coarsening during welding (tables 18,19).

(12) Boron changes the partitioning of iron and chromium which appear in the last liquid to solidify. The white etching nickel, titanium rich boundaries are thus replaces by a low melting point eutectic boride.

(13) Boron has little effect on the creep strength of A286, but has an adverse effect on the Charpy impact properties (table 13). This may offset the beneficial effects of boron and the weldability of A286.

# CHAPTER 12.   RECOMMENDATIONS.

The root cause of the intergranular embrittlement of highly alloyed steels such as A286 is the presence of intergranular microsegregates which are not broken down during hot working.  A study of the chemical composition of these deleterious, intergranular liquids and methods of removal or modification in commercial alloys is required.  In the case of A286 which is designed to resist hot deformation, the brittle as cast structure must be homogenized before welding is carried out.  Boron has been found to improve the cracking resistance of A286 and a controlled experiment to determine the optimum level is required.  In the case of high integrity weldments in creep resistant, ferritic, austenitic and nimonic alloys, an estimation of the degree of microsegregation is desirable prior to welding.  The casting and hot deformation histories of these alloys will serve as an approximate guide to their hot cracking resistances.

# CHAPTER 13.   ACKNOWLEDGEMENTS.

1.  Bashforth, G.R.  The Manufacture of Iron and Steel;  Vol.2, Steel Production, Chapman & Hall, 1963,  64.

2.  Middleton J.M., Foundry Trade Journal, 1967, 7, 319-327.

3.  Atlas of Defects in Castings, 1961.  Published by the Institute  of British Foundrymen.

4.  Barnard L. & Harris R.  'Hot Shortness in Forging Low Alloy Steels', 1968.  I.S.I. Publication 108, 167-177.

5.  Brammer, I.S. & Honeycombe, R.W.K.  J.I.S.I., 1964, 202, 335-342.

6.  Brammer, I.S.  J.I.S.I., 1963, 201, 752-761.

7.  Barnard, L. & Brook R.  J.I.S.I., 1967, 205, 756-762.

8.  Terminology used in Research & Development Department, Midland Group, British Steel Corporation.

9.  Blum, B.S.  Technical Documentary Report No. A.S.D.-T.R.61-678;  April 1962

10.  Bailey A.R.  'A text book of Metallurgy'.  Published by McMillan & Co. Ltd., London, 1960.

11.  Borland, J.C., & Younger, R.N.  Brit.Weld.J., 1960, 7, 22-59.

12.  Paton, B.E.  'Electroslag Welding'.  American Welding Soc.Inc., 1962.

13.  Whittenberger, J.E., & Rhines, F.N.  Trans.A.I.M.E., 1952, 4, 409-420.

14.  Kammer, P.A., Masubuchi, K., & Monroe, R.E.  'Cracking in High-Strength Steel Weldments - a Critical Review'.  D.M.I.C. Rep. 197, Batelle Memorial Inst., Columbus, 1, Ohio, 7 February, 1964.

15.  Boniszewski, T., & Watkinson F.  Brit.Weld.J., 1964, 11, 610-619.

16.  Baker, R.G., & Newman, R.P.  Met.Cons.1969, 1, Feb. (25), 1-4.

17.  Borland J.C., Brit.Weld.J., 7, 1960, 508-512.

18.  Brockhurst, P.J., & Muir, H.J.  J.Austral.Inst.Met., 10, 1965. 140-148.

19.  Hull, F.C.  Weld Res., 1967, 32, 399S-409S.

20.  Williams, J.A., & Singer, A.R.E.  J.Austral.Inst.Met., 1966, 11, 2-9

21.  Podgaetskii, V.V.  AVT. Svarka., 1968, No.3, 1-4.

22.  Lees, D.C.G.  J.Inst.Met., 1946, 72, 343.

23.  Singer, A.R.E., & Jennings, P.H.  J.Inst.Met., 1947, 73, 273.

24.  Van Eeghem, J., & De Sy, A.  Modern Castings, July, 1965, 100-110.

25. Pellini, W.S. 'Strain Theory of Hot Tearing', Foundry., 1952, <u>80</u>, <u>11</u>, 124-133, 192, 194, 196, 199.

26. Smith, C.S. Trans.Amer.Inst.Min.Met.Eng., 1948, <u>175</u>, 15.

27. Saveiko, V.N. Lit.Proiz., 1960, <u>8</u>, 33.

28. Griffiths, A.A. Phil.Trans.Roy.Soc., (A), 1920, <u>221</u>, 1963.

29. Eborall, R. & Gregory P. J.Inst.Metals, 1955, <u>84</u>, 88.

30. Rostoker, W. 'Embrittlement by Liquid Metals', New York, 1960. (Reinhold).

31. Stoloff, N.S., & Johnson, T.L. Acta.Met., 1960, <u>4</u>, 251.

32. Williams, J.A. & Singer, A.R.E. J.Inst.Met., 1968, <u>96</u>, 5-12.

33. Stroh, A.H. Proc.Roy.Soc.A., 1953, <u>218</u>, 391.

34. McLean, D. J.Inst.Met., 1952, <u>81</u>, 293.

35. Prokhorov, N.N. Lit.Proiz., 1962, <u>10</u>, 176.

36. Medovar, B.I. Automat.Weld., 1964, (6), 1-11.

37. Dorn, J.E. 'Mechanical Behaviour of Materials at Elevated Temperatures', McGraw Hill Brook Co., New York, 1961.

38. Garafolo, F. 'Fundamentals of Creep and Creep Rupture in Metals', McMillan Series in Material Science, 1965.

39. Hemsworth, B., Boniszewski, T. & Eaton N.F. 'Classification and Definition of High Temperature Welding Cracks in Alloys'. The Welding Institute Autumn Meeting, 1968; Metal Construction and British Welding Journal, 1969, <u>1</u>, February (28), 5-16.

40. Hemsworth, B. Welding Institute Autumn Meeting, 1968; Discussion Metal Construction and British Welding Journal, 1969, <u>1</u>, February (28), 104-106.

41. Eaton, N.F., Glossop, B.A., & Martin, N.S. The Welding of Austenitic Steels to be used in the Fabrication of The Supercritical Units, C.E.G.B. Research Report No. 11/65, N.W. Region, June, 1965, Figure 49.

42. Owczarski, W.A., Duvall, D.S., & Sullivan, C.P. A Model for Heat Affected Zone Cracking in Nickel Base Super-Alloys. Weld Res.1966, <u>31</u>, 145S-155S.

43. Rogerson, J.H., & Borland, J.C. Trans.A.I.M.E., 1963, <u>227</u>, 2-7.

44. Clews, K.J. Brit.Weld.J., 1965, <u>12</u>, 301-309.

45. Hemsworth, B., & Moore J.P.   Circumferential seam welding of 3%CrMo Steel by the electroslag welding process.  Group Research Laboratories Report No. R15/67-N4-1, 1967, English Steel Corporation Ltd., Midland Group, B.S.C. Ltd.

46. Petrov, G.L., & Zemzin, V.N.   Weld Prodn.1967, 14, (2), 1-4.

47. Shackleton, D.N.   "High Temperature Cracking Mechanism in the Heat Affected Zone of 25Cr 20% Ni Stainless Steel Welds".  Welding Inst. Report No. M/47/69, October, 1969.

48. Savage, W.F., Lundin, C.D., & Aronson, A.H.   Weld.Res., 1965, 30, 175S-181S.

49. Rhines, F.N., & Wray P.J.   Trans. A.S.M. 1961, 54 s, 117-128.

50. Haddrill, D.M. & Baker R.G.   Brit.Weld.J., 1965, 12, 8, 411-419.

51. Honeycombe, J., & Gooch, T.G.   'Microcracking in Fully Austenitic Stainless Steel Weld Metal'.  Welding Institute Report M39/3/69.  March, 1969.

52. Hemsworth, B.   High Temperature Weld Cracking Resistance of 3 Experimental 25Cr 20Ni Steels.  RD/M/N430.  1969.

53. British Patent 912, 814.   'Improvement in or relating to an austenitic Nickel-chromium-iron-base alloy'.  Allegheney Ledlum Steel Corporation, Jan.21, 1960.

54. Data Sheet Ref.M969, Jessop-Saville & Co. Ltd., Sheffield.

55. Marsh, A.E.   Role of high alloy steels in elevated temperature environments.  I.S.I. Publication, 117, 167-186, 1969.

56. Dyrkaez, W.W.   Iron Age, 1955, 176, 75.

57. Blum, B.S.   Technical Documentary Report No. A.S.D. -TR. 61-678, April, 1962.

58. Blum, B.S., & Witt, R.H.   Welding J., 1963, 10, 365.

59. Beattie, H.J., & Hagel, W.C.   Precipitation Processes in Steels, I.S.I., Spec.Rep.64, 98-107, 1959.

60. Ben Israel, D.A., & Fine, M.E.   Acta Met., 1963, 11, 1051-1059.

61. Wilson, F.G., & Pickering, F.B.   J.I.S.I., 1966, 204, 628-637.

62. Clarke, B.R., & Pickering, F.B.   J.I.S.I., 1967, 205, 70-84.

63. Mihalisin, J.R., & Decker, R.F.   Trans.A.I.M.E., 1960, 218, 507.

64.    Vogel, R., & Kasten, G.W.   Arch Eisenhutt, 1948, 19, 65.

65.    Elliott, J.F., & Gleiser, M.   'Thermochemistry for Steelmaking'.
       London, 1960.

66.    Gemmill, M.G., Hughes, H., Murray, J.D., Pickering, F.B., & Andrews, K.W.
       1956, 194, 122-144.

67.    Kiessling, R., & Lange, N.   'Non-Metallic Inclusions in Steel'.
       Part II, Iron and Steel Institute Publication No. 100, 1966, 139.

68.    Geiger, T., & Hengerer, F.   Revue de Metallurgie, 1967, 264-269.

69.    Gemmill, M.G.   'The Technology and Properties of Ferrous Alloys in
       High-Temperature Use'.   Newnes, 1966, 196-199.

70.    Allen, G.B.   Proceedings of the Conference on Stainless Steels for the
       Fabrication and User.   I.S.I. Publication 117, 1969, Discussion 98.

71.    Roberts, D.I., & Pucknell, D.J.   'Factors affecting the heat affected
       zone cracking behaviour of unstabilised 10/18 (type 303) austenitic
       stainless steel'.   Paper No. 7, The Welding Institute Autumn Meeting,
       London.   October - November, 1967.

72.    Medovar, B.I.   Automat Weld., 1964, 6, 1-11.

73.    Medovar, B.I., Pinchuk, N.I., Chekotilo, L.V., Pavliichuck, G.A., &
       Tabidze, A.I.   Avtomat Svarka, 1966, 12, 52-57.

74.    Medovar, B.I., Tabidze, A.I., Pinchuk, N.I., Us., V.I., & Yuskevich, Z.V.
       Avtomat Svarke, 1966, 19, (5), 87-90.

75.    Hemsworth, B. 'Proceedings of the Conference on Stainless Steels for
       the Fabricator and User'.   I.S.O. Publication, 117, 1969, Discussion, 98.

76.    Zitter, H., Weinger, H., & Matzer, F.   Radex Runds, 1966, 6, Oct.304-311.

77.    Behara, E.   J.I.S.I., 1966, 204, 48.

78.    Behara, E.   J.I.S.I., 1965, 203, 454.

79.    Borland, J.C.   Brit.Weld.J., 1960, 7, 508-512.

80.    Lancaster, J.F.   'The Metallurgy of Welding, Brazing and Soldering'.
       Allen & Unwin, 1965.

81.    Brockhurst, P.J., & Muir, H.   Welding Fabrication and Design, 1965, 9,
       80-86.

82.    Hull, F.C.   Weld.Res., 1967, 32, 399S-409S.

83.    Borland, J.C., & Robertson, J.M.   Brit.Weld.J., 1962, 9, (8), 494-499.

84. Houldcroft, P.T. Brit.Weld.J., 1955, 2, (10), 471-475.

85. Boudreau, J.S. Weld.Res., 1956, 35, (4), 1465-1685.

86. Rollason, E.C. The Welder, 1953, 22, (114). (New Series), 45-53.

87. Prokhorov, N.N. Svarochnoe Proizvodstvo, 1956, 6, 5-11.

88. Brockhurst, P.J., & Muir, H. J.Austral.Inst.Met., 1965, 10, 140-148.

89. Fredriks, H., & Van der Toorn, L.J. Brit.Weld.J., 1967, 14, 298-303.

90. Savage, W.F., & Lundin, C.D. Weld.Res. 1965, 44, (10), 4335-4425.

91. Astafiev, A.S., & Bardin, I.P. Svarochnoe Proizvodstvo., 1964, (7), 1-4.

92. Wilkinson, F.J., Cottrell, C.L.M., & Huxley, H.V. Brit.Weld.J., 1958, 5, 557-562.

93. Wolstenholme, D.A., Boniszewski, T., & Eaton, N.F. Metal Construction, 1969, 1, Feb. (5), 78-85.

94. Nippes, E.F., & Savage, W.F., & Grotke, G. Weld.Res.Council. Bull. (33), New York, February, 1957.

95. Russiyan, A.V., & Sakharnov, A.A. AVT. Svarka, 1964, (9), 22-27.

96. Hemsworth, B. 'Horizontal Tensile Machine Applied to High Temperature Weld Cracking Studies'. RD/M/N393, May, 1969. Welding and Metal Fabrication, 1970, 38, 76-79.

97. Lement, B.S., Averbach, B.K., & Cohen, M. Trans.A.S.M., 1954, 46, 851-854.

98. Da Silva, P.S.P. M.Met. Thesis, 1966. University of Sheffield.

99. Da Casa, C., & Nileshwar, V.B. J.I.S.I., 1969, 202, 1003-1009.

100. Hume-Rothery, W. Atomic theory for Students of Metallurgy, Institute of Metals Monograph and Report Series. No. 3, 1960, 388.

101. Buckley, R.A., & Hume-Rothery, W. J.I.S.I., 1963, 201, 227-232.

102. Hume-Rothery, W. J.I.S.I., 1965, 203, 1181-1193.
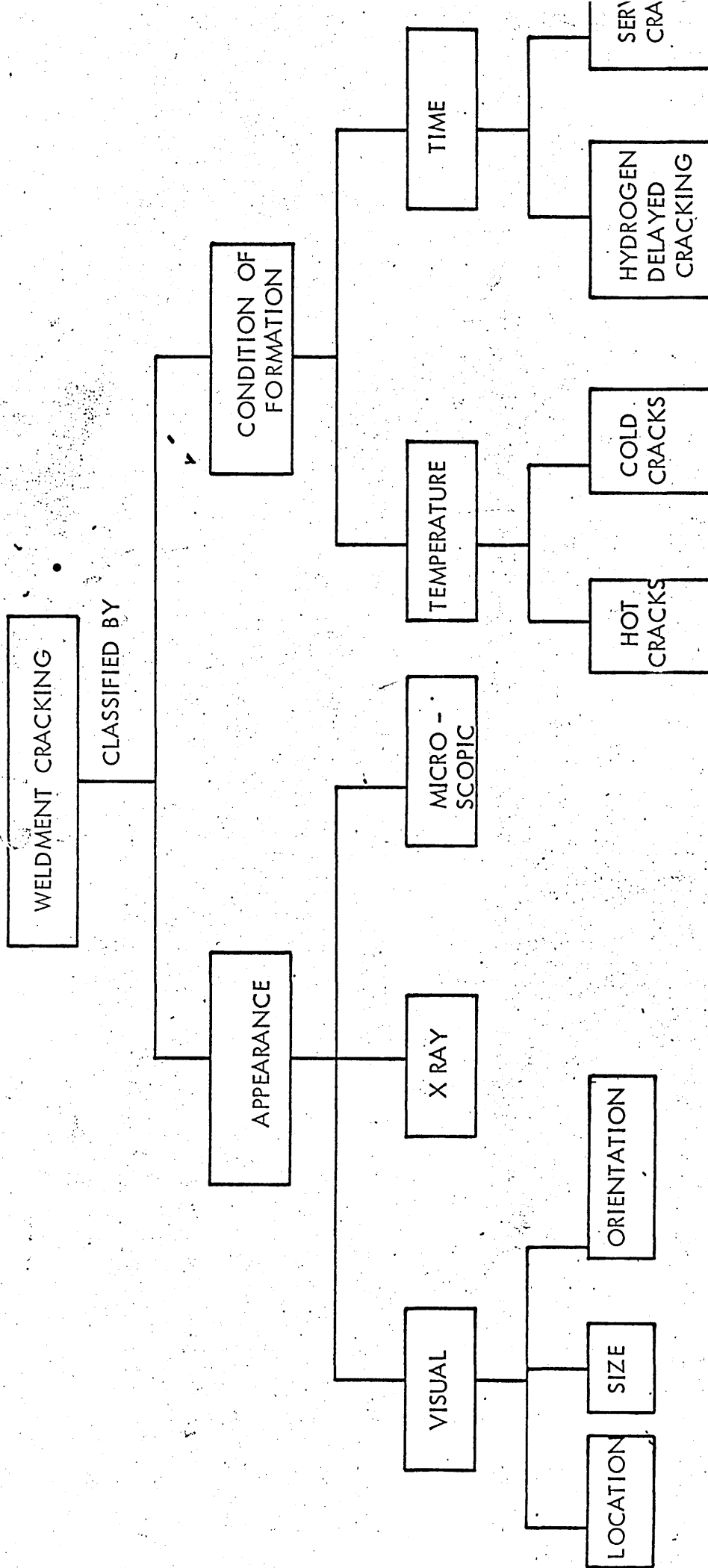
TABLE 1. CLASSIFICATION OF CRACKING IN TABULATED FORM ACCORDING TO KAMMER et al (14)

RD/M/R118

```
                    HIGH TEMPERATURE CRACKING

                    occurs during welding, casting and hot
                    working.


                              │
                              │   Classified by their microstructural
                              │   characteristics
                    ┌─────────┴─────────┐
                    │                   │
    ┌───────────────────────┐   ┌───────────────────────┐
    │       TYPE 1:         │   │       TYPE 2:         │
    │  SEGREGATION CRACKING │   │  DUCTILITY DIP CRACKING│
    │                       │   │                       │
    │ associated with micro-│   │ occurs at newly migrated grain
    │ segregation leading to│   │ boundaries free from films.
    │ intergranular films.  │   │                       │
    └───────────────────────┘   └───────────────────────┘
```

| TYPE 1A | TYPE 1B | TYPE 2A | TYPE 2B |
|---------|---------|---------|---------|
| SOLIDIFIC'N. CRACKING IN WELD METAL | LIQUATION CRACKING IN HAZ | DUCTILITY DIP CRACKING IN HAZ ( includes cavities ) | DUCTILITY DIP CRACKING IN PRIMARY WELD METAL ( includes cavities ) |
| Occurs in ingots and castings. | Occurs during the hot working of pre – worked metal. | Occurs during creep deformation and also hot working of pre – worked metal. | Occurs during creep deformation and the hot working of ingots. |

## TABLE 2. CLASSIFICATION OF INTERGRANULAR WELDING CRACKS

TABLE 3.

ABRIDGED DETAILS OF THE HORIZONTAL TENSILE MACHINE.

| | |
|---|---|
| Maximum effective cross-section of the test piece | 4" x $\frac{1}{2}$" |
| Minimum useful length of test piece | 6" |
| Adjustment of stationery wedge box | 12" x 3" steps |
| Maximum actual load | 20 tons |
| Load Cylinder | 6.5" bore x 4" stroke |
| Maximum hydraulic pressure | 1500 p.s.i. |
| Power of Motor | $\frac{3}{4}$ H.P. |

Crosshead speed 2/3" per minute to 4 inches per minute.

TABLE 4 – Grain Size Measurements.

| Test Plate Number. | Grain Coarsening Heat Treatment. | Length of Line "ℓ" (mm) | No. of Grain Boundary Intercepts, n | Mean Linear Intercept "d" (μm) | Average Spherical Grain Diameter 'L' D = 1.6485 d (μm) |
|---|---|---|---|---|---|
| 1 | 1200°C 1 hour Water Quench | 137 | 600 | 23 | 37.9 |
| 2 | 1200°C 2 hours Water Quench | 220 | 600 | 35 | 57.72 |
| 3 | 1200°C 6 hours Water Quench | 280 | 600 | 48 | 79.14 |
| 4 | 1200°C 24 hours Water Quench | 480 | 600 | 80 | 131.9 |
| 5 | 1200°C 70 hours Water Quench | 1000 | 600 | 166 | 27.37 |
| 6 | 1200°C 100 hours Water Quench | 1700 | 600 | 288 | 474.7 |
| 7 | 1200°C 2 hours Water Quench followed by 8 hours at 750°C | 140 | 600 | 24 | 39.6 |

TABLE 5.  Effect of Stress on the HAZ Cracking of AlSl/304

| Test Plate No. | Grain Coarsening Heat Treatment | Test Plate Cross Section | Load (tons) | Stress t.s.i. | Extension (thou in) | Welding Parameters | | |
|---|---|---|---|---|---|---|---|---|
| | | | | | | Amps | Volt | Time (secs) |
| 1 | 1200°C 1 hour Water Quench | 1.505" x 0.375" | 0 | 0 | 10 | 100 | 10 | 30 |
| 1 | " | " | 2 | 3.54 | 19 | " | " | " |
| 1 | " | " | 3 | 5.32 | 22 | " | " | " |
| 1 | " | " | 4 | 7.1 | 25 | " | " | " |
| 1 | " | " | $5\frac{1}{2}$ | 9.8 | 32 | " | " | " |
| 1 | " | " | $7\frac{1}{2}$ | 13.3 | 69 | " | " | " |
| 1 | " | " | 8 | 14.1 | 74 | " | " | " |
| 1 | " | " | 9 | 15.8 | 109 | " | " | " |
| 1 | " | " | $9\frac{1}{4}$ | 16.4 | fracture | " | " | " |
| 2 | 1200°C 2 hours Water Quench | 1.505" x 0.375" | 0 | 0 | 9 | " | " | " |
| 2 | " | " | 2 | 3.5 | 15 | " | " | " |
| 2 | " | " | 3 | 5.3 | 20 | " | " | " |
| 2 | " | " | 4 | 7.0 | 26 | " | " | " |
| 2 | " | " | 5 | 8.5 | 49 | " | " | " |

| | | | | | | | | | | | | | | |
|---|---|---|---|---|---|---|---|---|---|---|---|---|---|---|
| 2 | = | = | = | = | = | = | = | 5 | 8.5 | 49 | = | = | = | = |
| 2 | = | = | = | = | = | = | = | 6 | 10.0 | 68 | = | = | = | = |
| 2 | = | = | = | = | = | = | = | 7 | 12.6 | 98 | = | = | = | = |
| 3 | = | = | 1200°C 6 hours Water Quench | = | = | 1.5" x 0.375" | = | 0 | | 8 | = | = | = | = |
| 3 | = | = | = | = | = | = | = | 2 | 3.5 | 15 | = | = | = | = |
| 3 | = | = | = | = | = | = | = | 3 | 5.3 | 38 | = | = | = | = |
| 3 | = | = | = | = | = | = | = | 4 | 7.0 | 42 | = | = | = | = |
| 3 | = | = | = | = | = | = | = | 5 | 8.5 | 45 | = | = | = | = |
| 3 | = | = | = | = | = | = | = | 5.5 | 9.8 | 54 | = | = | = | = |
| 3 | = | = | = | = | = | = | = | 6.8 | 12.2 | 87 | = | = | = | = |
| 4 | = | = | 1200°C 24 hours Water Quench | = | = | 1.5" x 0.375" | = | 0 | 0 | 8 | = | = | = | = |
| 4 | = | = | = | = | = | = | = | 1 | 1.7 | 20 | = | = | = | = |
| 4 | = | = | = | = | = | = | = | 2 | 3.5 | 28 | = | = | = | = |
| 4 | = | = | = | = | = | = | = | 3 | 5.2 | 34 | = | = | = | = |
| 4 | = | = | = | = | = | = | = | 4 | 7.0 | 53 | = | = | = | = |
| 4 | = | = | = | = | = | = | = | 5 | 8.5 | 62 | = | = | = | = |
| 4 | = | = | = | = | = | = | = | 6.5 | 11 | 85 | = | = | = | = |

| | Treatment | Size | | | | | | |
|---|---|---|---|---|---|---|---|---|
| 5 | 1200°C 70 hours Water Quench | 1.52" x 0.395" | 0 | 0 | 15 | " | " | " |
| 5 | " | " | 2 | 3.5 | 23 | " | " | " |
| 5 | " | " | 3 | 5.2 | 31 | " | " | " |
| 5 | " | " | 4 | 7.0 | 40 | " | " | " |
| 5 | " | " | 4.5 | 7.4 | 45 | " | " | " |
| 6 | " | " | 0 | 0 | 18 | " | " | " |
| 6 | " | " | 0.5 | 0.9 | 18 | " | " | " |
| 6 | " | " | 1 | 1.7 | 22 | " | " | " |
| 6 | " | " | 2 | 3.5 | 26 | " | " | " |
| 6 | " | " | 3 | 5.2 | 26 | " | " | " |
| 6 | 1200°C 100 hrs Water Quench | " | 4 | 6.9 | 33 | 100 | 10 | 30 |
| 7 | 1200°C 1 hour Water Quench followed by 8 hours at 750°C | 1.5" x 0.375" | 0 | 0 | 9 | " | " | " |
| 7 | " | " | 2 | 3.54 | 20 | " | " | " |
| 7 | " | " | 3 | 5.32 | 22 | " | " | " |
| 7 | " | " | 4 | 7.1 | 25 | " | " | " |

| 7 | = | = | = | $5\frac{1}{2}$ | 9.8 | 30 | = | = | = |
| 7 | = | = | = | 7 | 12.4 | 74 | = | = | = |
| 7 | = | = | = | 8 | 14.1 | 95 | = | = | = |

TABLE 6. Stress and Extension Necessary to initiate HAZ Cracking in AISI 304 Stainless Steel.

| Test Plate Number. | Mean Linear intercept "d" ($\mu$m) | $\frac{1}{d^2}$ | $\frac{l_1}{d^2}$ | Stress to initiate HAZ Cracking t.s.i. | Extension to initiate Cracking over a 10 in. Gauge Length (thou in) |
|---|---|---|---|---|---|
| 1 | 23 | 4.796 | 0.2091 | 15.8 | 109 |
| 2 | 35 | 5.88 | 0.17 | 12.6 | 98 |
| 3 | 48 | 6.93 | 0.1431 | 12.2 | 87 |
| 4 | 80 | 8.94 | 0.1237 | 11.42 | 85 |
| 5 | 166 | 12.88 | 0.0786 | 7.4 | 45 |
| 6 | 288 | 16.97 | 0.0.594 | 6.933 | 33 |
| 7 | 24 | 4.9 | 0.2042 | 14.1 | 95 |

TABLE 7. Creep Testing Results.

| Cast No. | Test Temperature °C | Stress Tons per sq.in. | Time to Fracture (Hours). |
|---|---|---|---|
| A286 | 700 | 16.0 | $62\frac{3}{4}$ |
| A286 | 700 | 19.0 | 35 |
| A286 | 700 | 21.0 | 1 |
| A286 | 700 | 26.0 | Fractured on loading |
| A286 | 750 | 7.5 | 145 |
| A286 | 750 | 9.0 | $89\frac{3}{4}$ |
| A286 | 750 | 11.0 | $69\frac{1}{2}$ |
| A286 | 750 | 13.0 | $2\frac{1}{3}$ |
| A286 | 750 | 15.0 | $3\frac{3}{4}$ |
| A286 + 0.39 wt % B | 700 | 8 | 1800 |
| A286 + 0.39 wt % B | 700 | 9 | 1434 |
| A286 + 0.39 wt % B | 700 | 10 | 313 |
| A286 + 0.39 wt % B | 700 | 11 | 501.5 |

TABLE 8.  Effect of Solution Treatment Temperature on the Grain Size
of A286.

| Heat Treatment | Type of steel | No. of grain inter-section "n" | Length of line "1" section | Mean Linear intercept "d" | Average Spherical Grain diameter "L" multiply by 1.6485 |
|---|---|---|---|---|---|
| 980°C 2 hrs water quench | A286 | 600 | 18,000 | 30 ( μm) | 51 ( μm) |
| 1050°C 2 hrs water quench | A286 | 600 | 21,600 | 36 ( μm) | 60 ( μm) |
| 1150°C 2 hrs water quench | A286 | 600 | 24,000 | 40 ( μm) | 65 ( μm) |

TABLE 9. Chemical Analysis of W.R.K.S10 Experimental Electrodes.

| Cast No. | Element wt % | | | | | | | | | | | | |
|---|---|---|---|---|---|---|---|---|---|---|---|---|---|
| | C | Mn | Si | S | P | Ni | Cr | Mo | V | Al | Ti | B | Co |
| A286 | 0.05 | 1.82 | 0.76 | 0.008 | 0.012 | 24.96 | 14.76 | 1.02 | 0.39 | 0.145 | 1.50 | S0.007 10.005 | - |
| Coating of W.R.K.S10 | 1.83 | 0.79 | 1.17 | 0.23 | 0.017 | 5.48 | 0.08 | 1.53 | - | - | 2.96 | | 32.5 |
| Filler Metal | 0.05 | 0.87 | 1.68 | 0.025 | 0.015 | 21.12 | 23.21 | 0.17 | - | - | 0.04 | | 0.26 |
| 10 S.W.G. Electrode | 0.20 | 0.55 | 0.57 | 0.025 | 0.018 | 14.84 | 12.36 | 8.40 | - | - | 0.10 | | 15.84 |
| 8 S.W.G. Electrode | 0.21 | 0.53 | 0.50 | 0.026 | 0.018 | 15.20 | 12.38 | 8.36 | - | - | 0.075 | | 16.2 |
| 6 S.W.G. Electrode | 0.23 | 0.52 | 0.46 | 0.026 | 0.019 | 15.48 | 12.38 | 8.33 | - | - | 0.05 | | 16.89 |

TABLE 10.  Bead on Plate Tests on A286

| Steel | Solution Treatment | Manual Arc Electrode | Preheat | Gauge | Current | Voltage | Pole | Examination of HAZ Dye Penetrant Testing. |
|---|---|---|---|---|---|---|---|---|
| A286 | 1150°C WQ | WRKS 10 | NONE | 10 | 150 | 25 | DC + ve | extensive cracking |
| A286 | 1050°C WQ | " | NONE | 10 | 150 | 25 | DC + ve | extensive cracking |
| A286 | 980°C WQ | " | NONE | 10 | 150 | 25 | DC + ve | extensive cracking |
| A286 | 1150°C | " | NONE | 8 | 190 | 25 | DC + ve | cracking |
| A286 | 1050°C | " | NONE | 8 | 190 | 25 | DC + ve | cracking |
| A286 | 980°C | " | NONE | 8 | 190 | 25 | DC + ve | cracking |
| A286 | 1150°C | " | NONE | 6 | 240 | 25 | DC + ve | cracking |
| A286 | 980°C | " | NONE | 6 | 240 | 25 | DC + ve | slight cracking |
| A286 | 1050°C | " | NONE | 6 | 240 | 25 | DC + ve | cracking |
| A286 | 1150°C | " | 200°C | 10 | 150 | 25 | DC + ve | cracking |
| A286 | 1050°C | " | 200°C | 10 | 150 | 25 | DC + ve | cracking |
| A286 | 980°C | " | 200°C | 10 | 150 | 25 | DC + ve | cracking |
| A286 | 1150°C | " | 200°C | 8 | 190 | 25 | DC + ve | cracking |

TABLE 10 (Continued).

| Steel | Solution Treatment | Manual Arc Electrode | Preheat | Gauge | Current | Voltage | Pole | Examination of HAZ Dye Penetrant Testing |
|---|---|---|---|---|---|---|---|---|
| A286 | 1050°C | " | 200°C | 8 | 190 | 25 | DC + ve | cracking |
| A286 | 980°C | " | 200°C | 8 | 190 | 25 | DC + ve | no cracking |
| A286 | 1150°C | " | 200°C | 6 | 240 | 25 | DC + ve | cracking |
| A286 | 1050°C | " | 200°C | 6 | 240 | 25 | DC + ve | no cracking |
| A286 | 980°C | " | 200°C | 6 | 240 | 25 | DC + ve | no cracking |
| A286 | 1150°C | " | -20°C | 10 | 150 | 25 | DC + ve | extensive cracking |
| A286 | 1050°C | " | -20°C | 10 | 150 | 25 | DC + ve | extensive cracking |
| A286 | 980°C | " | -20°C | 10 | 150 | 25 | DC + ve | extensive cracking |
| A286 | 1150°C | " | -20°C | 8 | 190 | 25 | DC + ve | cracking |
| A286 | 1050°C | " | -20°C | 8 | 190 | 25 | DC + ve | cracking |
| A286 | 980°C | " | -20°C | 8 | 190 | 25 | DC + ve | cracking |
| A286 | 1150°C | " | -20°C | 6 | 240 | 25 | DC + ve | cracking |
| A286 | 1050°C | " | -20°C | 6 | 240 | 25 | DC + ve | cracking |
| A286 | 980°C | " | -20°C | 6 | 240 | 25 | DC + ve | cracking |

TABLE 11.    Microscopic Examination of Incidence of HAZ Cracking in A286

| Solution Treatment Temperature 2 hours water quench | Preheat Temperature °C | Gauge of Electrode | Incidence of HAZ Cracking No. of Cracks per cm to nearest whole number |
|---|---|---|---|
| 1150 | 20 | 10 | 10 |
| 1050 | 20 | 10 | 8 |
| 980 | 20 | 10 | 6 |
| 1150 | 20 | 8 | 5 |
| 1050 | 20 | 8 | 4 |
| 980 | 20 | 8 | 3 |
| 1150 | 20 | 6 | 2 |
| 1050 | 20 | 6 | 1 |
| 980 | 20 | 6 | 1 |
| 1150 | -20 | 10 | 10 |
| 1050 | -20 | 10 | 8 |
| 980 | -20 | 10 | 7 |
| 1150 | -20 | 8 | 6 |
| 1050 | -20 | 8 | 4 |
| 980 | -20 | 8 | 3 |
| 1150 | -20 | 6 | 2 |
| 1050 | -20 | 6 | 1 |
| 980 | -20 | 6 | 1 |
| 1150 | +200 | 10 | 4 |
| 1050 | +200 | 10 | 4 |
| 980 | +200 | 10 | 3 |
| 1150 | +200 | 8 | 1 |
| 1050 | +200 | 8 | 1 |
| 980 | +200 | 8 | 1 |
| 1150 | +200 | 6 | 1 |
| 1050 | +200 | 6 | 1 |
| 980 | +200 | 6 | 1 |

TABLE 12. Effect of Heat Input on the HAZ Grain Coarsening Tendencies of A286, Preheat 20°C.

| Cast No. | Solution Treatment Temperature 2 hrs water quench | Parent Metal Grain Size Average Spherical Grain Diameter ($\mu$m) | Electrode | Gauge S.W.G | Current | Volts | HAZ Grain Size Average Spherical Grain Diameter ($\mu$m) |
|---|---|---|---|---|---|---|---|
| A286 | 980 | 51 | WRKS 10 | 10 | 150 | 25 | 72 |
| A286 | 980 | 51 | WRKS 10 | 8 | 190 | 25 | 75 |
| A286 | 980 | 51 | WRKS 10 | 6 | 240 | 25 | 77 |
| A286 | 1050 | 60 | WRKS 10 | 10 | 150 | 25 | 84 |
| A286 | 1050 | 60 | WRKS 10 | 8 | 190 | 25 | 88 |
| A286 | 1050 | 60 | WRKS 10 | 6 | 240 | 25 | 92 |
| A286 | 1150 | 65 | WRKS 10 | 10 | 150 | 25 | 88 |
| A286 | 1150 | 65 | WRKS 10 | 8 | 190 | 25 | 94 |
| A286 | 1150 | 65 | WRKS 10 | 6 | 240 | 25 | 102 |

TABLE 13. Room Temperature Impact Properties of A286 and A286B.

| Temperature (°C) | Time (hours) | Charpy Impact Properties ft.lbs. | |
| --- | --- | --- | --- |
| | | A.286 | A.286 + 0.39 wt % B. |
| 800 | 0.5 | 31 | 20 |
| 800 | 1 | 40 | 16 |
| 800 | 2 | 38 | 28 |
| 800 | 4 | 35 | 29 |
| 800 | 8 | 35 | 16 |
| 800 | 24 | 33 | 18 |
| 800 | 48 | 32 | 16 |
| 800 | 70 | 29 | 17 |
| 750 | 0.5 | 33 | 20 |
| 750 | 2 | 36 | 23 |
| 750 | 4 | 29 | 13 |
| 750 | 8 | 25 | 25 |
| 750 | 24 | 24 | 17 |
| 750 | 48 | 23 | 13 |
| 750 | 70 | 21 | 15 |
| 700 | 0.5 | 30 | 18 |
| 700 | 2 | 32 | 20 |
| 700 | 4 | 36 | 16 |
| 700 | 8 | 34 | 23 |
| 700 | 24 | 29 | 18 |
| 700 | 48 | 30 | 16 |
| 700 | 70 | 28 | 15 |
| 980 water quench. | 0 | 37 | 20 |

TABLE 14.    Bead on Plate Tests on A286 plus 0.39 wt % Boron.

| Cast No | Preheat Temperature | Gauge SWG | Current (amps) | Volts | Examination of HAZ by Dye Penetrant Testing. |
|---------|---------------------|-----------|----------------|-------|----------------------------------------------|
| A286B   | 20                  | 10        | 150            | 25    | HAZ cracking                                 |
| A286B   | 20                  | 8         | 190            | 25    | No cracking                                  |
| A286B   | 20                  | 6         | 240            | 25    | No cracking                                  |
| A286B   | -20                 | 10        | 150            | 25    | HAZ cracking                                 |
| A286B   | -20                 | 8         | 190            | 25    | No cracking                                  |
| A286B   | -20                 | 6         | 240            | 25    | No cracking                                  |
| A286B   | 200                 | 10        | 150            | 25    | No cracking                                  |
| A286B   | 200                 | 8         | 190            | 25    | No cracking                                  |
| A286B   | 200                 | 6         | 240            | 25    | No cracking                                  |

TABLE 15.    Effect of Heat Input on the HAZ Grain Coarsening Tendencies

of A286 Plus a 0.39 wt % Boron Addition

| Cast No. | Solution Temperature, 1 hour water quench °C | Parent Metal Grain Size Average Spherical Grain dia. (μm) | Electrode | Gauge SWG | Current (amps) | Volts | HAZ Grain Size Averag Spherical Grain dia. (μm) |
|---|---|---|---|---|---|---|---|
| A286B | 980 | 22 | WRKS 10 | 10 | 150 | 25 | 27 |
| A286B | 980 | 22 | WRKS 10 | 8 | 190 | 25 | 34 |
| A286B | 980 | 22 | WRKS 10 | 6 | 240 | 25 | 33 |
| A286B | 1050 | 24 | WRKS 10 | 10 | 150 | 25 | 34 |
| A286B | 1050 | 24 | WRKS 10 | 8 | 190 | 25 | 38 |
| A286B | 1050 | 24 | WRKS 10 | 6 | 240 | 25 | 40 |
| A286B | 1150 | 27 | WRKS 10 | 10 | 150 | 25 | 37 |
| A286B | 1150 | 27 | WRKS 10 | 8 | 190 | 25 | 39 |
| A286B | 1150 | 27 | WRKS 10 | 6 | 240 | 25 | 43 |

TABLE 16. Effect of High Temperature Heat Treatment on the
Liquation Tendencies of A286.

| Cast No. | Heat Treatment temperature °C followed by Water Quench | Time (hours). | Microscopical Examination |
|---|---|---|---|
| A286 | 1200 | 1 | No observed liquation |
| A286 | 1250 | 1 | No observed liquation |
| A286 | 1300 | 1 | Chinese script shaped second phase plus intergranular cracking. |
| A286 | 1325 | 1 | Chinese script shaped liquated second phase plus intergranular cracking. |
| A286 | 1350 | 1 | Extensive liquated second phase plus excessive intergranular cracking. |
| A286 | 1400 | 1 | Complete melting |

TABLE 17.   Effect of High Temperature Heat Treatment on the Liquation
Tendencies of A286 + 0.39 wt % Boron.

| Cast No. | Heat Treatment Temperature °C | Time | Microscopical Examinatio |
|---|---|---|---|
| A286B | 1200 | 1 | No signs of liquation. |
| A286B | 1250 | 1 | Small amount of liquated second phase. |
| A286B | 1300 | 1 | Liquated second phase. |
| A286B | 1325 | 1 | Excessive liquated second phase plus intergranular cracking. |
| A286B | 1350 | 1 | Extensive liquated second phase plus intergranular cracking. |
| A286B | 1400 | 1 | Total fusion of test specimen. |

TABLE 18.  Effect of Heat Treatment on the Grain Coarsening
Tendencies of A286.

| Cast No. | Heat Treatment Temperature °C followed by water quench | Time (Hours) | Grain size.  Average Spherical Grain Diameter "L" ( $\mu$m). |
|---|---|---|---|
| A286 | 1200 | 1 | 90 |
| A286 | 1250 | 1 | 96 |
| A286 | 1300 | 1 | 108 |
| A286 | 1325 | 1 | 110 |
| A286 | 1350 | 1 | 135 |
| A286 | 1400 | 1 | Total fusion of test specimen. |

TABLE 19.    Effect of Heat Treatment on the Grain Coarsening Tendencies
of A286 Plus 0.39 wt % Addition of Boron:

| Cast No. | Heat Treatment Temperature °C followed by water quench | Time (hours) | Grain Size Average Spherical Grain Diameter ($\mu$m) |
|---|---|---|---|
| A286B | 1200 | 1 | 60 |
| A286B | 1250 | 1 | 65 |
| A286B | 1300 | 1 | 65 |
| A286B | 1325 | 1 | 79 |
| A286B | 1350 | 1 | 84 |
| A286B | 1400 | 1 | Total melting of test specimen. |

# APPENDIX 1

## SELECTED AREA ELECTRON DIFFRACTION

**SHEET 1**

| EXPERIMENTAL DATA — EMMA INDICATIONS Ti, S. | | | | | | | | ASTM X-RAY STANDARDS | | | |
|---|---|---|---|---|---|---|---|---|---|---|---|
| Al STANDARD PLATE No. 523 | | | | UNKNOWN PLATE No. 522 DENDRITIC FILM | | | | $T_{15}S_4$ 12 - 402 | Tau phase $T_{12}S$ | $T_{13}S_4$ 9 - 294 | T S 9 - 28 |
| log d | Cr | log 2rd | log 2rd | 2r | log 2r | log d | d | d spacings | d spacings | d spacings | d spac |
| 0.3694 | 18.6 | 1.2695 | 1.6389 | 17.2 | 1.2355 | 0.4034 | 2.531 | 2.58 | 2.69 | 2.63 | 2.5 |
| 0.3694 | 18.7 | 1.2718 | 1.6412 | 17.9 | 1.2529 | 0.3883 | 2.445 | 2.47 | 2.22 | 2.34 | 2.3 |
| 0.3064 | 21.4 | 1.3304 | 1.6368 | 22.2 | 1.3464 | 0.2904 | 1.952 | 2.02 | 1.96 | 2.06 / 1.90 | 1.9 |
| 0.1563 | 30.65 | 1.4864 | 1.6427 | 27.1 | 1.4330 | 0.2097 | 1.621 | 1.67 | 1.596 | 1.64 / 1.60 | 1.6 |
| 0.1563 | 30.5 | 1.4843 | 1.6406 | 27.9 | 1.4456 | 0.1950 | 1.567 | 1.51 | 1.542 | 1.60 / 1.47 | 1.5 |

**General Comments:** Electron microscopy reveals a large fern which was liquated during welding and was present in the HAZ of A 286.

Electron Microscope Micro-Analysis (EMMA) indicated the particle to be titanium and sulphur rich.

Selected area diffraction would tend to indicate the phase is $T_{15}S_4$.

# SELECTED AREA ELECTRON DIFFRACTION

## EMMA INDICATION Ti, S

### SHEET 2

| Al STANDARD PLATE 523 | | | UNKNOWN PLATE 519 fern shaped region | | | | | ASTM XRAY INDEX 12 - 402 $Ti_5S_4$ |
|---|---|---|---|---|---|---|---|---|
| log d | 2r | log 2r | log 2rd | 2r | log 2r | log d | d | d spacings |
| 0.3694 | 18.5 | 1.2672 | 1.6366 | 15.75 | 1.1973 | 0.4393 | 2.75 | 2.70 |
| 0.3064 | 21.5 | 1.3324 | 1.6388 | 21.5 | 1.3324 | 0.3064 | 2.025 | 2.02 |
| 0.3064 | 21.6 | 1.3345 | 1.6409 | 22.5 | 1.3522 | 0.2937 | 1.99 | 1.86 |
| 0.1563 | 30.5 | 1.4843 | 1.6406 | 30.00 | 1.4771 | 0.1635 | 1.457 | 1.49 |

General Comments:

Liquated phase which could quite well be $Ti_5S_4$.

**SHEET 3**

## SELECTED AREA ELECTRON DIFFRACTION

| EXPERIMENTAL DATA A1 STANDARD PLATE No. 704 | | | | UNKNOWN PLATE 702 | | | | X-RAY DATA. | |
|---|---|---|---|---|---|---|---|---|---|
| log d | 2r | log 2r | log 2rd | 2r | log 2r | log d | d | d spacings M6C | d spacings M23 C6 |
| 0.3694 | 19.65 | 1.2934 | 1.6628 | 8.3 | 0.9191 | 0.7437 | 5.543 | 5.541 | 5.31 |
| 0.3064 | 22.6 | 1.3541 | 1.6605 | 11.6 | 1.0645 | 0.5960 | 3.945 | 3.918 | 3.755 |
| 0.3694 | 19.65 | 1.2934 | 1.6628 | 8.35 | 0.9217 | 0.7411 | 5.51 | 5.541 | 5.541 |
| 0.3064 | 22.60 | 1.3541 | 1.6605 | 11.65 | 1.0664 | 0.5941 | 3.926 | 3.918 | 3.755 |

| d | $d^2$ | hkl | $a^2$ |
|---|---|---|---|
| 5.543 | 30.72 | 002 | 121.88 |
| 3.945 | 15.56 | 022 | 124.48 |
| 5.51 | 30.36 | 002 | 121.44 |
| 3.926 | 15.42 | 022 | 121.36 |
| | | | $a^2$ = 489.16 |

$a^2 = 124.78 \qquad a = 11.$

General Comments:    The dendritic shapes phase is M6C carbide.
F.C.C. [001] Zone.

## SELECTED AREA DIFFRACTION

| | EXPERIMENTAL DATA | | | | SHATTERED FILMS | | | | ASTM XRAY INDEX |
|---|---|---|---|---|---|---|---|---|---|
| A1 STANDARD PLATE No. 697 | | | | EMMA INDICATIONS Ti, V and S | UNKNOWN PLATE No. 696 | | | | $T - T_{i2}S$ 11 - 664 Tau TITANIUM SULPHI |
| log d | 2r | log 2r | log 2rd | | 2r | log 2r | log d | d | d spacings |
| 0.3694 | 19.5 | 1.2900 | 1.6594 | | 16.2 | 1.2095 | 0.4499 | 2.812 | 2.77 |
| 0.3064 | 22.2 | 1.3464 | 1.6528 | | 22.5 | 1.3522 | 0.3006 | 1.998 | 1.963 |
| 0.3064 | 22.2 | 1.3464 | 1.6528 | | 23.0 | 1.3617 | 0.2911 | 1.955 | 1.963 |
| 0.1563 | 32.0 | 1.5051 | 1.6614 | | 33.0 | 1.5185 | 0.1429 | 1.39 | 1.381 |

General Comments:

EMMA indications are Ti, V and S compound. Selected area electron diffraction would indicate an $M_2CS$ type compound.

## SELECTED AREA ELECTRON DIFFRACTION

| A1 STANDARD PLATE 420 | | | | UNKNOWN PLATE 419 SHATTERED FILMS EMMA INDICATIONS Ti, V, S. | | | | 11 - 664 Ti$_2$S Y Phase and Phase | | | |
|---|---|---|---|---|---|---|---|---|---|---|---|
| log d | 2r | log 2r | log 2rd | 2r | log 2r | log d | dÅ | I | dÅ | I$_2$ | hkl |
| 0.3694 | 16.4 | 1.2148 | 1.5842 | 13.8 | 1.1399 | 0.4443 | 2.728 | S | 2.77 | 50 | |
| 0.3694 | 16.55 | 1.2188 | 1.5882 | 14.4 | 1.1584 | 0.4298 | 2.690 | S | 2.69 | 20 | |
| 0.3694 | 16.50 | 1.2175 | 1.5869 | 14.3 | 1.1553 | 0.4316 | 2.702 | S | 2.69 | 20 | |
| 0.3064 | 19.1 | 1.2810 | 1.5874 | 24.25 | 1.3847 | 0.2027 | 1.595 | Mq | 1.60 | 70 | |
| 0.1563 | 27.0 | 1.4314 | 1.5877 | 25.2 | 1.4014 | 0.1863 | 1.537 | M | 1.542 | 50 | |

General Comments:

The strong lines of  phase Ti$_2$S are 2.22, 1.60, 1.38, 2.77 with intensity ratings 100, 70, 60, 50 respectively.

The above phase does not have 2.22 and 1.38 and may not be tau phase.  However, probe indications of Ti, V, S may mean the V has altered structure of the film.  M$_2$(CS).

## SELECTED AREA ELECTRON DIFFRACTION

### EMMA indications Ti, V and S

| Al STANDARD No. 659 | | | | UNKNOWN PLATE No. 658 SHATTERED FILMS | | | | ASTM XRAY INDEX T − Ti$_{12}$S |
|---|---|---|---|---|---|---|---|---|
| log d | 2r | log 2r | log 2rd | 2r | log 2 | log d | d | Tau Titanium Sulph |
| 0.3694 | 19.7 | 1.2945 | 1.6639 | 21.3 | 1.3284 | 0.3355 | 2.165 | 2.22 |
| 0.3694 | 19.9 | 1.2989 | 1.6683 | 21.2 | 1.3243 | 0.3440 | 2.208 | 2.22 |
| 0.1563 | 32.25 | 1.5086 | 1.6649 | 29.8 | 1.4742 | 0.1907 | 1.552 | 1.60 |
| 0.0867 | 35.4 | 1.5490 | 1.6357 | 31.9 | 1.5038 | 0.1319 | 1.355 | 1.38 |

General Comments:

Strongest d spacings for tau phase (Ti$_2$S) are as follows 2.22, 1.60, 1.38 and the "d" spacings of unkn[own] are similar and, therefore, the phase is possibly Ti$_2$S. EMMA indications are Ti, V and S would indicate phase is M$_2$CS

## SELECTED AREA ELECTRON DIFFRACTION

### EXPERIMENTAL DATA EMMA INDICATIONS Fe and Ti

| Al STANDARD No. 761 | | | | UNKNOWN PLATE No. 760 DENDRITIC FILM. | | | | ASTM XRAY INDEX Ti Fe2  3 - 1049 | Fe2Ti (66)  a = 4.766Å  c = 7.59 Å |
|---|---|---|---|---|---|---|---|---|---|
| log d | 2r | log 2r | log 2rd | 2r | log 2r | log d | d | | |
| 0.3694 | 19.4 | 1.2878 | 1.6572 | 8.7 | 0.9395 | 0.7177 | 5.22 | | 2.3828 |
| | | | | | | | | 2.40 | 2.1915 |
| 0.3064 | 22.8 | 1.3579 | 1.6643 | 26.8 | 1.4281 | 0.2362 | 1.72 | 2.20 | 2.0635 |
| | | | | | | | | 2.04 | 2.0303 |
| 0.1563 | 32.1 | 1.5065 | 1.6628 | 29.6 | 1.4713 | 0.1915 | 1.554 | 2.00 | 1.3757 |
| | | | | | | | | 1.96 | 1.3358 |
| | | | | | | | | 1.83 | 1.2931 |

General Comments:

Liquated particle appears as dendritic ferns and EMMA indicates Fe and Ti. Selected area electron diffraction pattern was not solved.

## SELECTED AREA ELECTRON DIFFRACTION

| EXPERIMENTAL DATA | | | | | | | | ASTM XRAY INDEX | |
| Al STANDARD PLATE No. 862 | | | | UNION JACKS UNKNOWN PLATE 861 | | | | TiC 6 - 0614 | TiN 6 - 0642 |
| log d | 2r | log 2r | log 2 rd | 2r | log 2r | log d | d | d spacing | d spacing |
|---|---|---|---|---|---|---|---|---|---|
| 0.3694 | 19.6 | 1.2923 | 1.6617 | 21.4 | 1.3304 | 0.3313 | 2.144 | 2.18 | 2.12 |
| 0.1563 | 32.2 | 1.5079 | 1.6642 | 35.6 | 1.5514 | 0.1128 | 1.296 | 1.311 | 1.277 |
| 0.1563 | 32.2 | 1.5079 | 1.6642 | 35.5 | 1.5502 | 0.1140 | 1.300 | 1.311 | |
| 0.0678 | 40.0 | 1.6021 | 1.6699 | 46.6 | 1.6684 | 0.0015 | 1.003 | 1.086  0.997 | 1.059 |

General Comments:

Particles appear as "Union Jacks" shaped films because they have differential contrast under the elect
beam. No EMMA results possible but SAED would indicate Ti (CN). These small films appear dispersed on the
fracture surfaces of cracks which are thermal faceted.

## SELECTED AREA DIFFRACTION

| EXPERIMENTAL DATA | | | | | | | | ASTM XRAY DATA | |
| --- | --- | --- | --- | --- | --- | --- | --- | --- | --- |
| Al STANDARD PLATE No. 1032 | | | | UNION JACKS UNKNOWN PLATE No. 1031 | | | | Ti C 6 - 0614 | Ti N 6 - 0644 |
| log d | 2r | log 2r | log 2rd | 2r | log 2r | log d | d | d spacings | d spacing |
| 0.3694 | 19.7 | 1.2945 | 1.6639 | 21.5 | 1.3324 | 0.3304 | 2.14 | 2.18 | 2.12 |
| 0.3694 | 19.6 | 1.2923 | 1.6617 | 21.2 | 1.3263 | 0.3354 | 2.16 | 2.18 | 2.12 |
| 0.3064 | 22.9 | 1.3598 | 1.6662 | 30.4 | 1.4829 | 0.1833 | 1.53 | 1.535 | 1.50 |
| 0.3064 | 22.8 | 1.3579 | 1.6643 | 30.4 | 1.4829 | 0.1814 | 1.52 | 1.535 | 1.50 |
| 0.3064 | 22.8 | 1.3579 | 1.6643 | 30.4 | 1.4829 | 0.1814 | 1.52 | 1.535 | 1.50 |

General Comments:

Particles appear as arrays of "Union Jack" shaped films. It was not possible to carry out Electron Microscope-Micro-Analysis, EMMA, but Selected Area Electron Diffraction would indicate Titanium Carbonitride. The diffraction pattern is streaky and only possible to index two radii which are consistent with Ti(CN).

Critical amount of strain for tearing

Film stage reached

Strain less than critical amount

Strain greater than critical amount
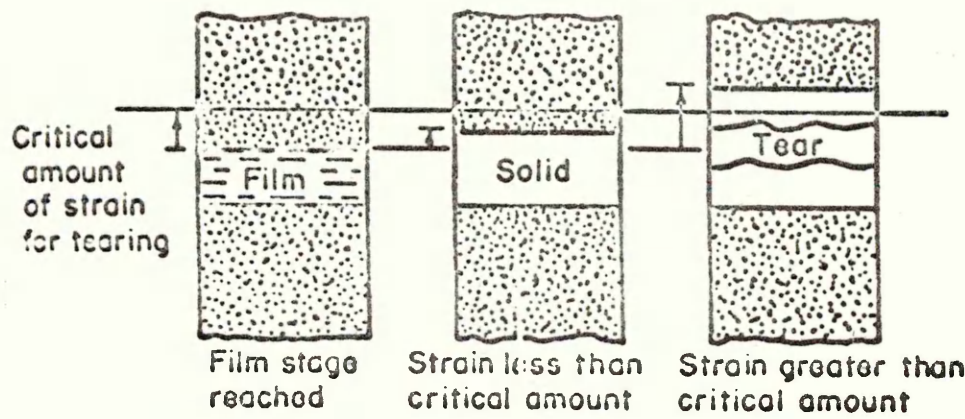
Total strain developed during film-life period depends on:

(1) Strain rate
(2) Time of film life

Effect of segregates is severe due to increased film life
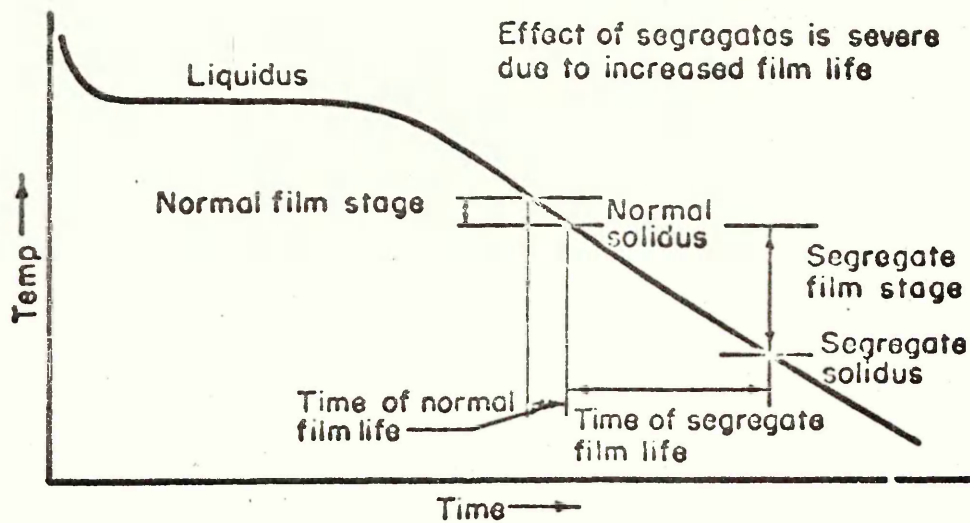
FIG. 1  STRAIN THEORY OF HOT TEARING IN CASTINGS  (25)
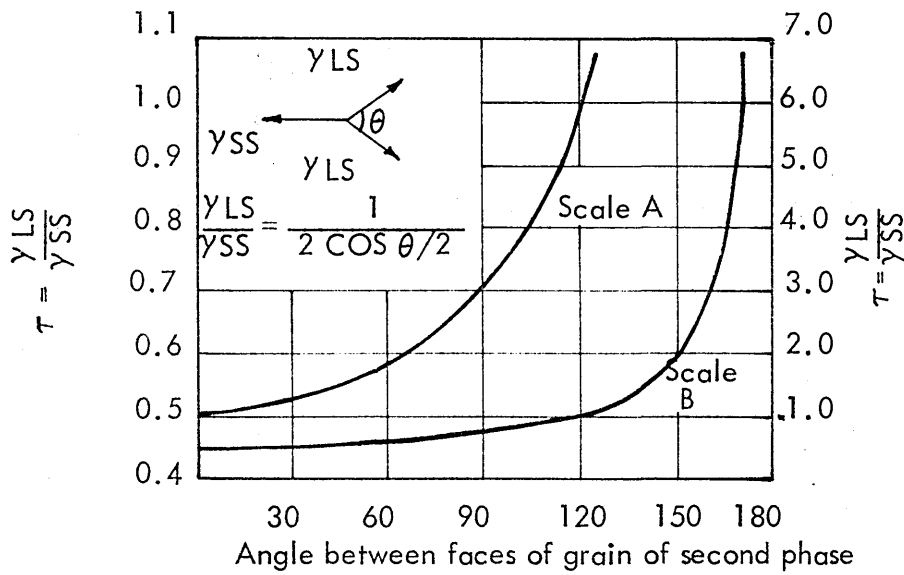
FIG. 2a    RATIO OF INTERPHASE BOUNDARY TENSION AND GRAIN BOUNDARY TENSION AS A FUNCTION OF DIHEDRAL ANGLE OF SECOND PHASE ( SMITH ) (26)



$180° > \theta > 60°$ liquid forms isolated particles on grain boundaries and triple points

$\theta = 60°$ liquid forms continuous film around the grain edges

$\theta < 60$   liquid spreads further over grain surfaces until $\theta = 0°$ complete coverage
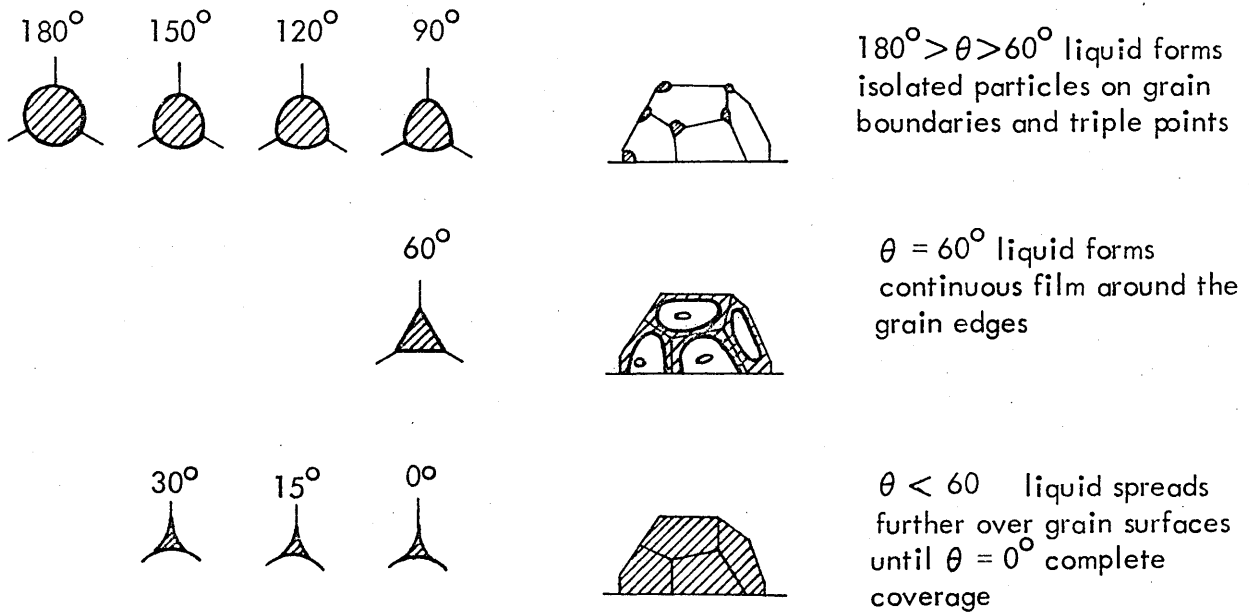
FIG. 2b    EFÈECT OF DIHEDRAL ANGLE ON THE SHAPE OF LIQUID PARTICLES ( SMITH )(26
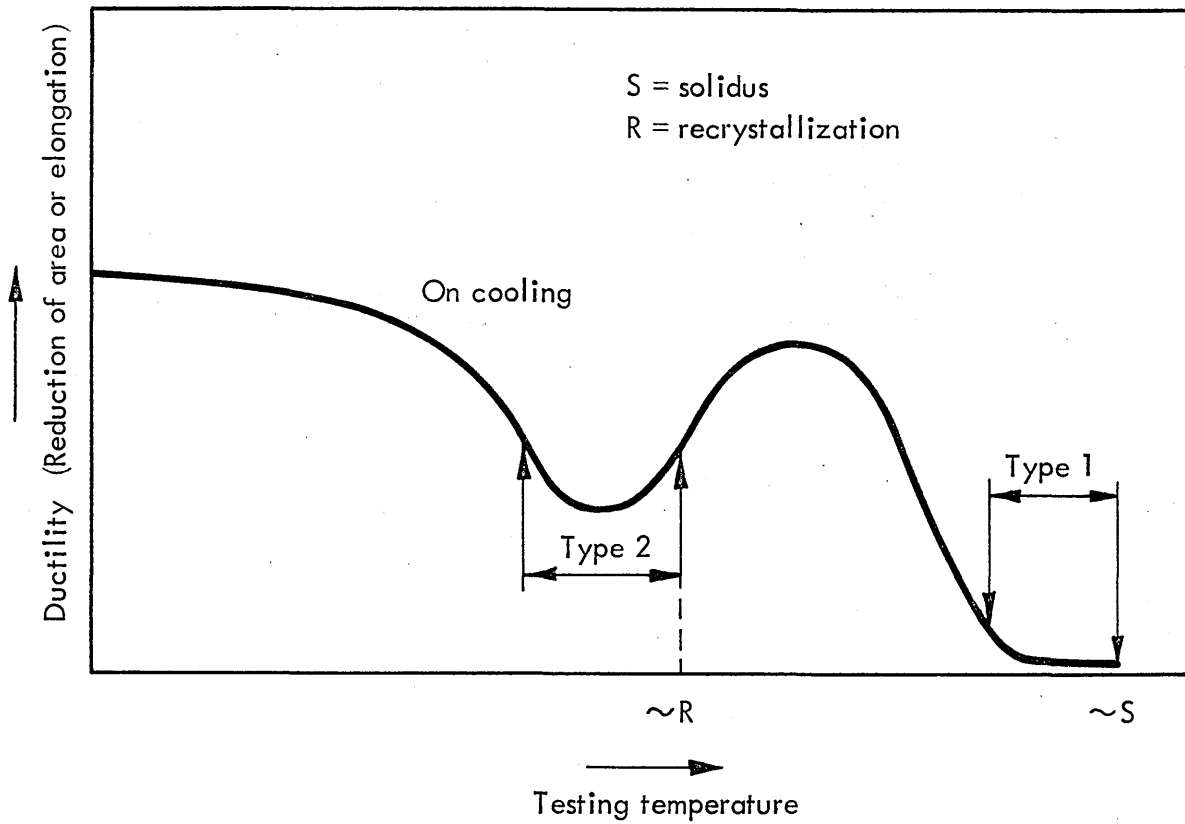
FIG. 3  SCHEMATIC REPRESENTATION OF THE TWO BASIC TEMPERATURE RANGES IN
WHICH A DUCTILITY MINIMUM IS CONDUCIVE TO WELDMENT CRACKING
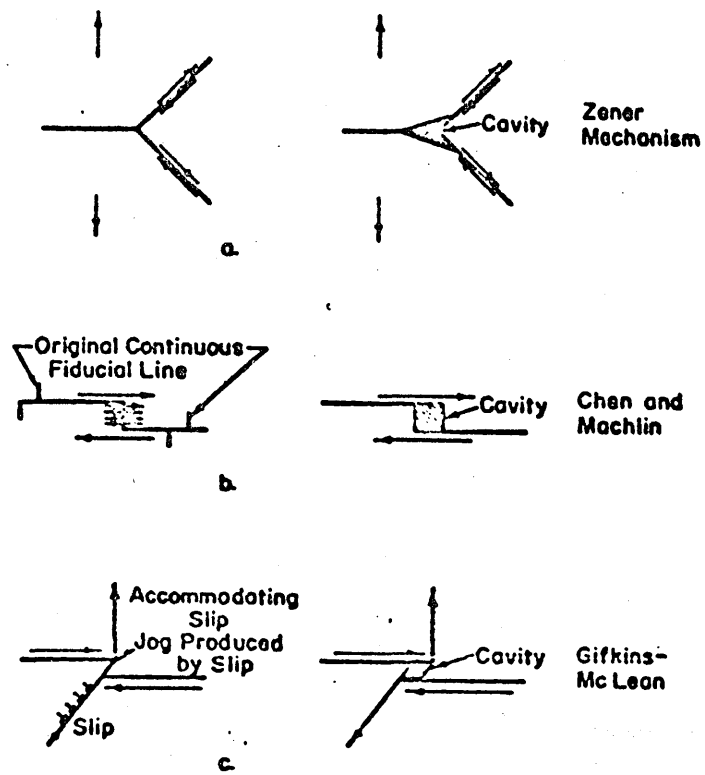
FIG. 4   POSSIBLE MECHANISMS OF CAVITY GROWTH AT GRAIN BOUNDARIES(14)
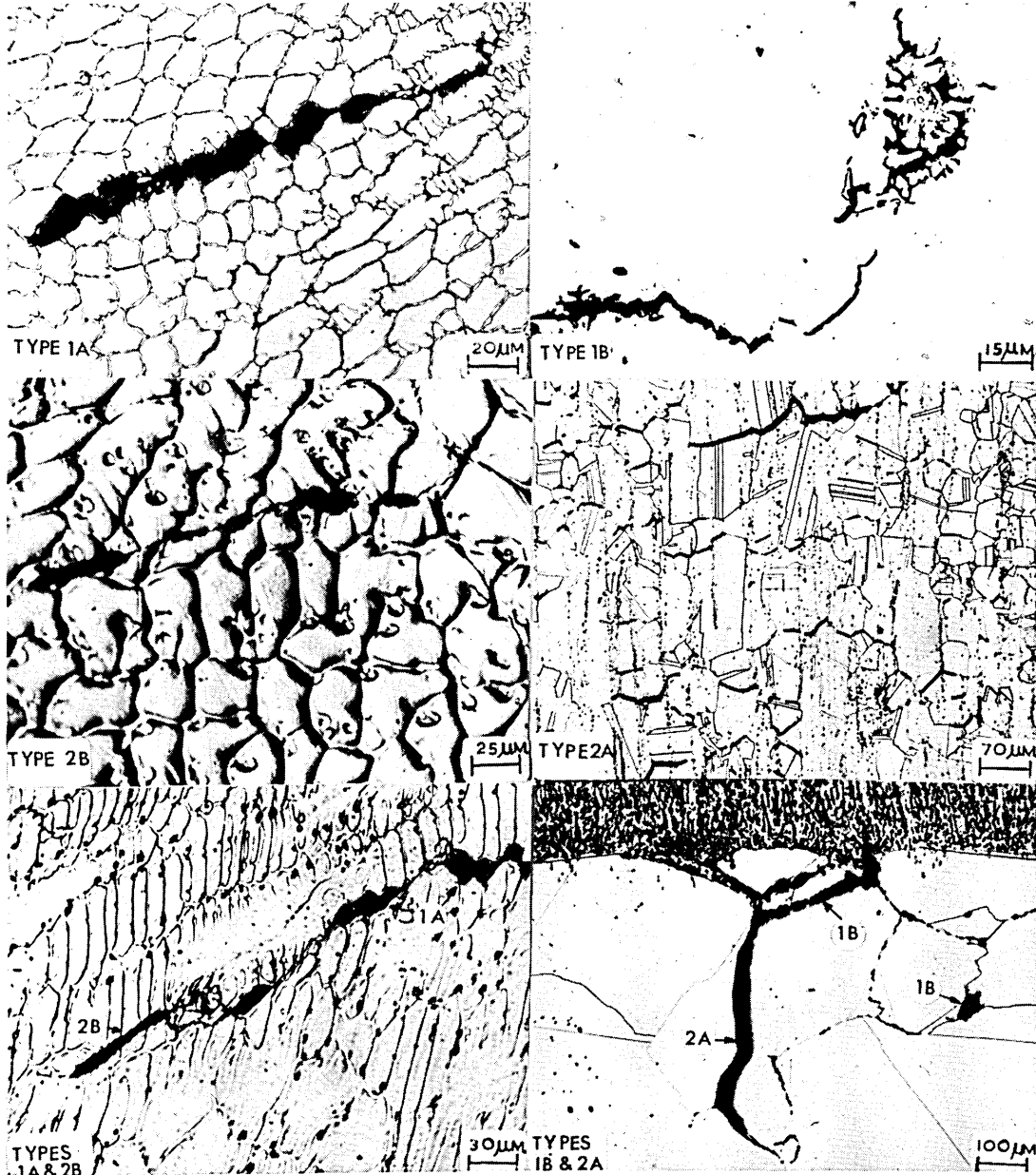
## FIG. 5  CLASSIFICATION OF HIGH TEMPERATURE WELD CRACKING

Type 1A:  Intercellular solidification cracking intimately associated with the solidification structure in an 18Cr 10Ni weld metal.

Type 1B:  HAZ liquation cracking in A286 (a25Ni 15Cr intermetallic strengthened austenitic steel)

Type 2B:  Trans-cellular ductility dip cracking which ignores the solidification structure in 18Cr 10Ni weld metal

Type 2A:  HAZ ductility dip cracking in AISI 310 (a25Cr 20Ni austenitic steel)

Merging of the two main types

Type 1A propagating as Type 2B in an 18Cr 10Ni weld metal

Type 1B propagating as Type 2A in AISI 304 steel  (an 18Cr 10Ni alloy)
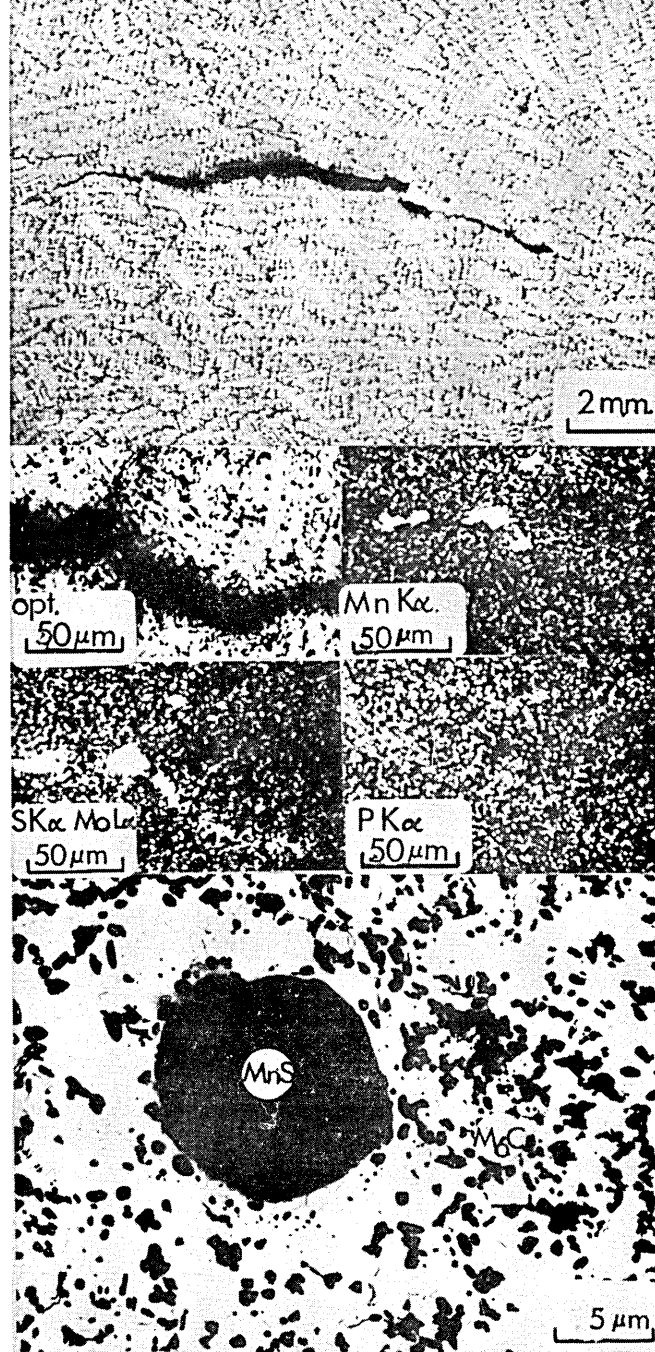
## FIG. 6   WELD METAL SOLIDIFICATION CRACKING   (TYPE 1A)

Shows the composition of the interdendritic microsegregate in a $2\frac{1}{2}$Cr 1Mo electroslag
weld metal.   The microsegregate consists of manganese sulphide, molybdenum carbide
($M_6C$), and phosphorus which increases the fluidity of the interdendritic liquid.
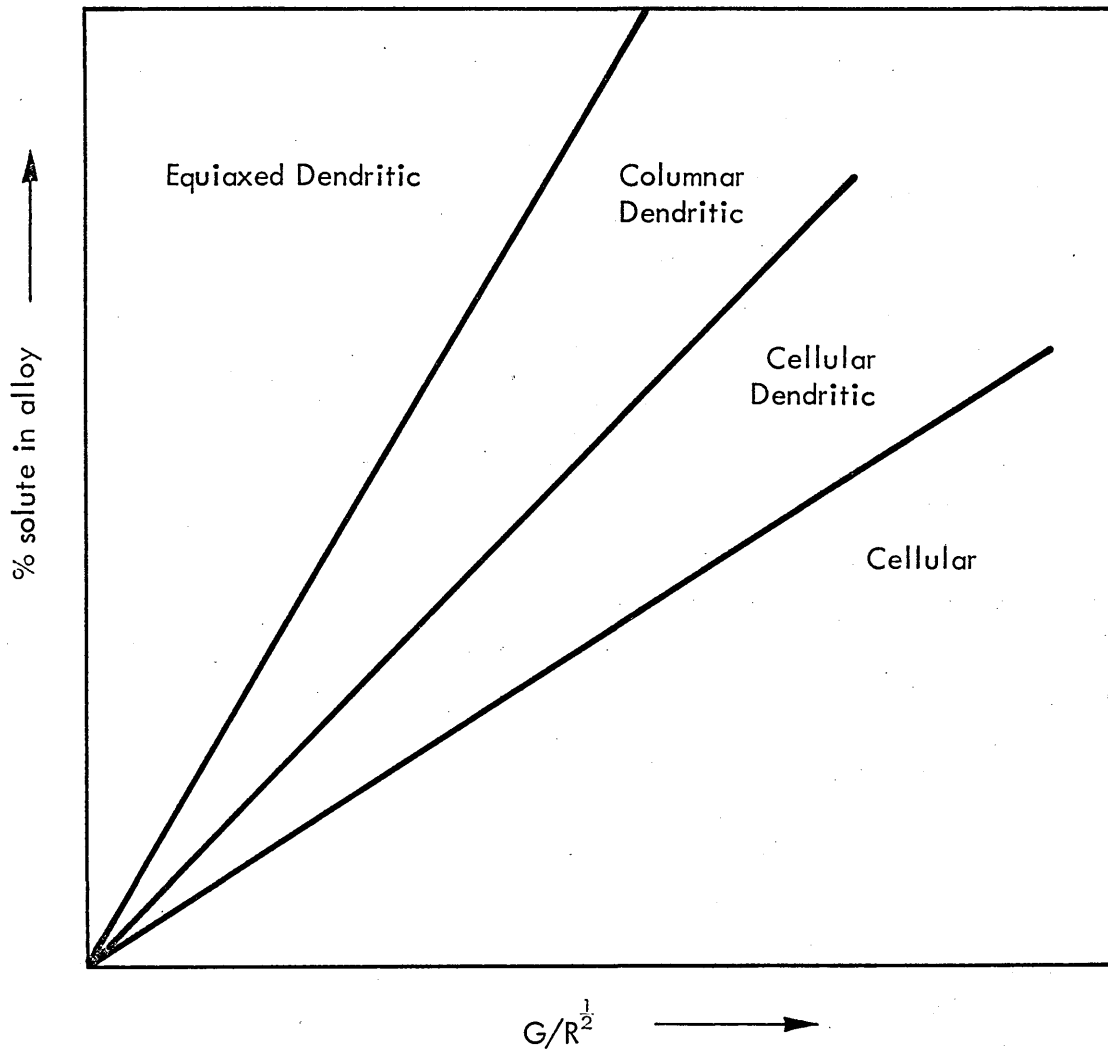
FIG. 7   SCHEMATIC REPRESENTATION OF THE INFLUENCE OF THE TEMPERATURE GRADIENT IN THE LIQUID, "G" AND THE RATE OF GROWTH "R"
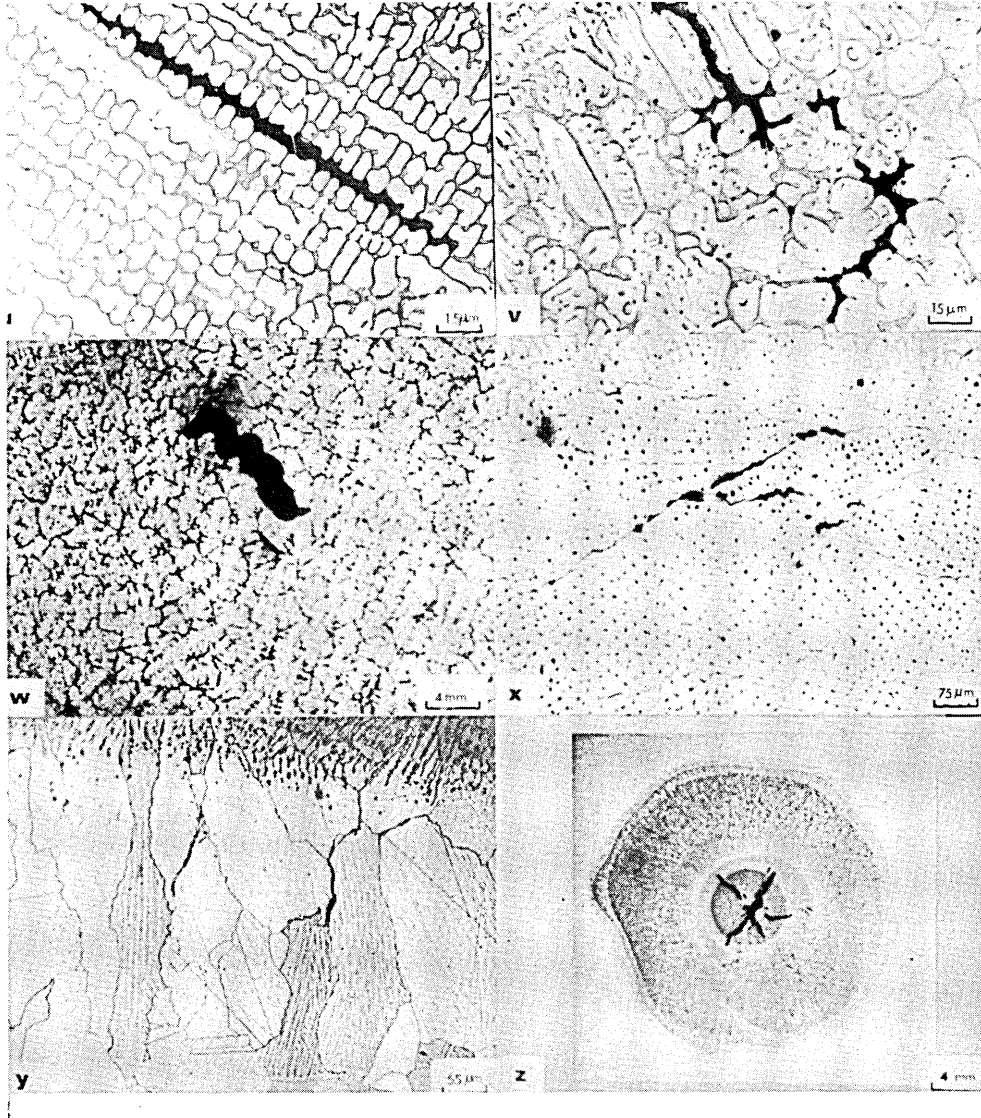
FIG. 8 VARIOUS FORMS OF WELD METAL SOLIDIFICATION CRACKING (TYPE 1A)

(u) Intercellular weld metal solidification cracking in 18Cr 10Ni steel plus 0.5% P. Cracking is seen to propate along the second phase "Ledeburite $Fe_3P$)

(v) Solidification cracking in the cellular – dendritic region of the weld metal in 18Cr 10Ni plus 0.5% P.

(w) Interdendritic weld metal solidification cracking in $2\frac{1}{4}$Ni Cr Mo V electroslag weld metal

(x) Solidification cracking along the blocks of cells in Incoloy 800 weld metal

(y) Solidification cracking in the epitaxial growth region in 18Cr 10Ni weld metal

(z) Solidification cracking in 25Cr 20Ni weld metal having the morphology of a crater. This is known as crater cracking.
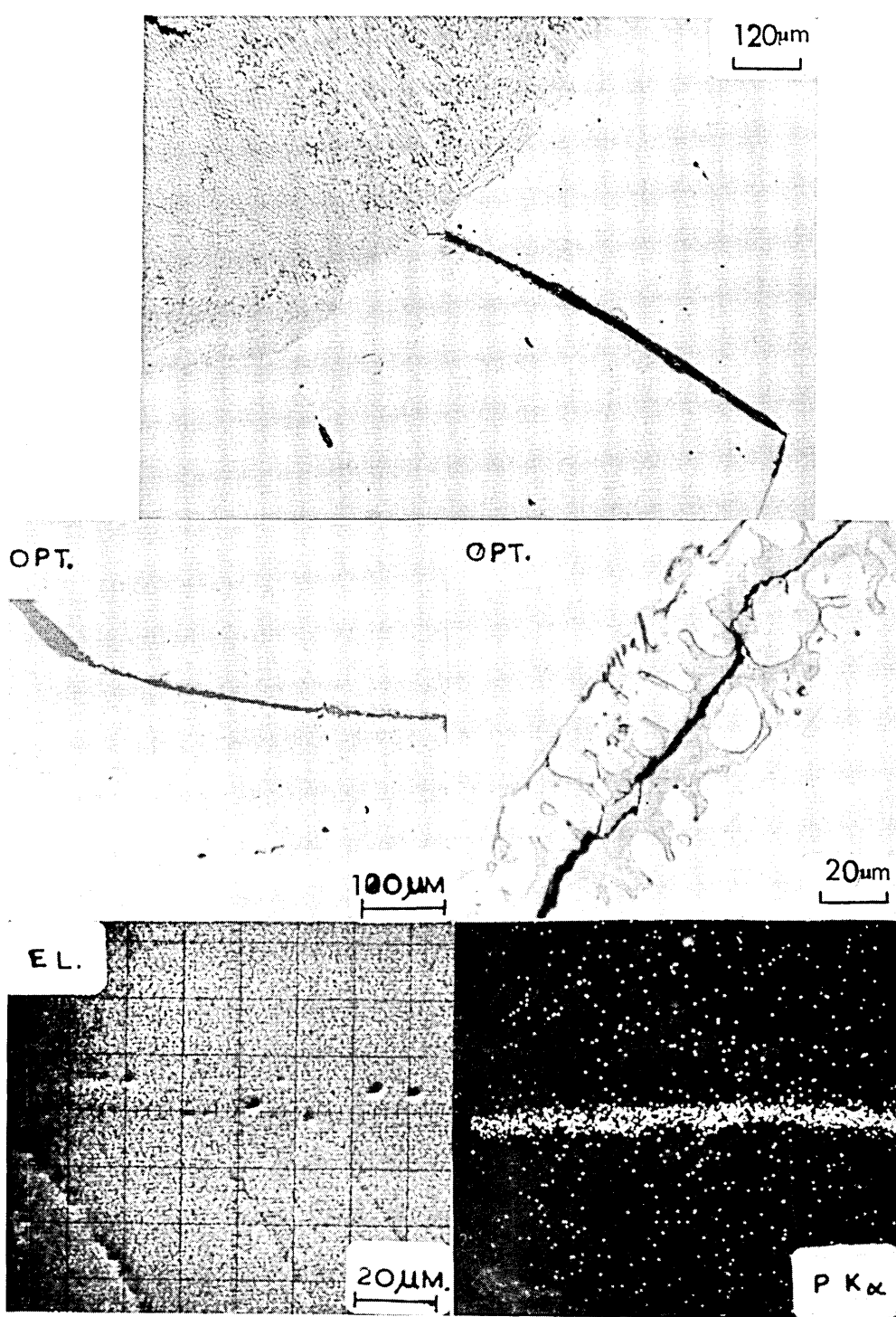
FIG. 9   THE ADDITION OF LEDEBURITE(Fe$_3$P) TO A MELT RUN IN AN 18Cr 10Ni
STEEL LED TO GRAIN BOUNDARY PENETRATION OF THE LIQUID PHOSPHIDE
AND THE RESULTANT HAZ EMBRITTLEMENT

RD/M/R 118
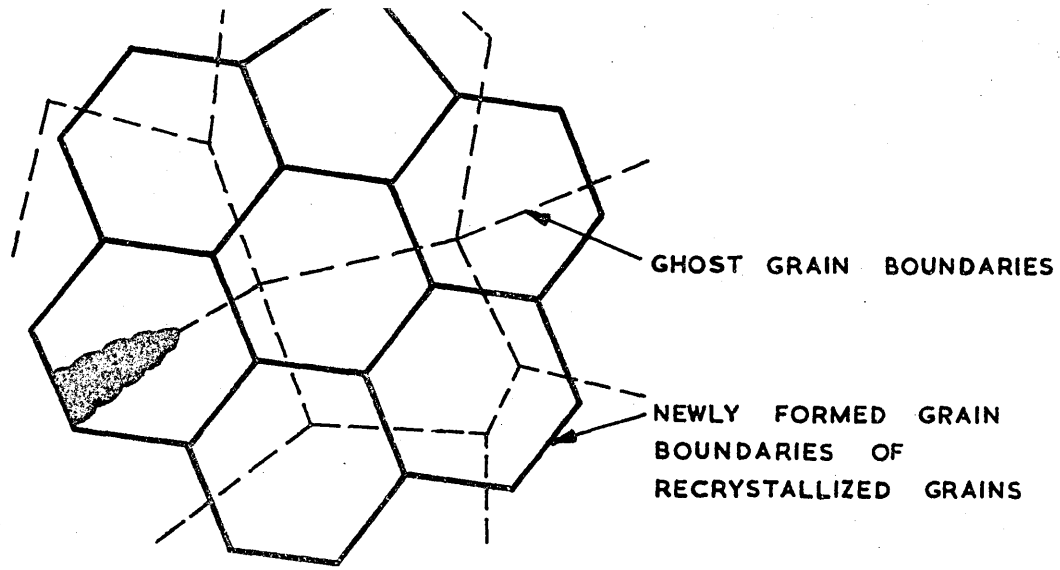
(a) SEEMINGLY TRANSCRYSTALLINE CRACK STRANDED WITHIN A RECRYSTALLIZED GRAIN. OBSERVED IN THE HAZ
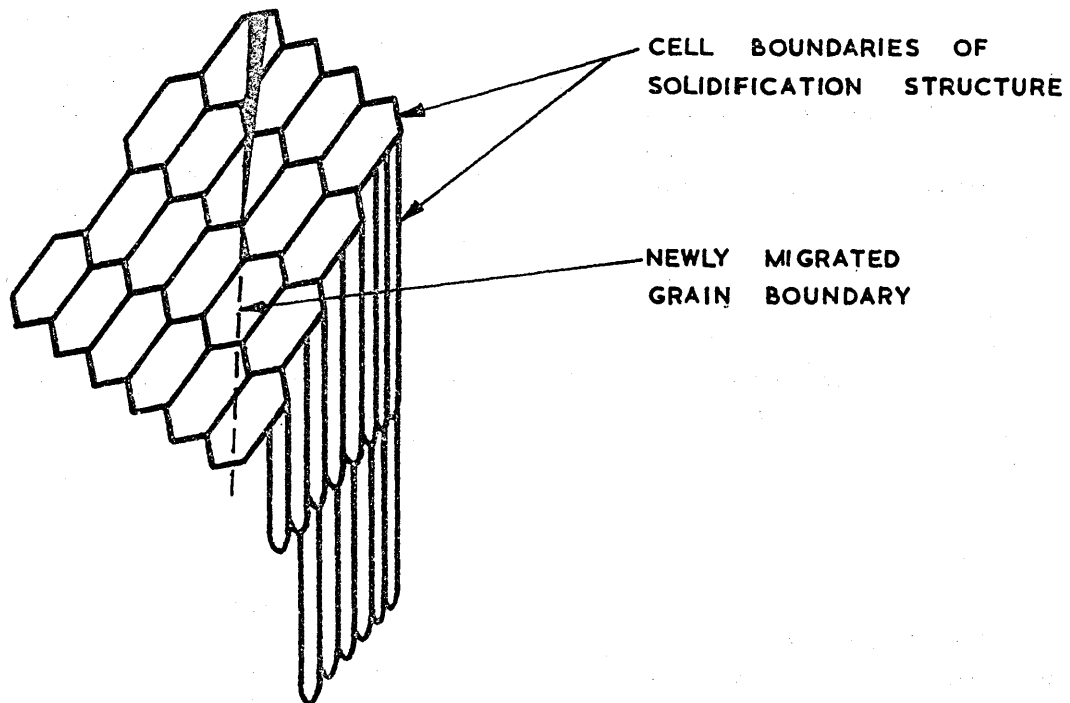


(b) SEEMINGLY TRANSGRANULAR TRANS-CELLULAR CRACK. OBSERVED IN THE WELD METAL

FIG. 10 EXAMPLES OF APPARENTLY TRANSGRANULAR HIGH TEMPERATURE CRACKING
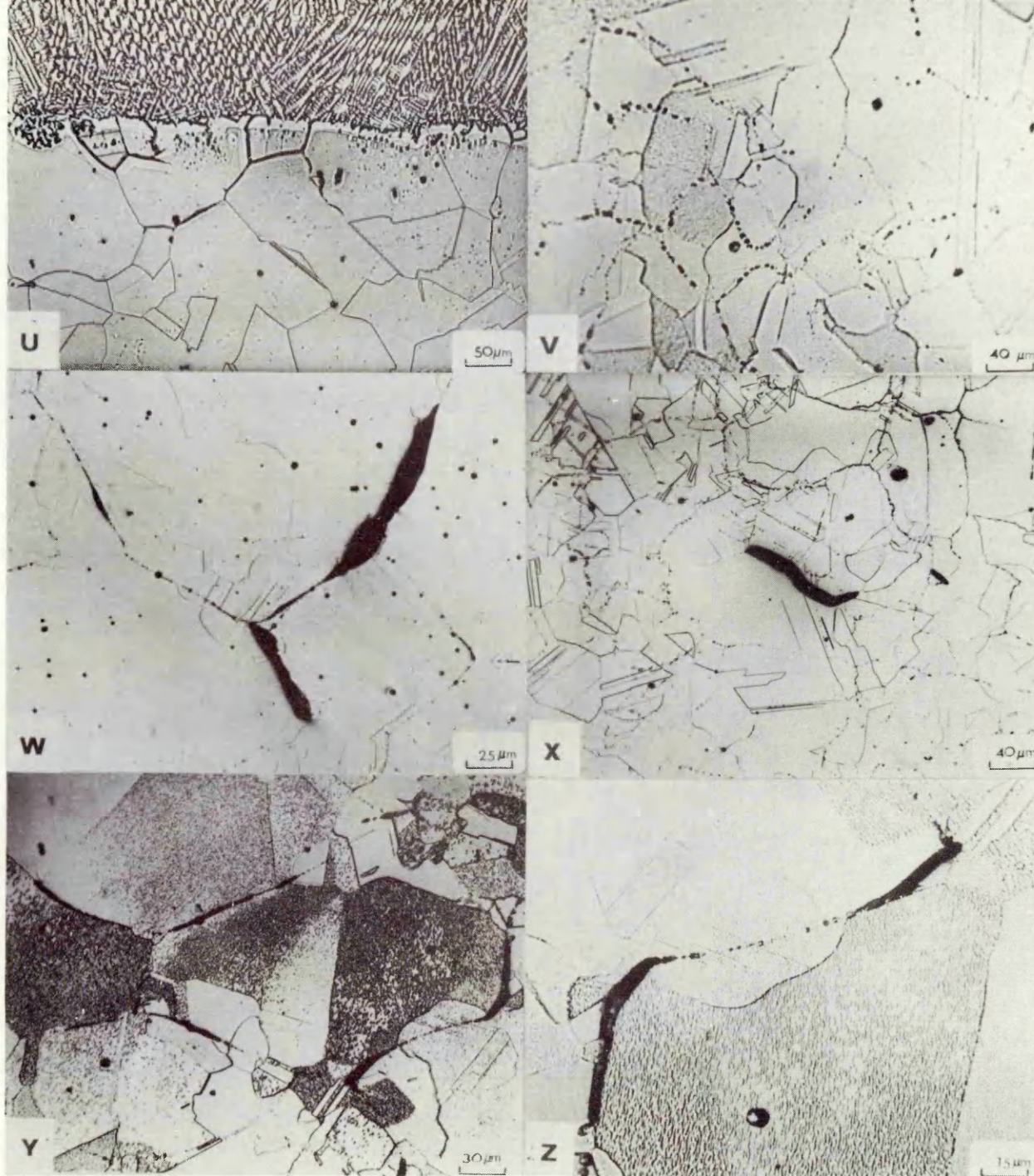
FIGURE 11. EFFECT OF GHOST BOUNDARIES IN AISI 304 ( AN 18 Cr 10Ni STEEL)

(u) Shows grain boundary migration in the fusion boundary and notice the grains have recrystallized stranding the $M_{23}$(BC) as ghost boundaries.

(v) Detail of ghost boundaries

(w) HAZ liquation cracking along ghost boundaries ( Type 1B )

(x) HAZ ductility dip cracking along recrystallized grain boundaries ( Type 2A )

(y) HAZ ductility dip cracking (2A) associated with cavitation along the ghost boundaries,

(z) Detail of Figure y showing cavitation along ghost boundaries.
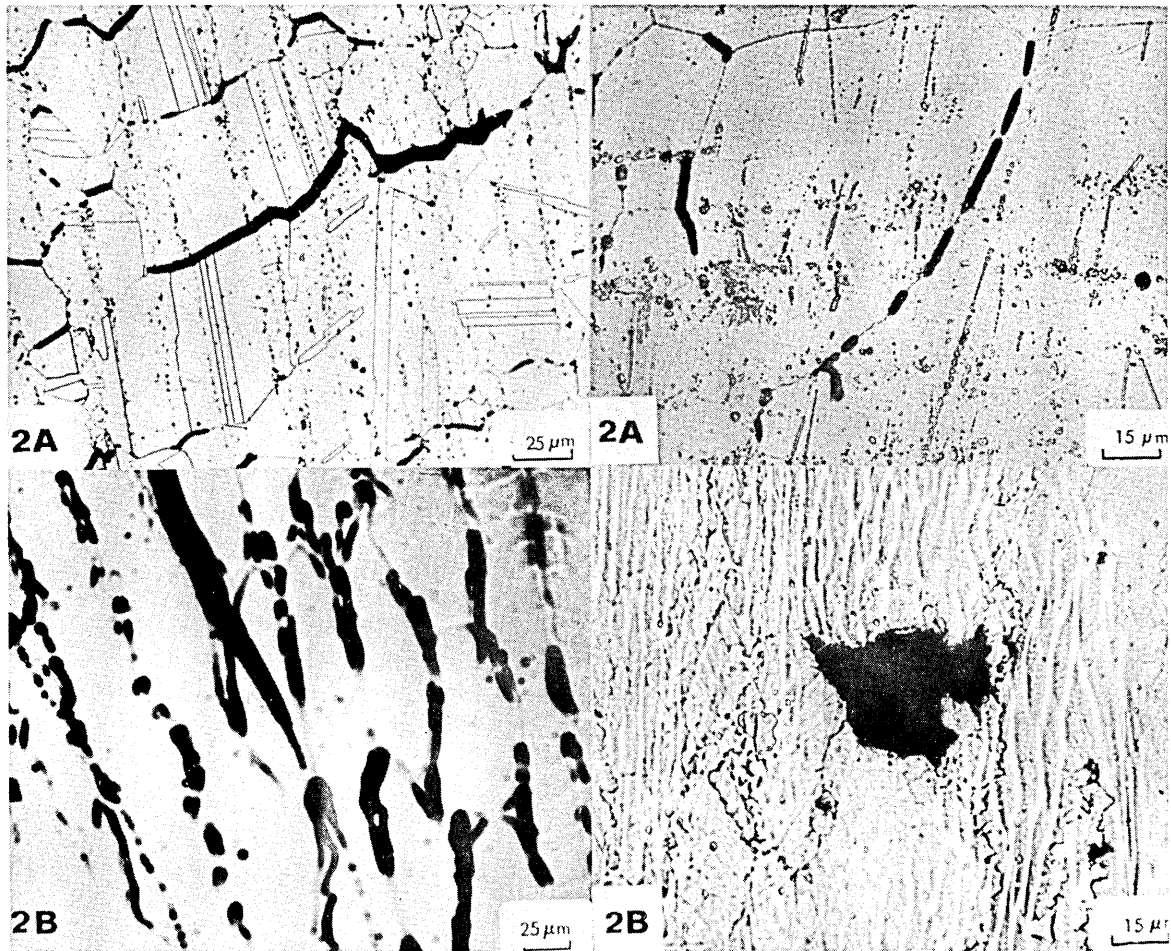
FIGURE 12. TYPE 2: DUCTILITY-DIP CRACKING

Type 2A HAZ wedge shaped cracking with tension axis in direction of mechanical fibre in 25 Cr 20 Ni steel (top left)
Type 2A Cavitation in the HAZ of 25 Cr 20 Ni steel (top right)
Type 2B Trans-cellular weld metal cracking in 25 Cr 20 Ni steel (King B.L.;B.W.R.A. Report C139/A2/65 (bottom left)
Type 2B Cavitation in an 18 Cr 10 Ni weld metal. Note the formation of recrystallized boundaries (bottom right)

RD/M/R118

FIGURE 13. HIGH TEMPERATURE CRACK STRADDLING
FUSION BOUNDARY          x 280
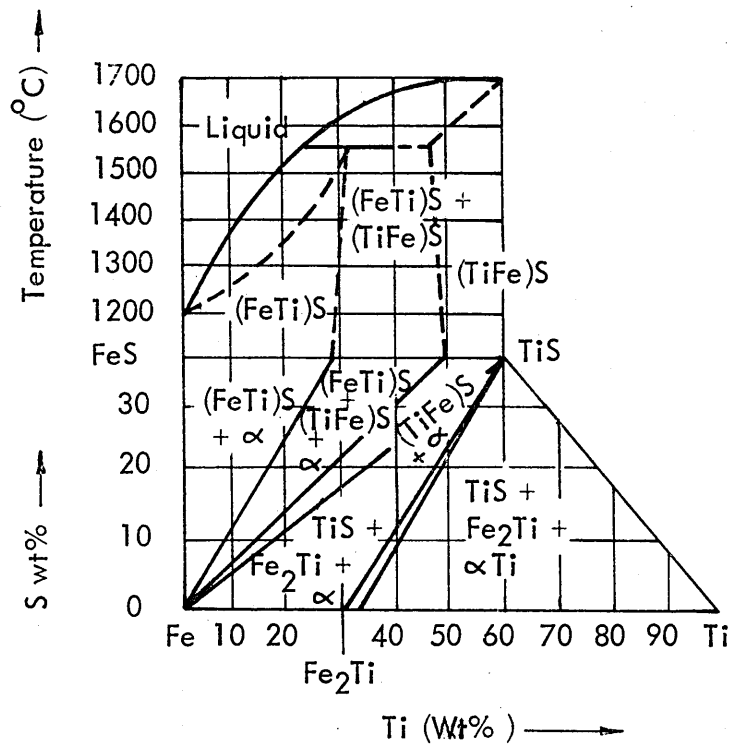
**FIG. 14.   Fe – Ti – S SYSTEM PHASE DIAGRAM (VOGEL & KASTEN )(64)**
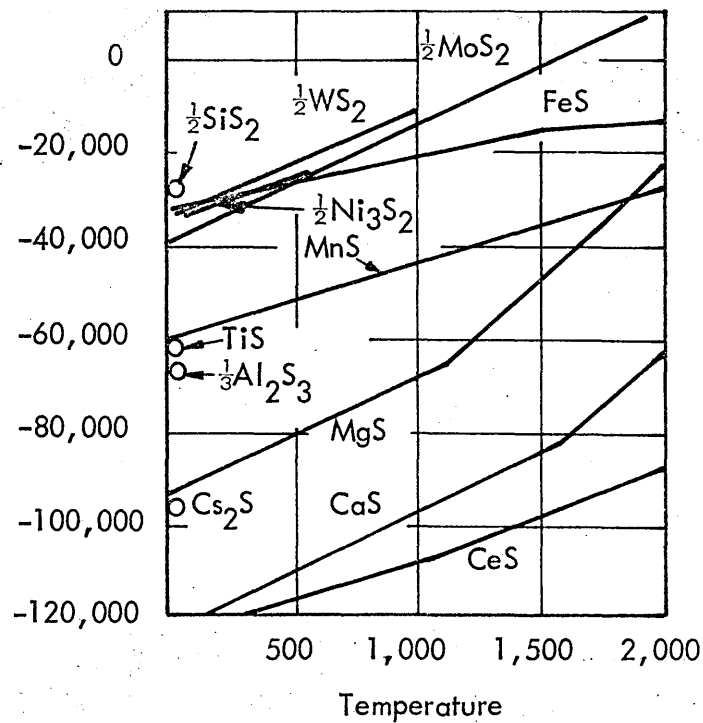
FIG. 15.  FREE ENERGY OF FORMATION OF BINARY SULPHIDES

( ELLIOTT et al ) (65)

| Cast No | C | Mn | Si | S | Ni | Cr | Mo | V | Al | Ti | B | N |
|---------|-----|------|------|-------|------|------|------|------|------|------|--------|-------|
| A286 | 0.07 | 1.94 | 0.86 | 0.016 | 25.6 | 15.1 | 1.40 | 0.28 | 0.58 | 1.91 | 0.0045 | 0.016 |
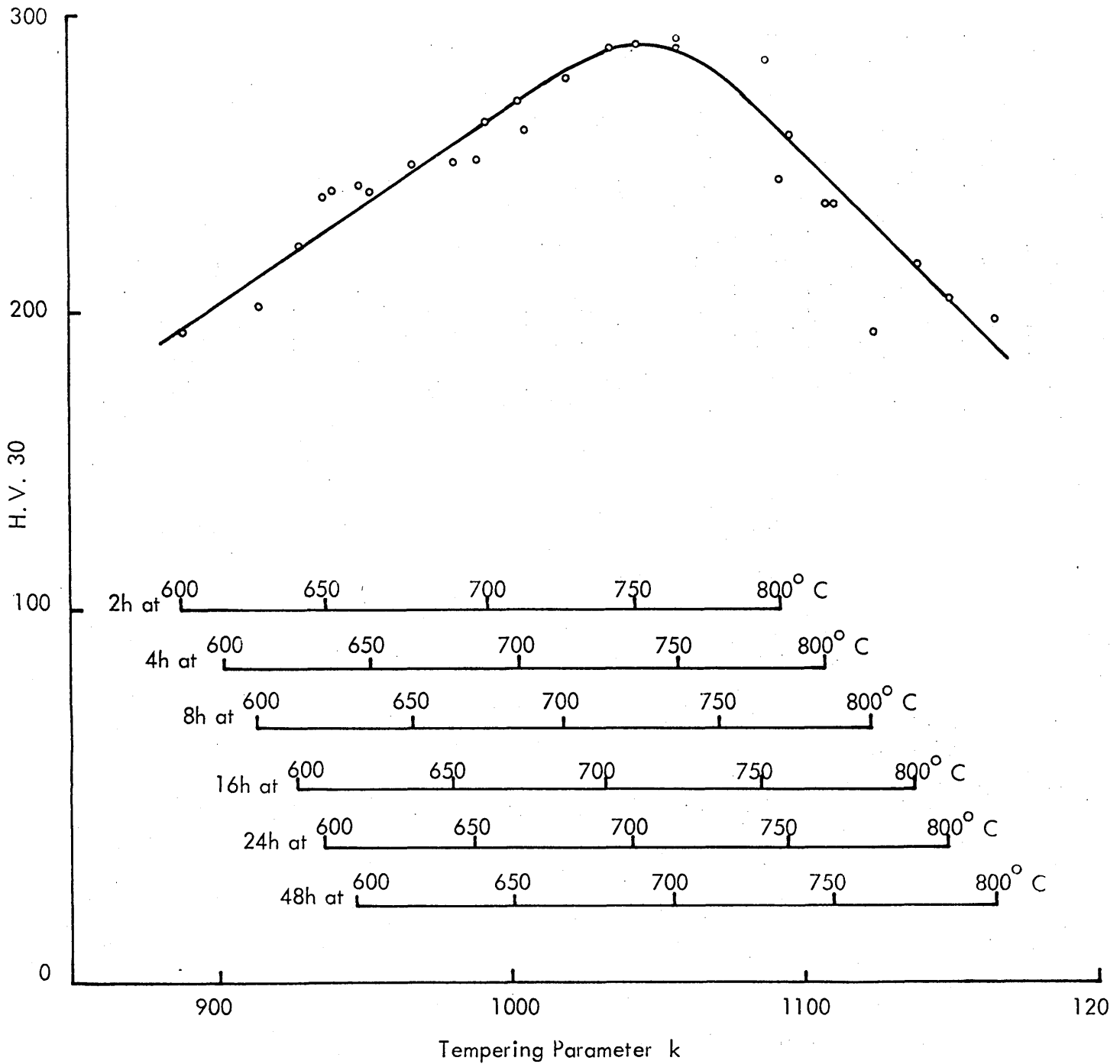


FIG. 16. AGEING CHARACTERISTICS OF A286 AFTER SOLUTION

TREATING AT 980° C ( E.S.C. DATA )

RD/M/R118
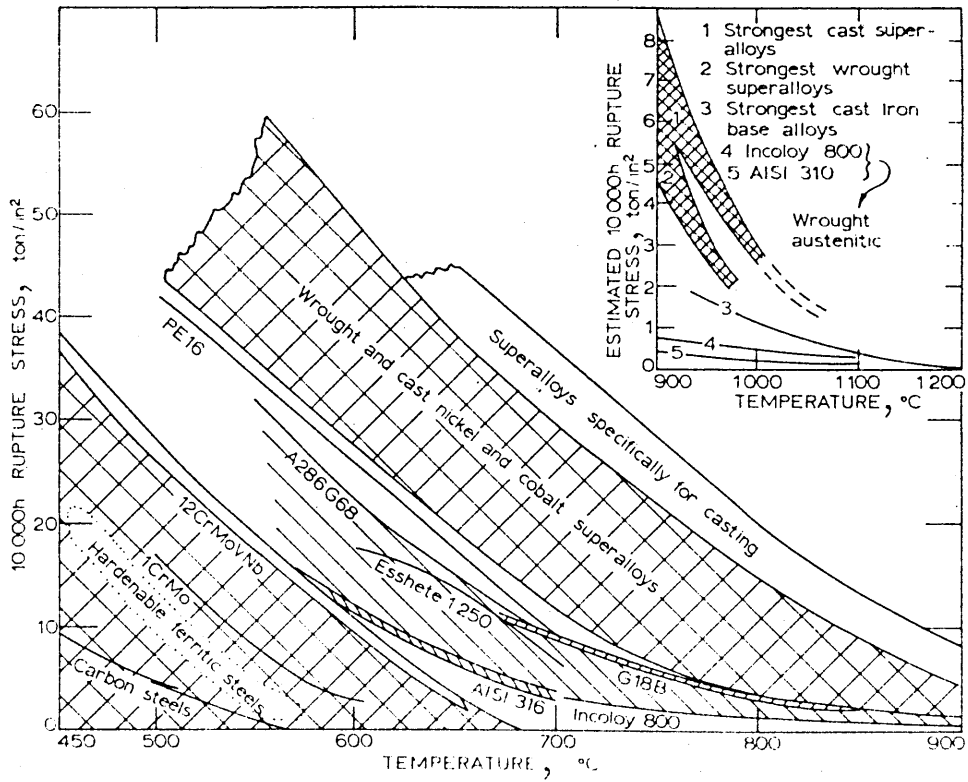
FIGURE 17. COMPARISON OF THE 10,000 HOURS RUPTURE STRENGTH OF
A286 WITH OTHER COMMERCIAL ALLOYS. ( MARSH 55 )
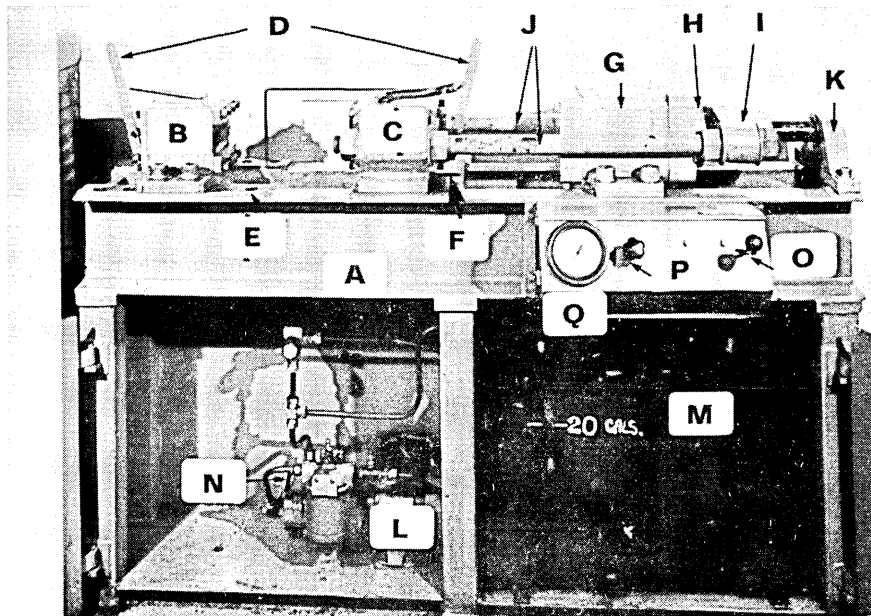
MAIN STRUCTURE

(A) Simple fabricated structure.

WEDGE BOXES

(B) Stationary wedge box.
(C) Moving wedge box.
(D) Lever for opening wedge boxes.
(E) Adjustment of stationary wedge box.
(F) Slot for the tee-piece.

CYLINDER.

(G) Cylinder
(H) Piston Rod Unit
(I) Crosshead
(J) Tie Rods
(K) Support for Piston rod end.

HYDRAULIC SYSTEM.

(L) Pre-coupled pump/motor unit.
(M) Hydraulic Reservoir Tank.
(N) Lever for adjusting crosshead speed.
(O) Directional Valve.
(P) Pressure relief valve.
(Q) Pressure gauge.

## FIGURE 18. DETAILED ILLUSTRATION OF THE HORIZONTALLY OPPOSED TENSILE MACHINE
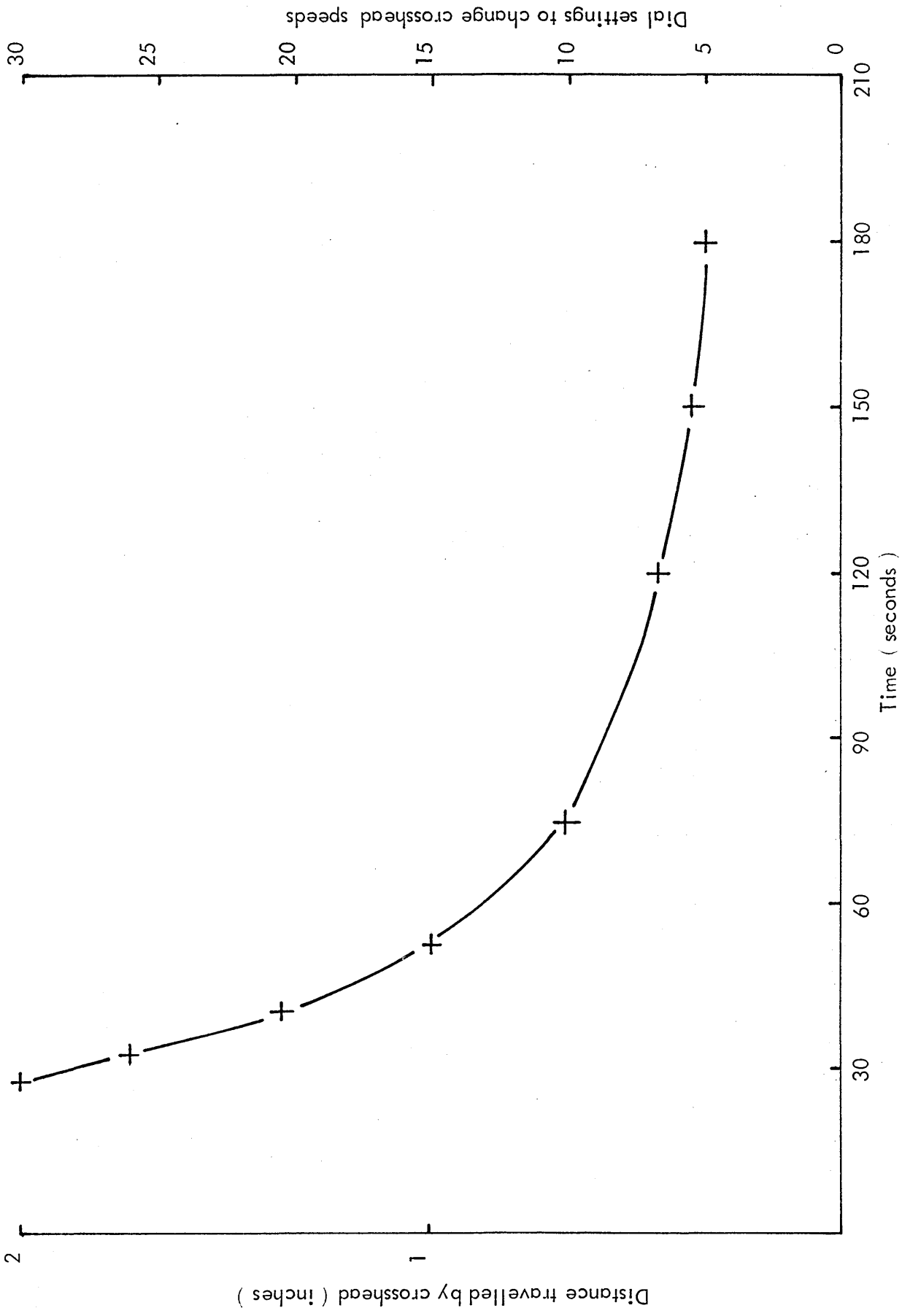
FIG. 19.  CALIBRATION OF RANGE OF TRAVEL SPEEDS OF THE HORIZONTALLY OPPOSED TENSILE MACHINE

RD/M/R 118
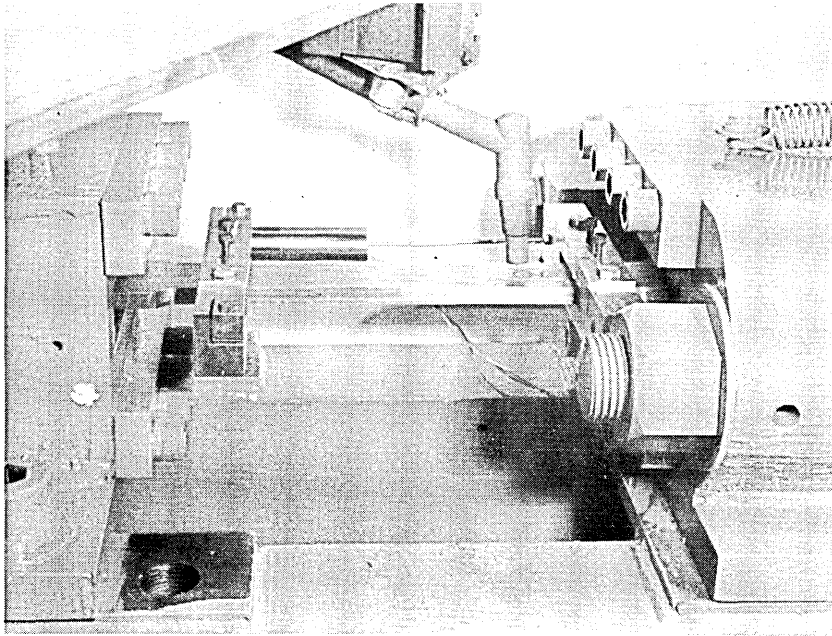
FIGURE 20. CLOSE UP OF T.I.G. WELDING TORCH IN
POSITION TO CARRY OUT A MELT RUN
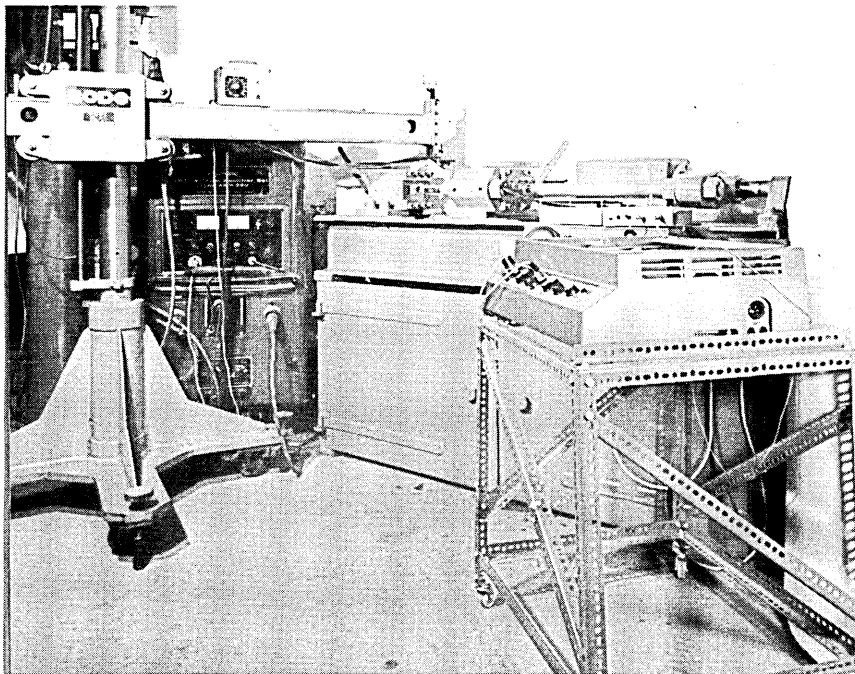


FIGURE 21. SHOWS OVERALL SET UP OF TENSILE
MACHINE AND X-Y RECORDER
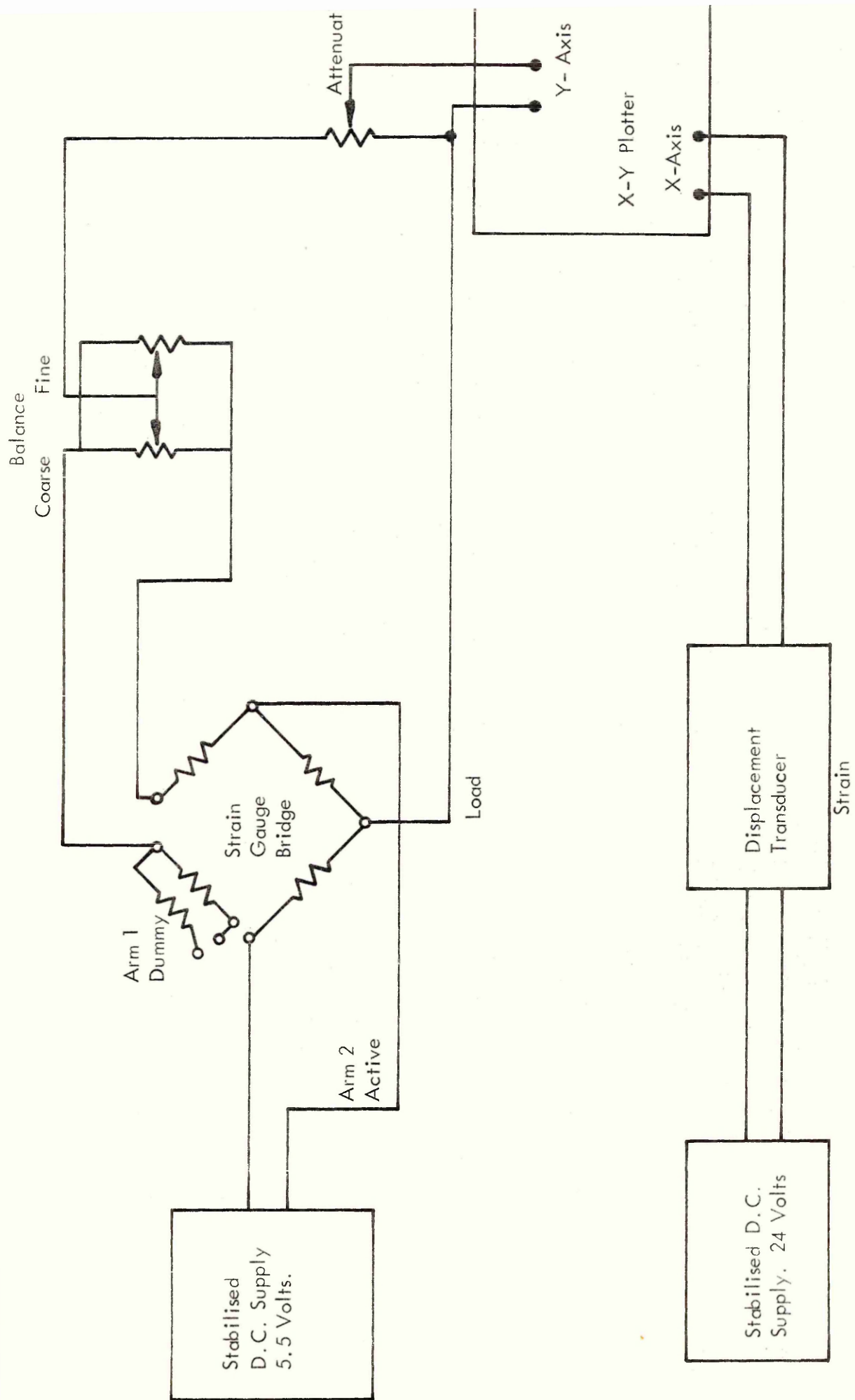
FIG. 22. ELECTRICAL CIRCUIT FOR MEASUREMENT OF APPLIED STRESS AND EXTENSION

RD/M/R118
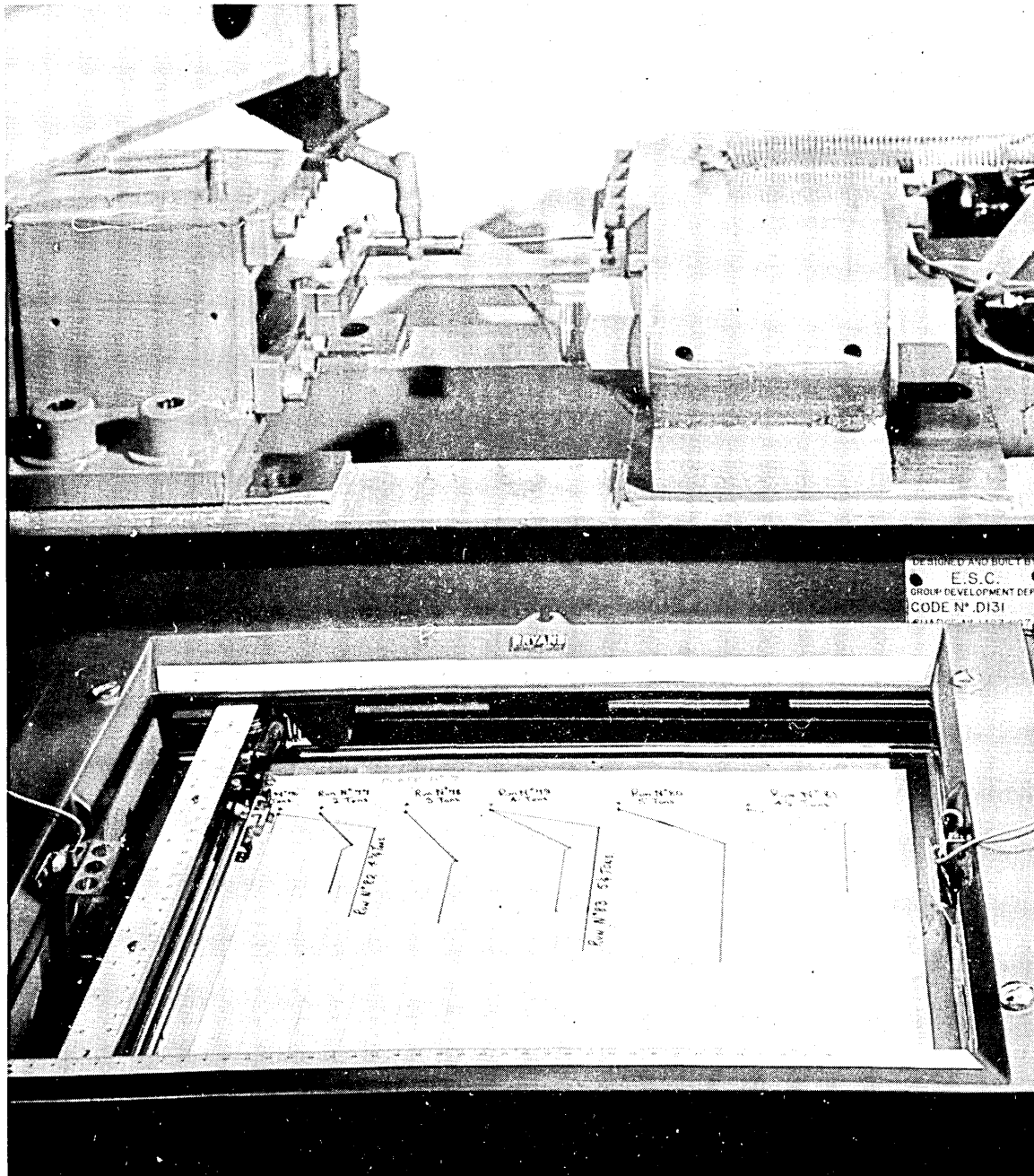
FIG. 23. SHOWS THE READ OUT OF APPLIED STRESS AGAINST OVERALL
EXTENSION FOR A MELT RUN
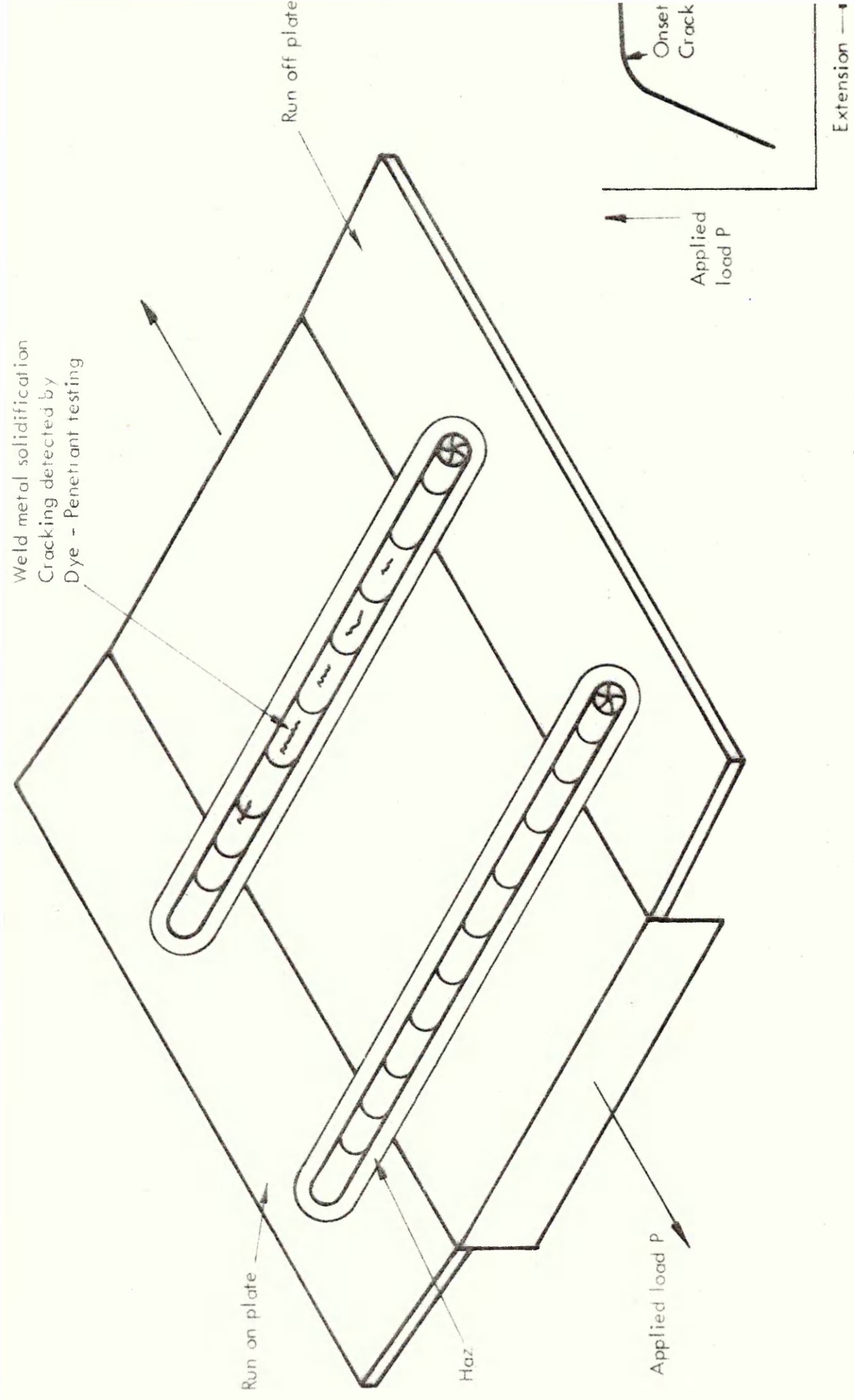
Weld metal solidification
Cracking detected by
Dye – Penetrant testing

Run off plate

Onset
Crack

Extension

Applied
load P

Run on plate

Haz

Applied load P

FIGURE 24. SCHEMATIC REPRESENTATION OF THE SET UP FOR

EVALUATING MANUAL ARC ELECTRODES

RD/M/R118
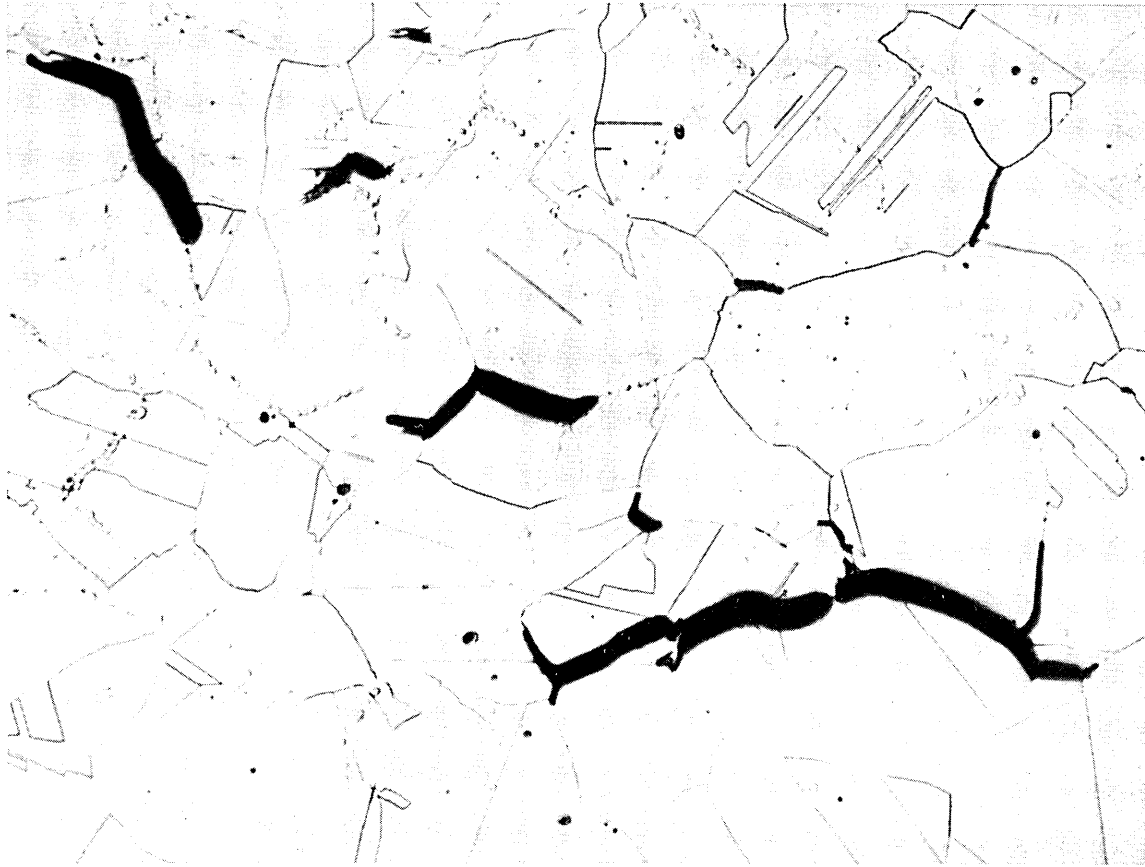
FIG. 25. HAZ DUCTILITY DIP CRACKING IN AISI 304 STEEL
ETCHED IN 10% HCL IN METHANOL, ELECTROLYTIC 5V x 270
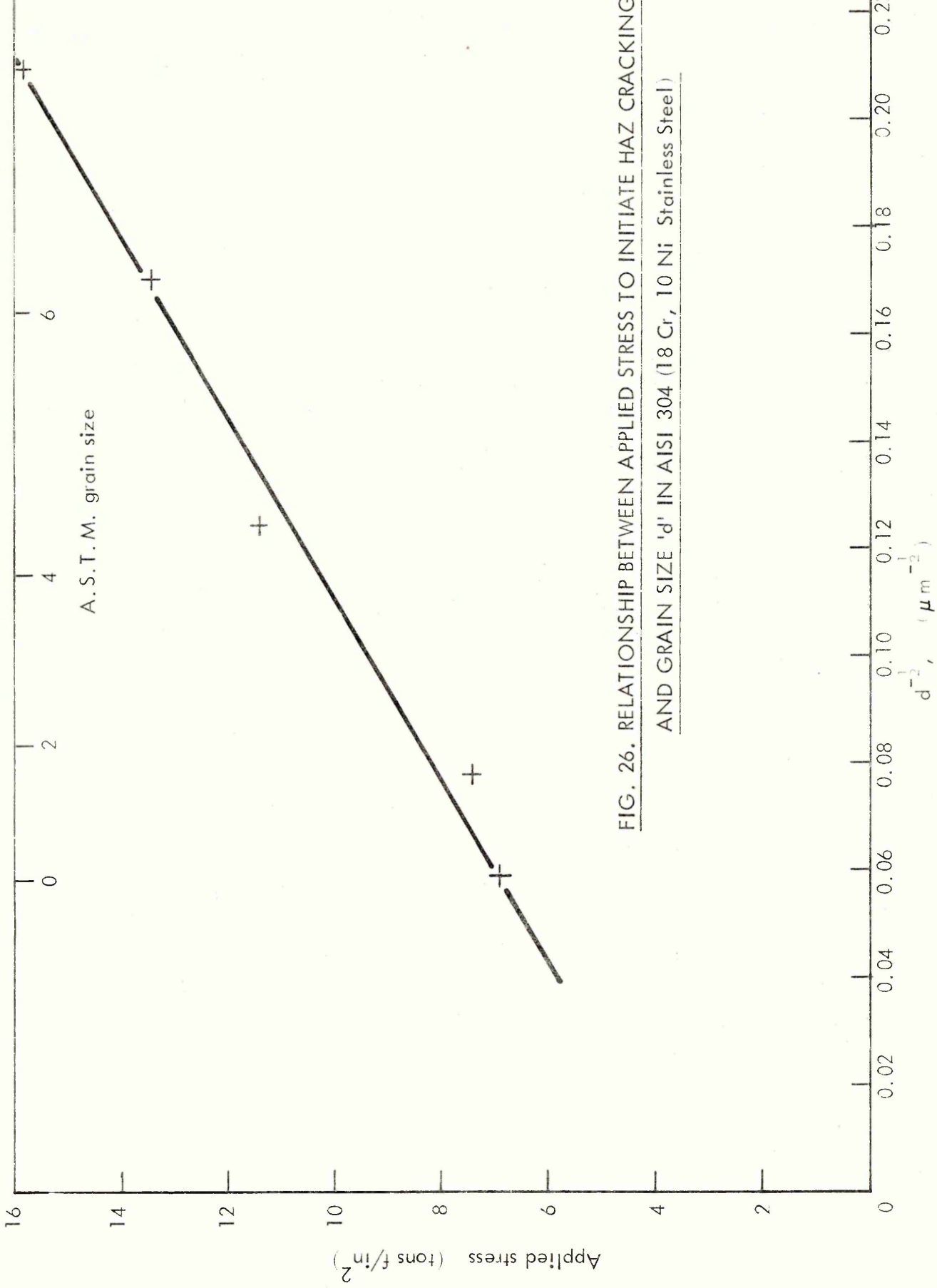
FIG. 26. RELATIONSHIP BETWEEN APPLIED STRESS TO INITIATE HAZ CRACKING
AND GRAIN SIZE 'd' IN AISI 304 (18 Cr, 10 Ni Stainless Steel)
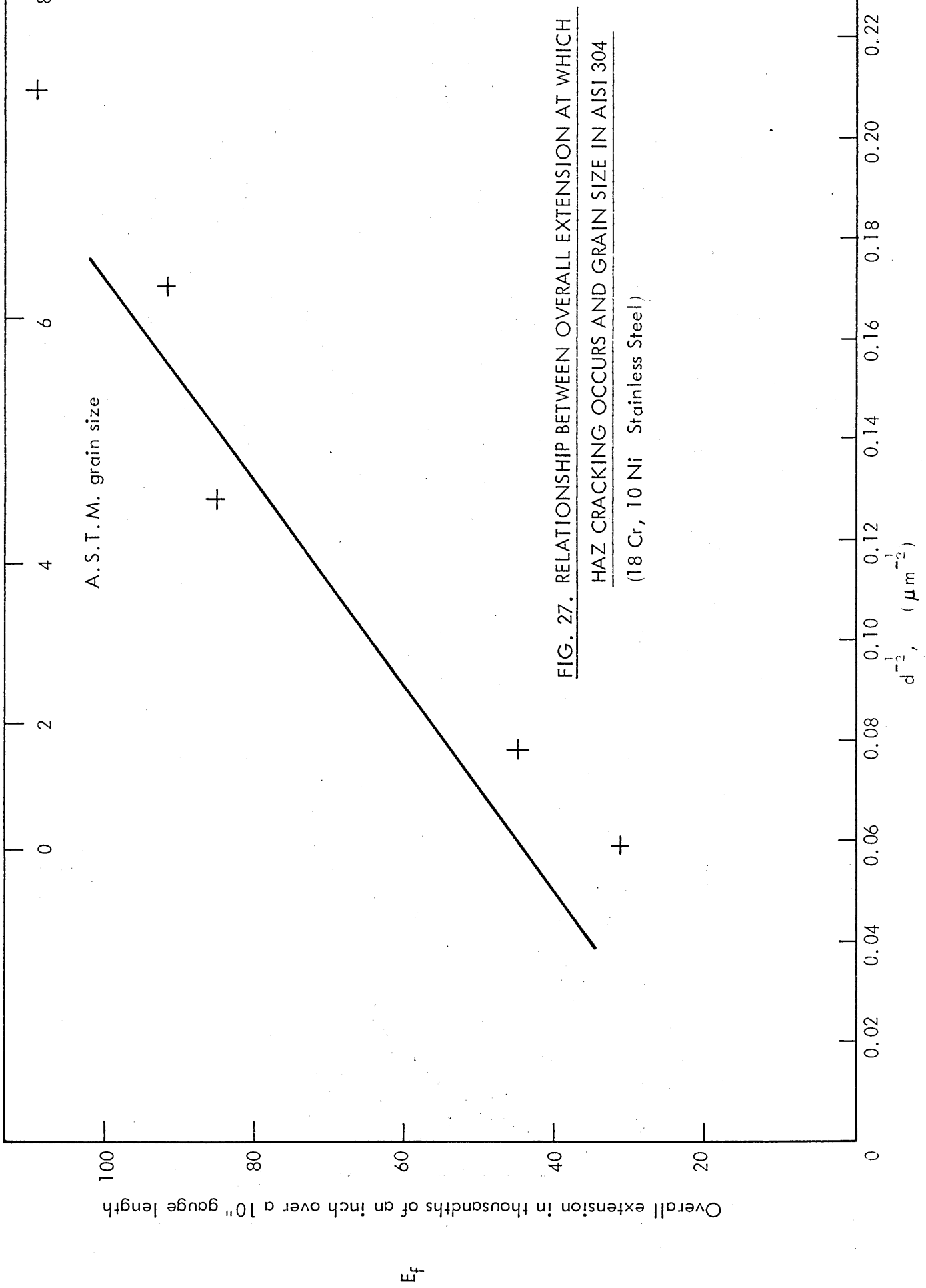
FIG. 27. RELATIONSHIP BETWEEN OVERALL EXTENSION AT WHICH
HAZ CRACKING OCCURS AND GRAIN SIZE IN AISI 304

(18 Cr, 10 Ni Stainless Steel)

A.S.T.M. grain size

Overall extension in thousandths of an inch over a 10" gauge length

$E_f$

$d^{-\frac{1}{2}}$, ( $\mu$ m $^{-\frac{1}{2}}$ )

FIG. 28. GRAPH OF VICKERS HARDNESS PLOTTED AGAINST AGEING TIME FOR A286

Time ( hours )

HV₃₀

△  600°C    +  750°C
⊙  650°C    ●  800°C
X  700°C

RD/M/R118
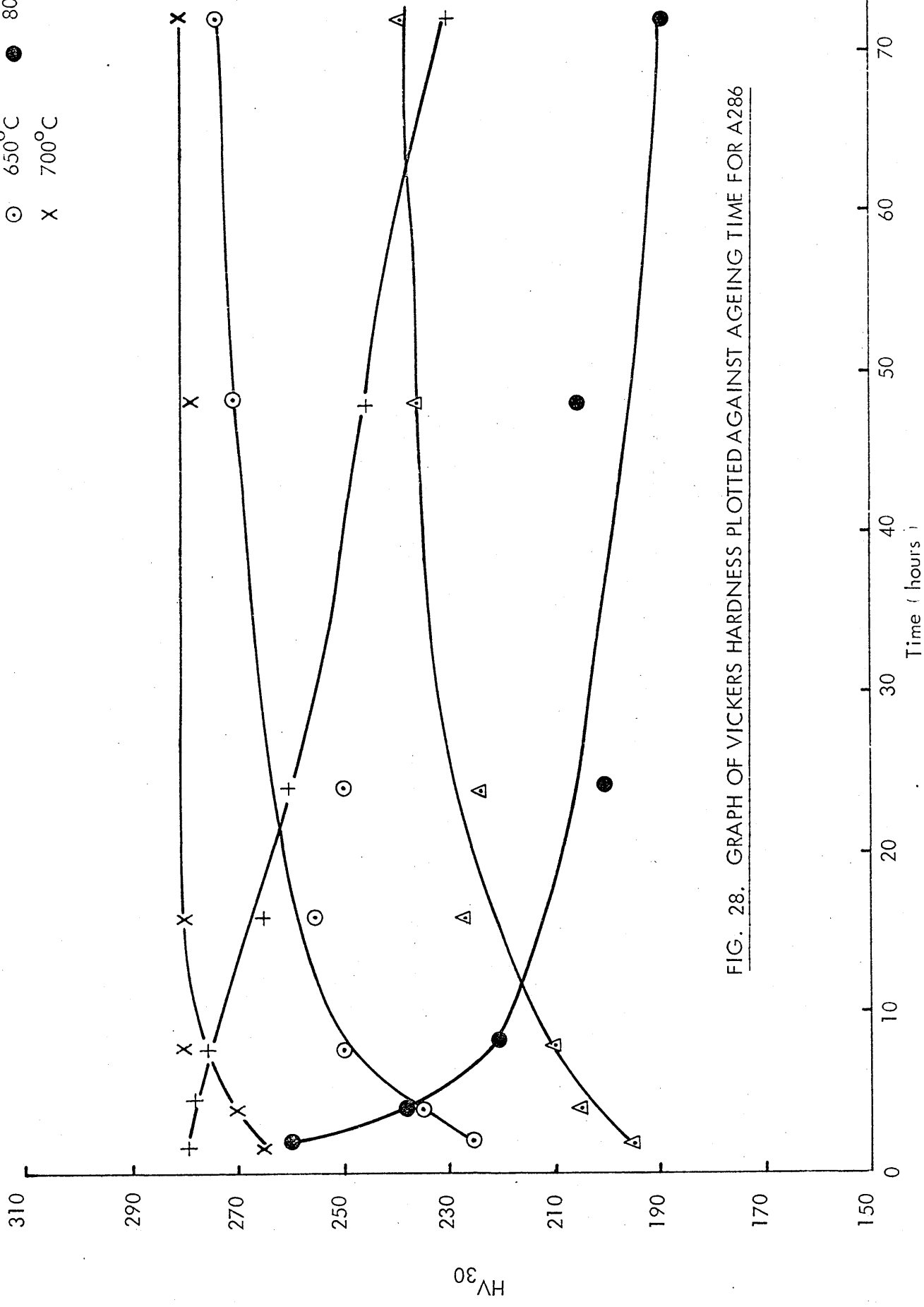
FIG. 29. BEAD ON PLATE TEST FOR A286 USING W.R.K.S.10 EXPERIMENTAL MANUAL ARC ELECTRODE

Extensive Haz cracking

Slight Haz cracking

9"

1"

10"

Ten gauge weld deposit

Eight gauge weld deposit

Six gauge weld deposit

Ten gauge weld deposit
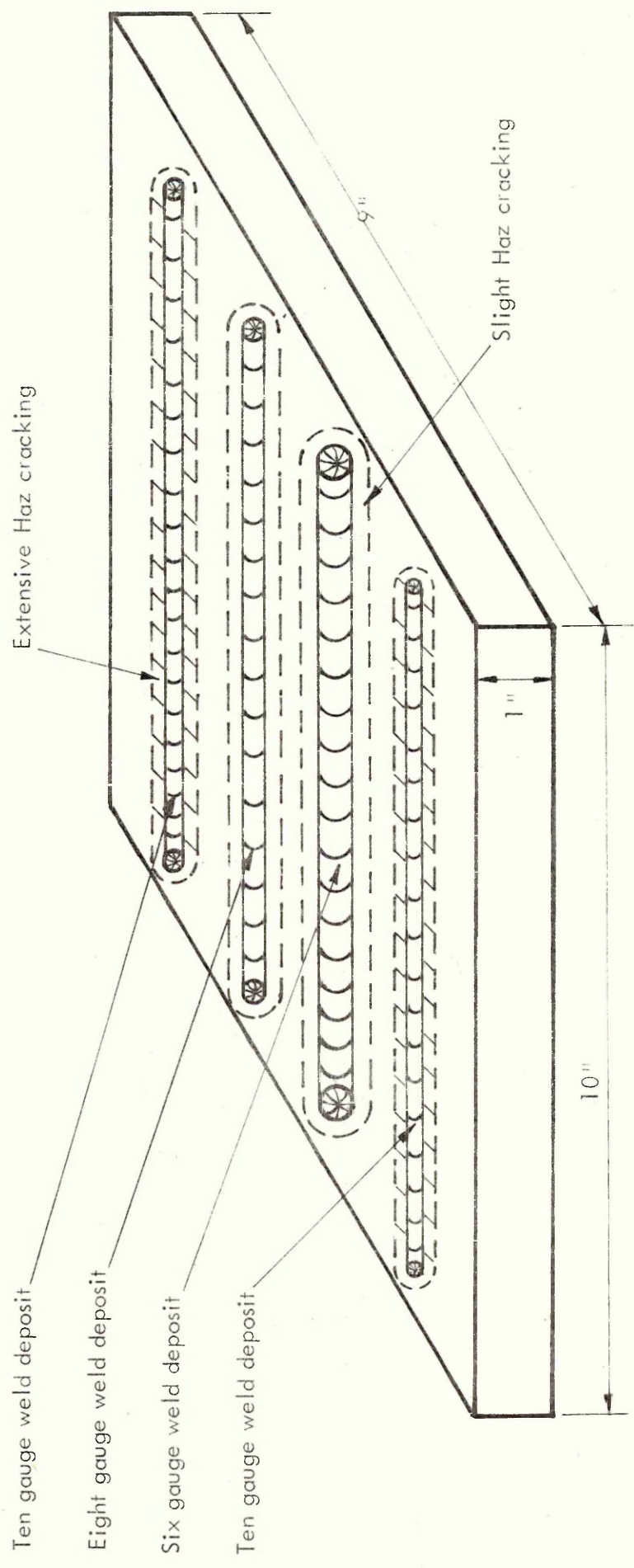
FIG. 30. SHOWS ROSETTE SHAPED CAVITIES ASSOCIATED WITH "CHINESE
SCRIPT" ORIENTATED LIQUATION PHASES IN THE HAZ   N560 x1000

x 750

N 558

FIG. 31   HAZ LIQUATION REGION ASSOCIATED WITH STRAIGHTER EDGED CRACKING

WHICH IS PRESUMABLY WETTED BY THE EXCESS LIQUID
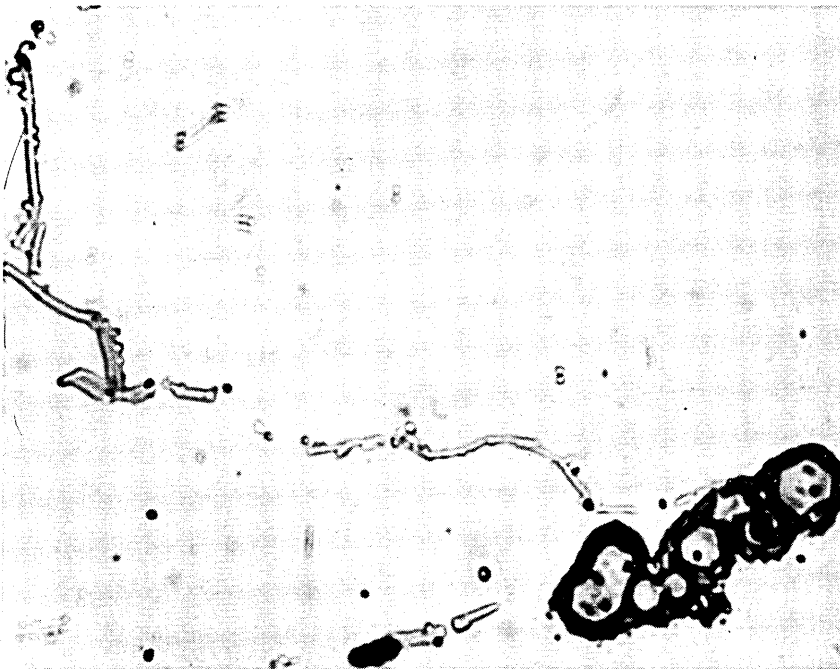


x 750

N 556

FIG. 32   NON-METALLIC FILMS IN THE HAZ OF A286
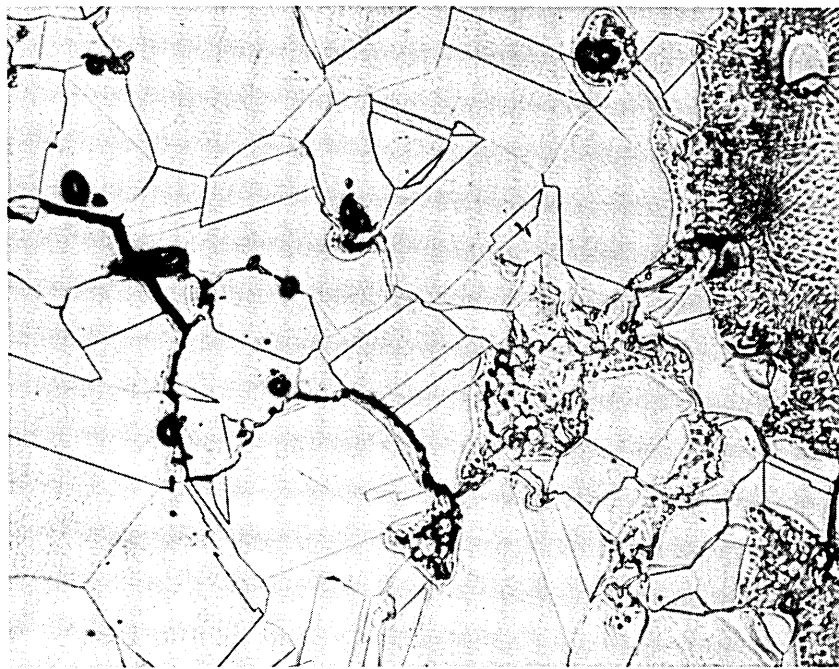
FIG. 33    SHOWS HAZ CRACKS PROPAGATING NORMAL TO THE FUSION

BOUNDARY.    ETCHED IN METHAREGIA
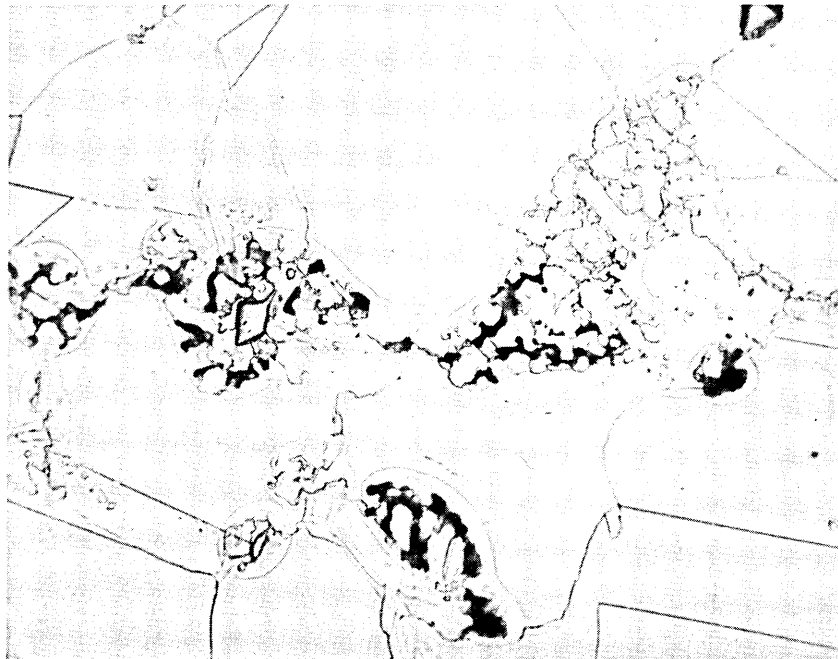
× 550

N 1354

FIG. 34   SHOWS DETAIL OF JAGGED SHAPED LIQUATION CRACKS IN THE HAZ.

NOTE THEIR ASSOCIATION WITH A TITANIUM CARBONITRIDE PARTICLE

ETCHED IN METHAREGIA
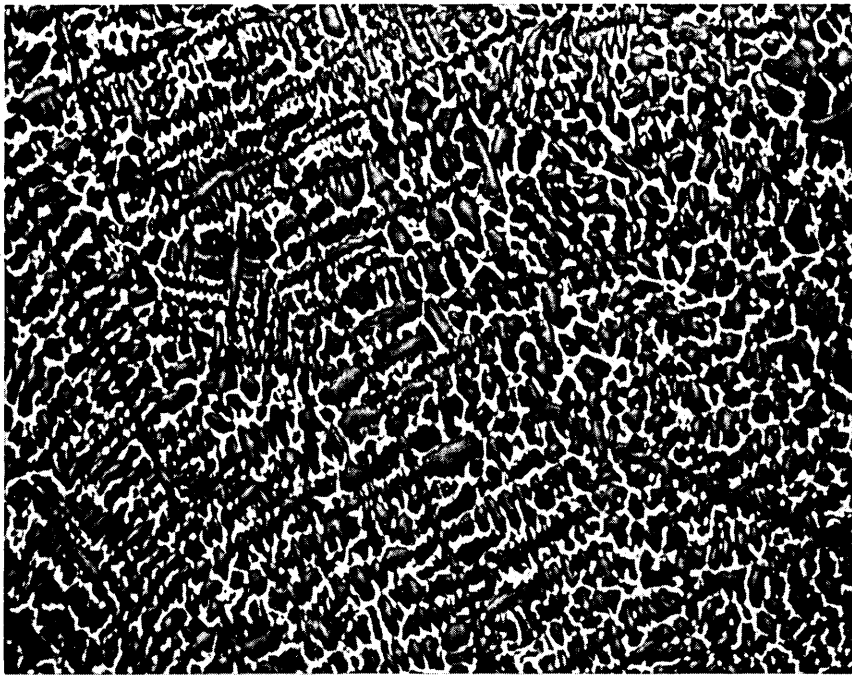
× 25

N 1597

FIG. 35    SHOWS THE HEAVILY MICROSEGREGATED PARENT METAL AFTER
SELECTIVELY ETCHING IN THE MIXED ACIDS REAGENT.
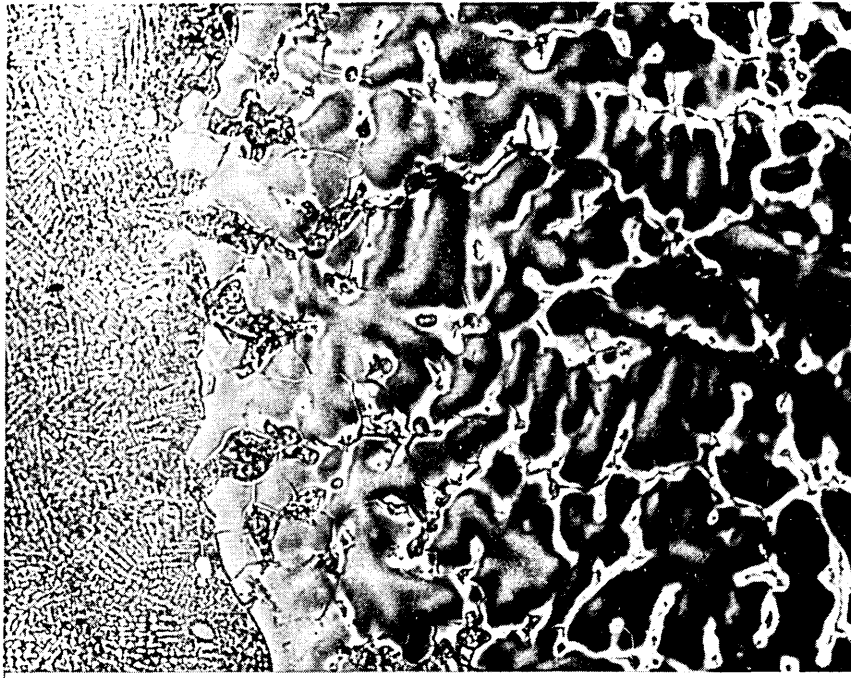


× 150

FIG. 36    SHOWS THE FUSION BOUNDARY AND HAZ AFTER SELECTIVELY ETCHING
IN THE MIXED ACIDS REAGENT    (COMPARE WITH FIG. 33)
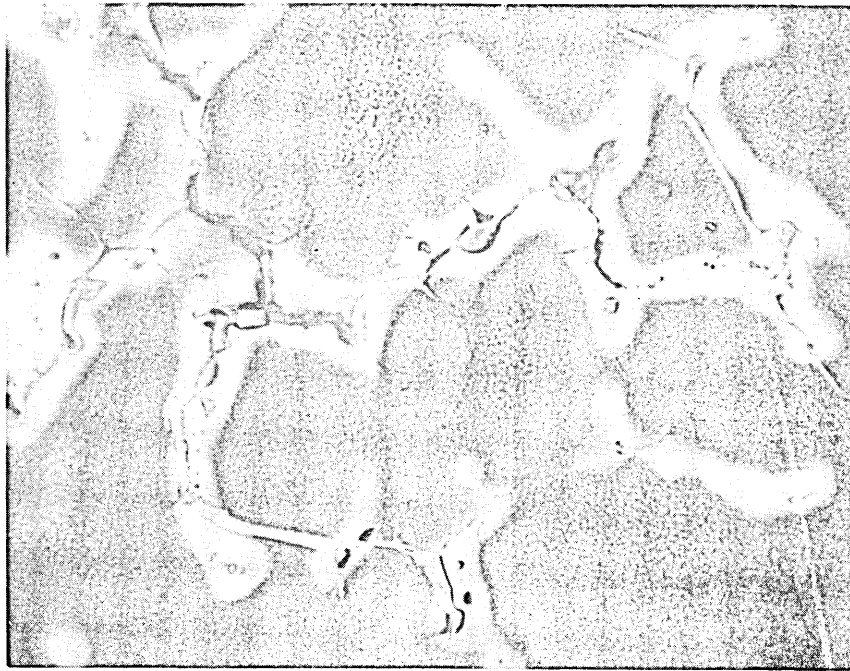
x 300

FIG. 37    DETAIL OF WHITE ETCHING REGIONS SHOWING THAT THEY ARE
A PREFERENTIAL PATH FOR CRACK PROPAGATION
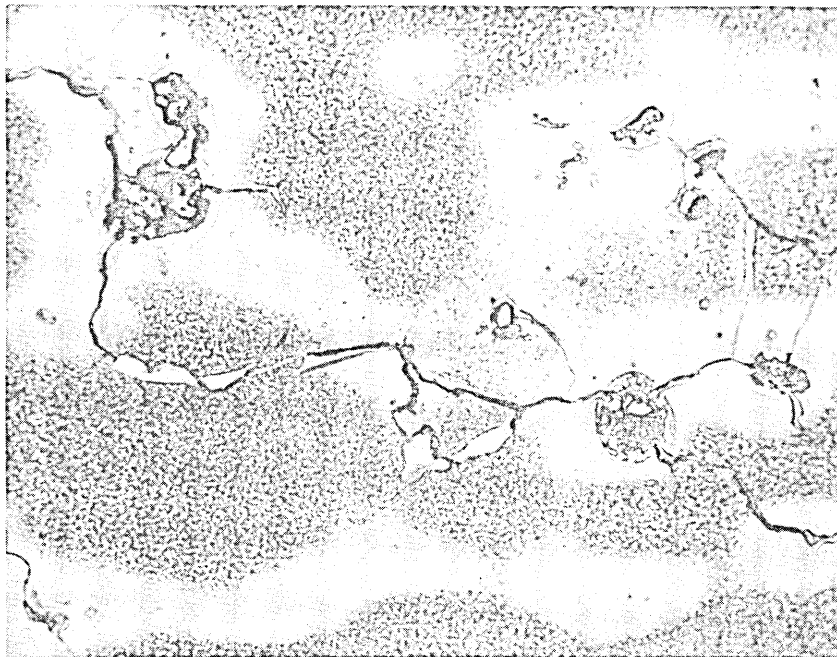


x 430

N 1596

FIG. 38    SHOWING ROSETTE SHAPED LIQUATION CRACKS IN THE WHITE
ETCHING REGIONS

OPT.    EL.

20µM    20µM

Ti Kα.    S Kα.
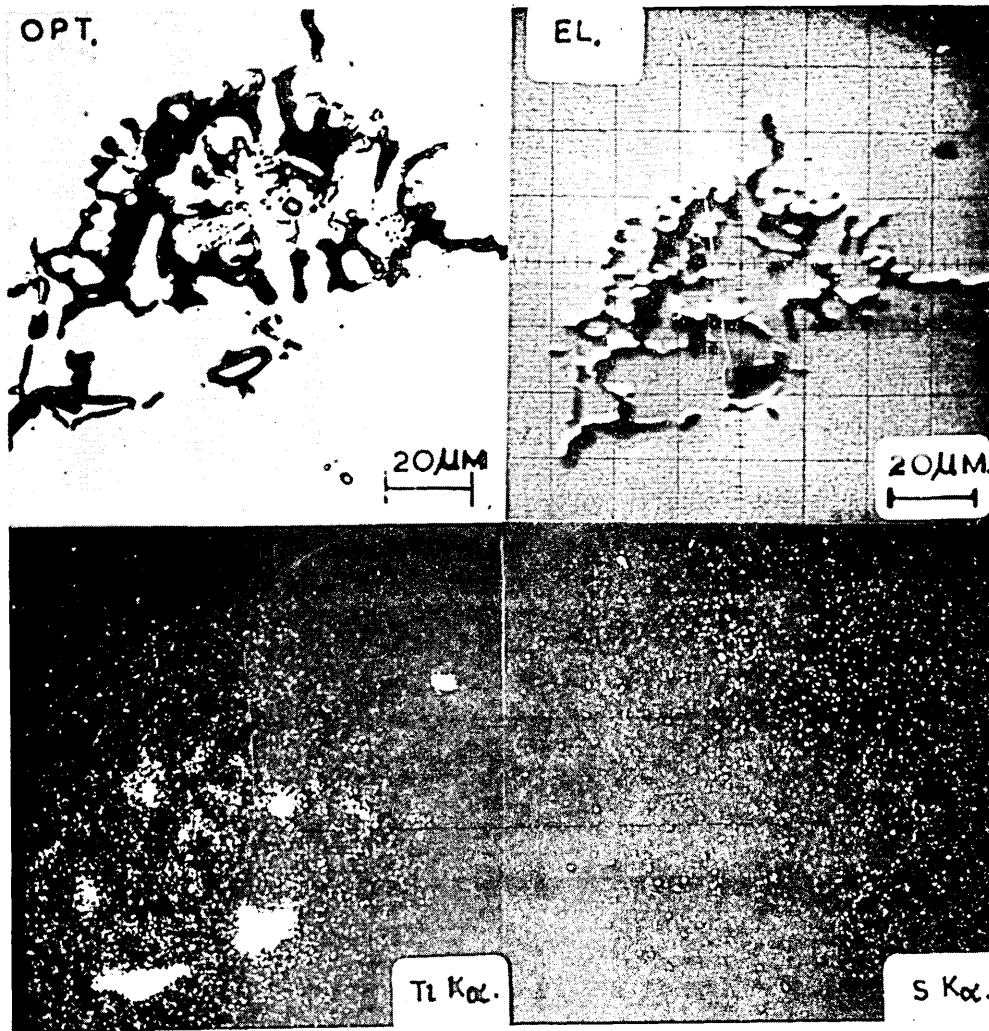
FIG. 39  SHOWS LIQUATION CRACKING ASSOCIATED WITH A TITANIUM RICH PHASE
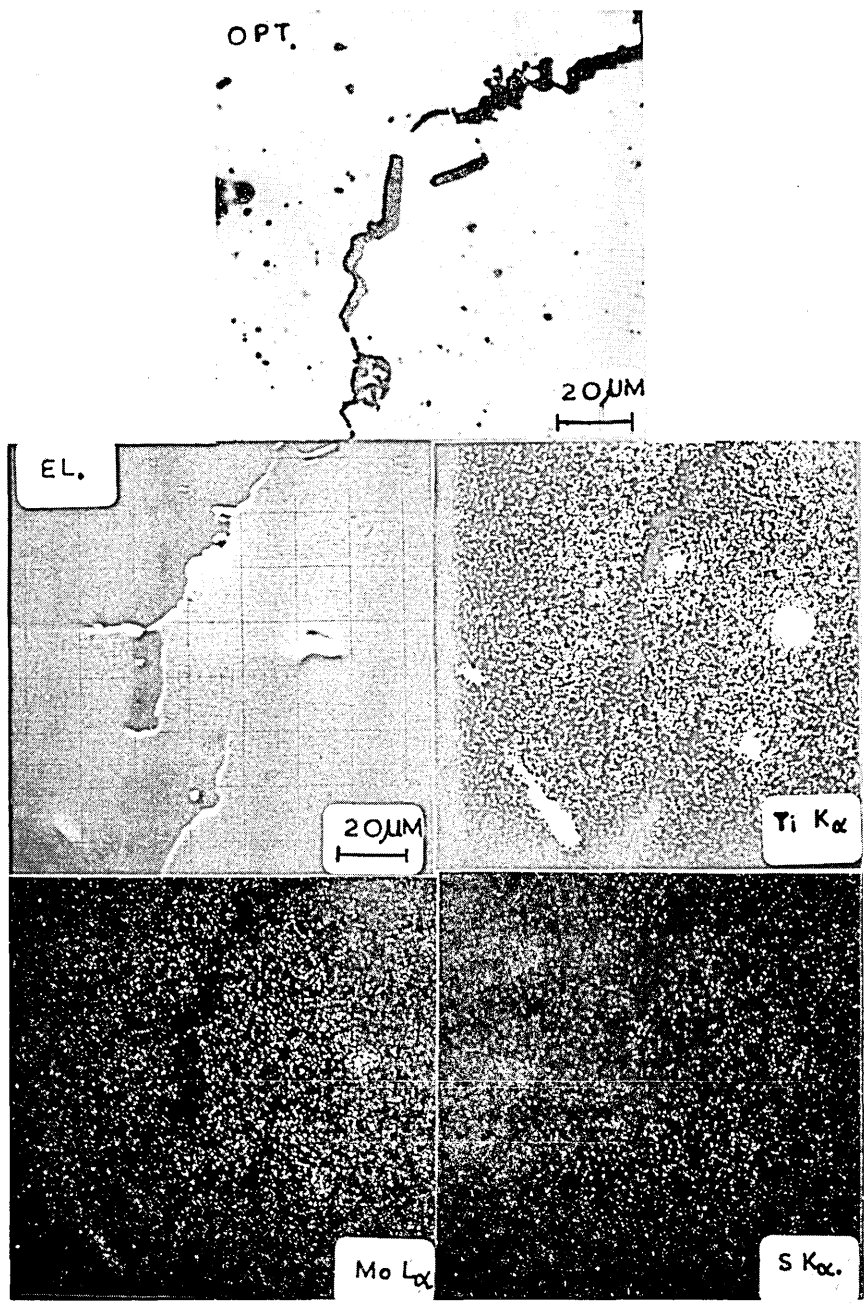
FIG. 40 SHOWS THAT REGIONS WHICH LIQUATE ARE ENRICHED IN Ti AND Mo BUT THEY ARE NOT NECESSARILY AT GRAIN BOUNDARIES WHERE THE CRACKS INITIATE
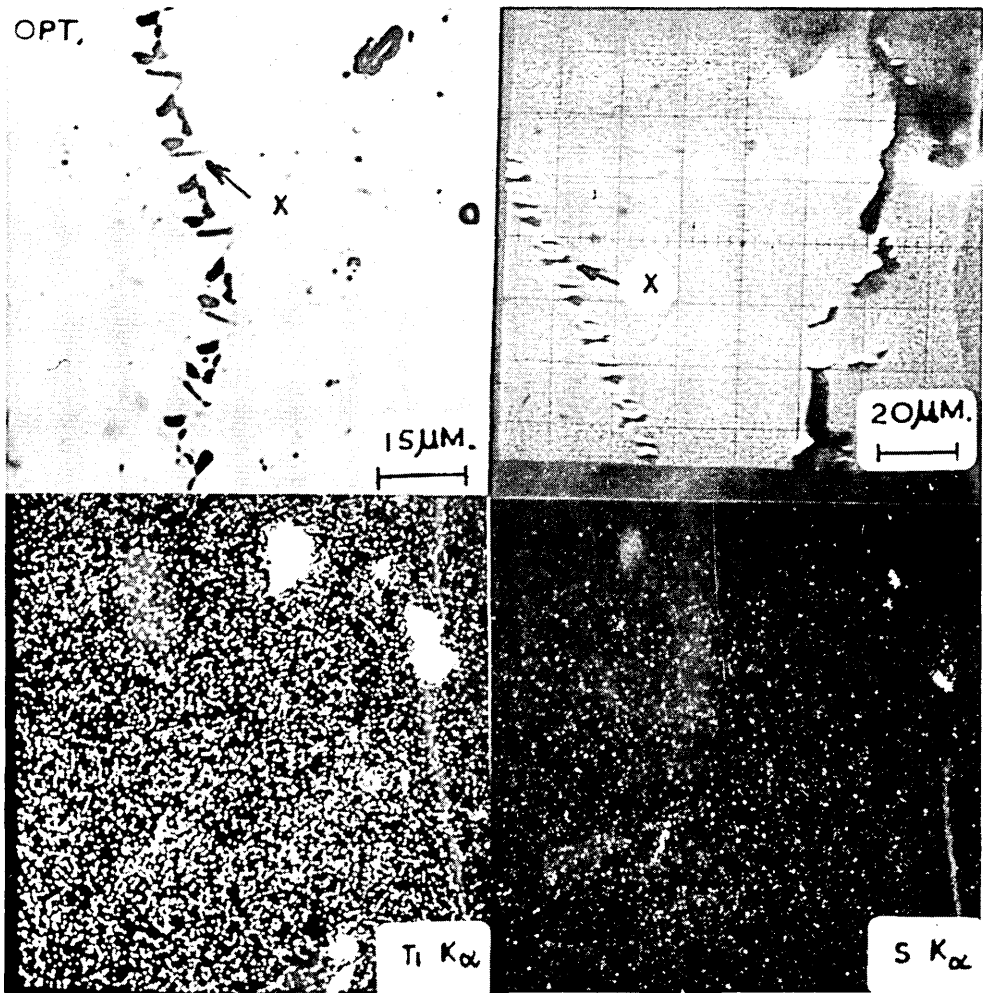
FIG. 41. FILM LIKE ARRAYS OF POSSIBLY Y PHASE ($M_2CS$)
WHICH ARE TOO THIN TO DETECT BY ELECTRON –
MICRO – PROBE ANALYSIS
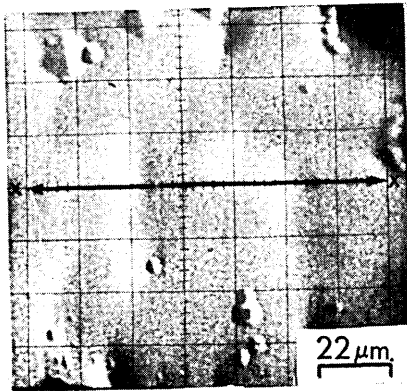
LINE TRACE 120μm ALONG
X-X . Ti, Ni ENRICHMENT.
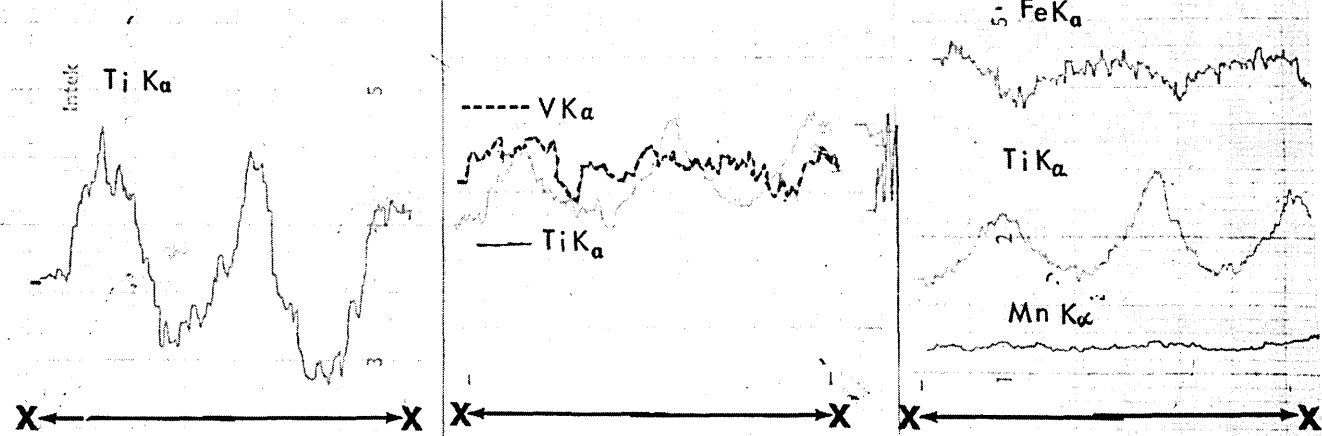
FIG. 42. SHOWS THE COMPOSITION OF THE WHITE ETCHING REGION TO BE
ENHANCED IN TITANIUM AND NICKEL, AND DEPLETED IN IRON AND
CHROMIUM ( SEE FIGS. 37 & 38 )

FIG. 43. SHOWS LIQUATED TITANIUM SULPHIDE IN ZONE 1 OF THE HAZ OF A286. ELECTRON MICROSCOPE MICRO ANALYSIS INDICATES Ti AND S
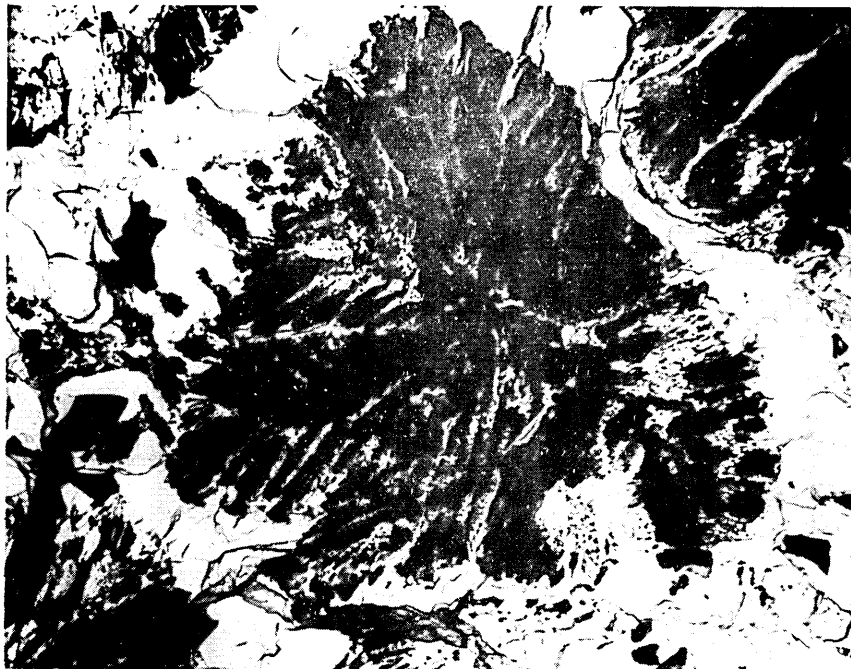


FIG. 44. SHOWS FERN SHAPED $Ti_5S_4$. INDEXED SELECTED AREA DIFFRACTION PATTERN SHEET 1, APPENDIX 1. ELECTRON MICROSCOPE MICRO ANALYSIS INDICATES Ti AND S $\times$ 4500

N521 ( 15 )

FIG. 45. DENDRITIC SULPHIDES OF TITANIUM INDICATED
BY ELECTRON MICROSCOPE MICRO ANALYSIS

x 6000   N680 ( 31 )
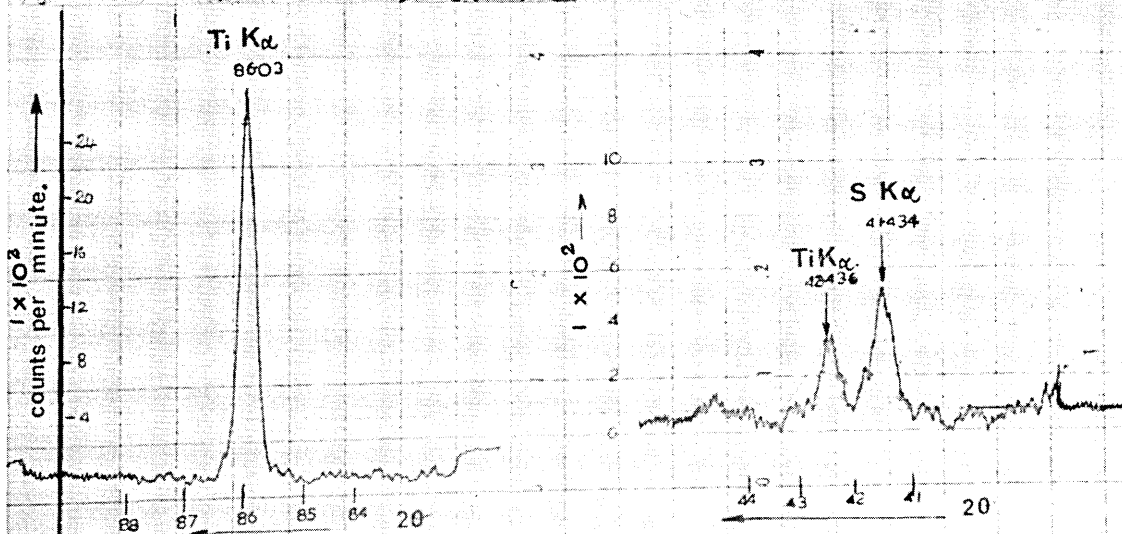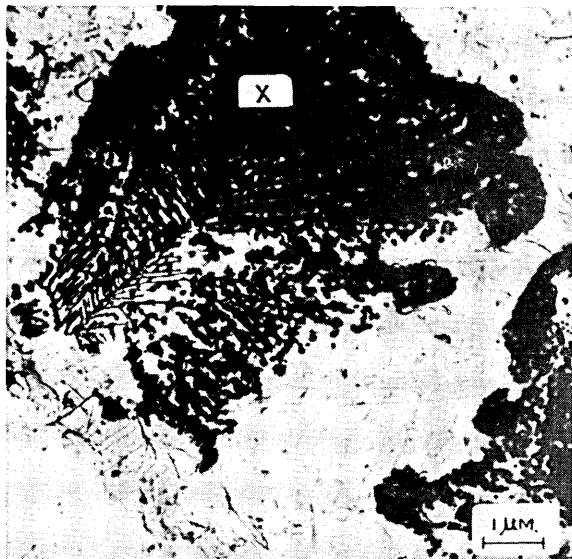


FIG. 46. DENDRITIC $Ti_5S_4$. SELECTED AREA ELECTRON DIFFRACTION
PATTERN INDEXED SHEET 2   APPENDIX 1
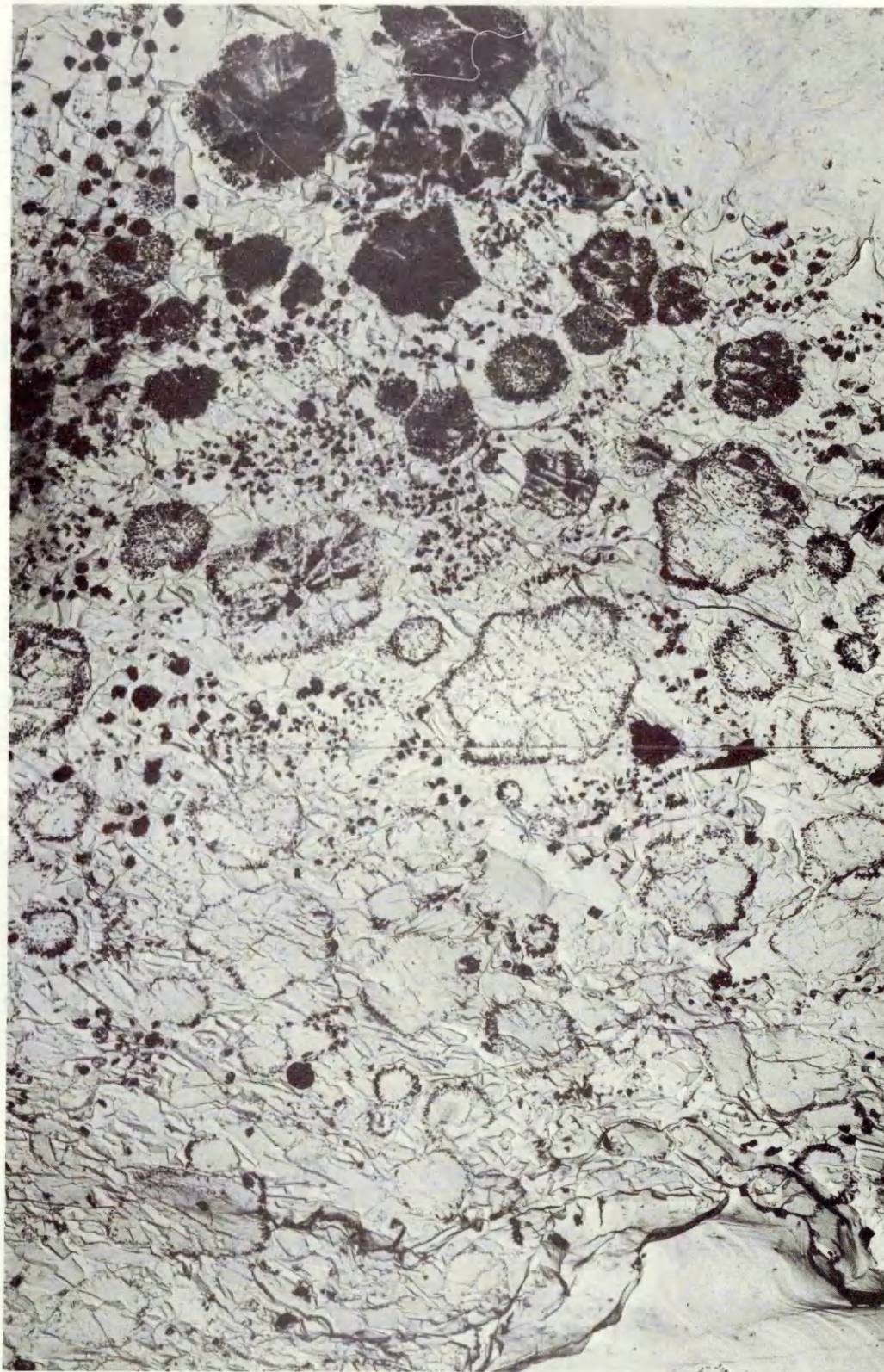
FIG. 47. M$_6$C IN THE HAZ OF A286. x 5000     N879 ( 38)
                                                N880 (39 )
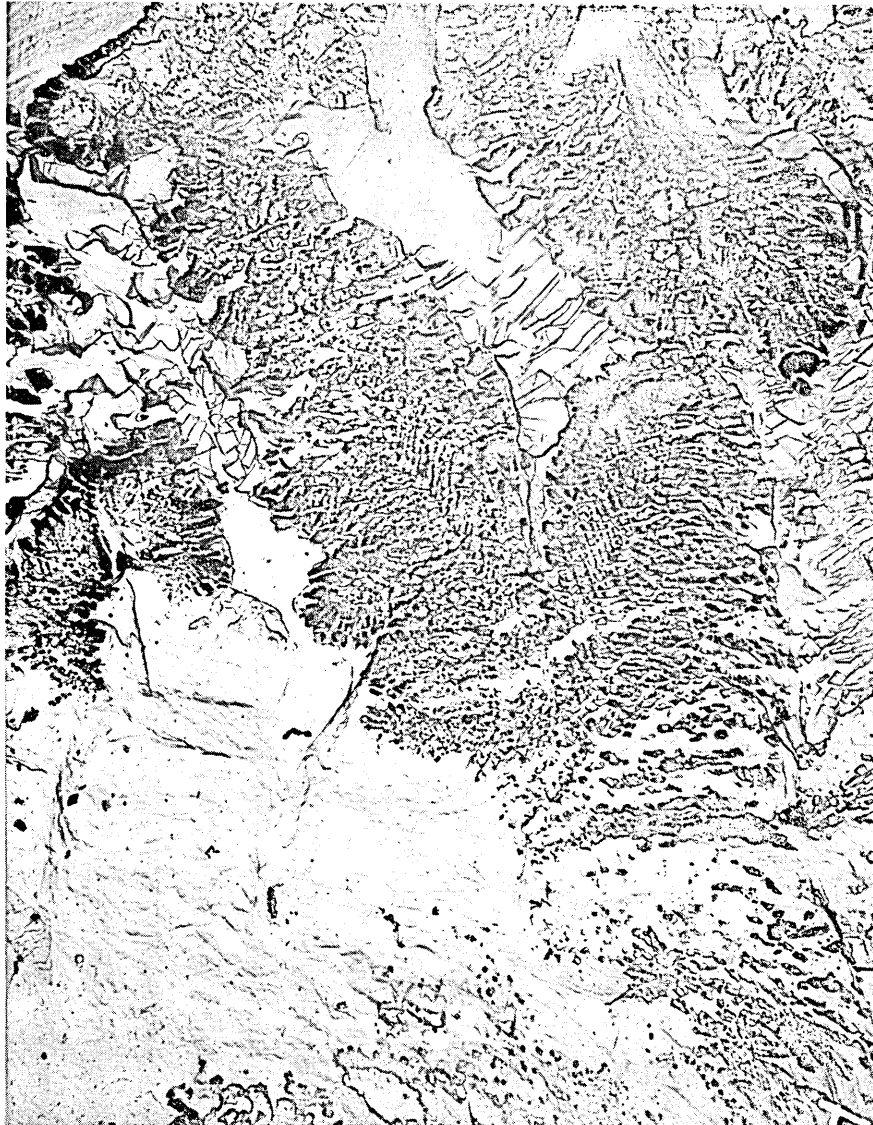
FIG. 48. M$_6$C IN A DENDRITIC MORPHOLOGY x 3600

N701 ( 4 )
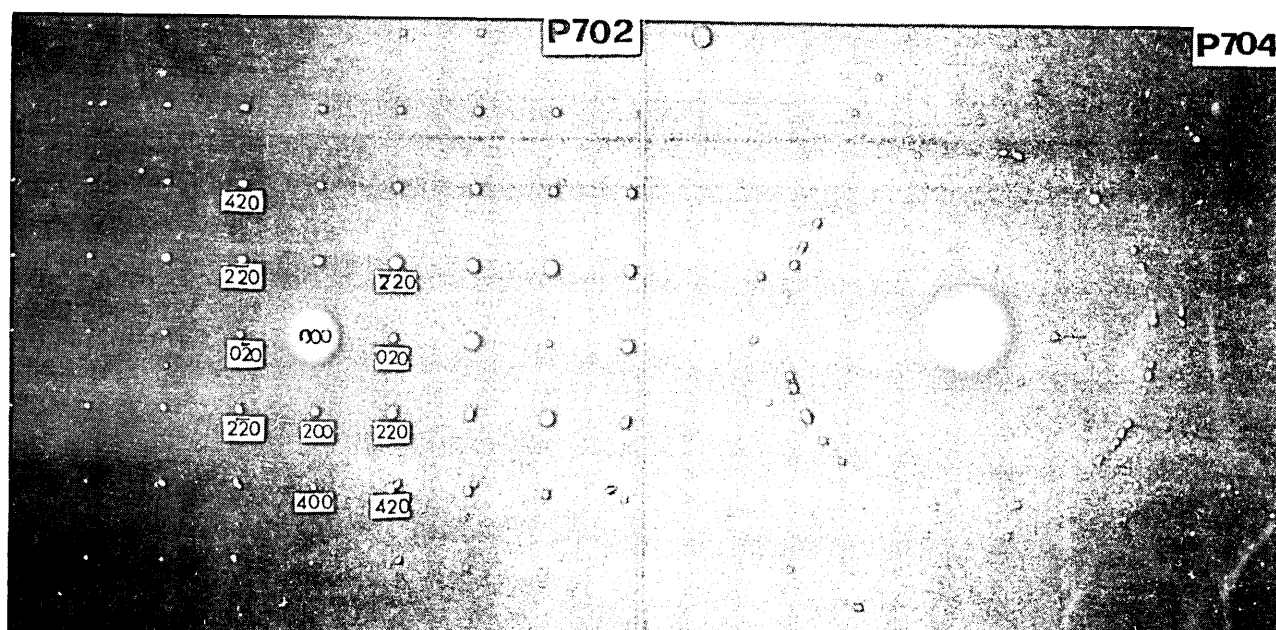


FIG. 49. M$_6$C [001] ZONE

F.C.C. a$_o$=11.18 Å

( SHEET 3. APPENDIX )

ALUMINIUM STANDARD

RD/M/R118

FIG. 50. Fe – Ti PHASE      x 3000

N766( 21 )
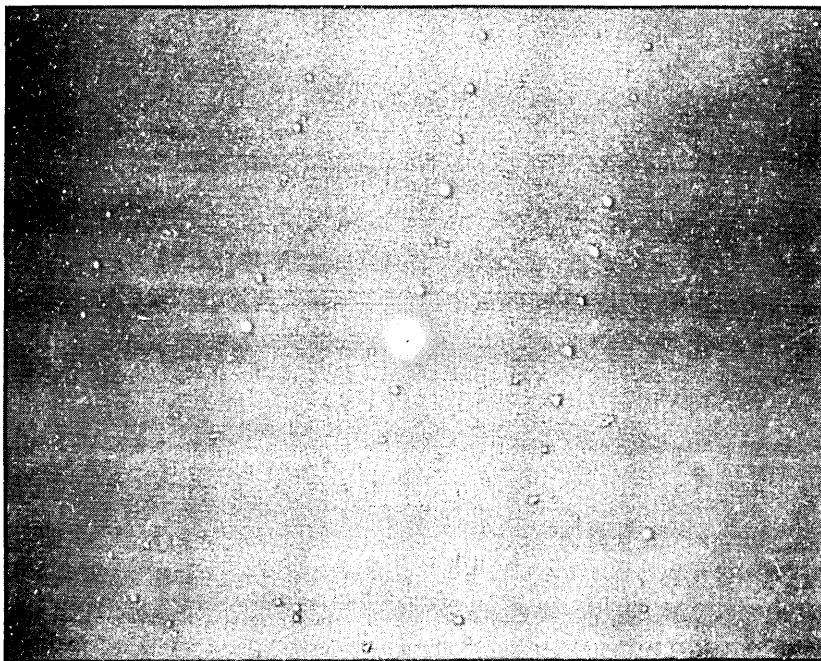


FIG. 51. SELECTED AREA ELECTRON DIFFRACTION OF

ABOVE PHASE      N( 760 ) 15
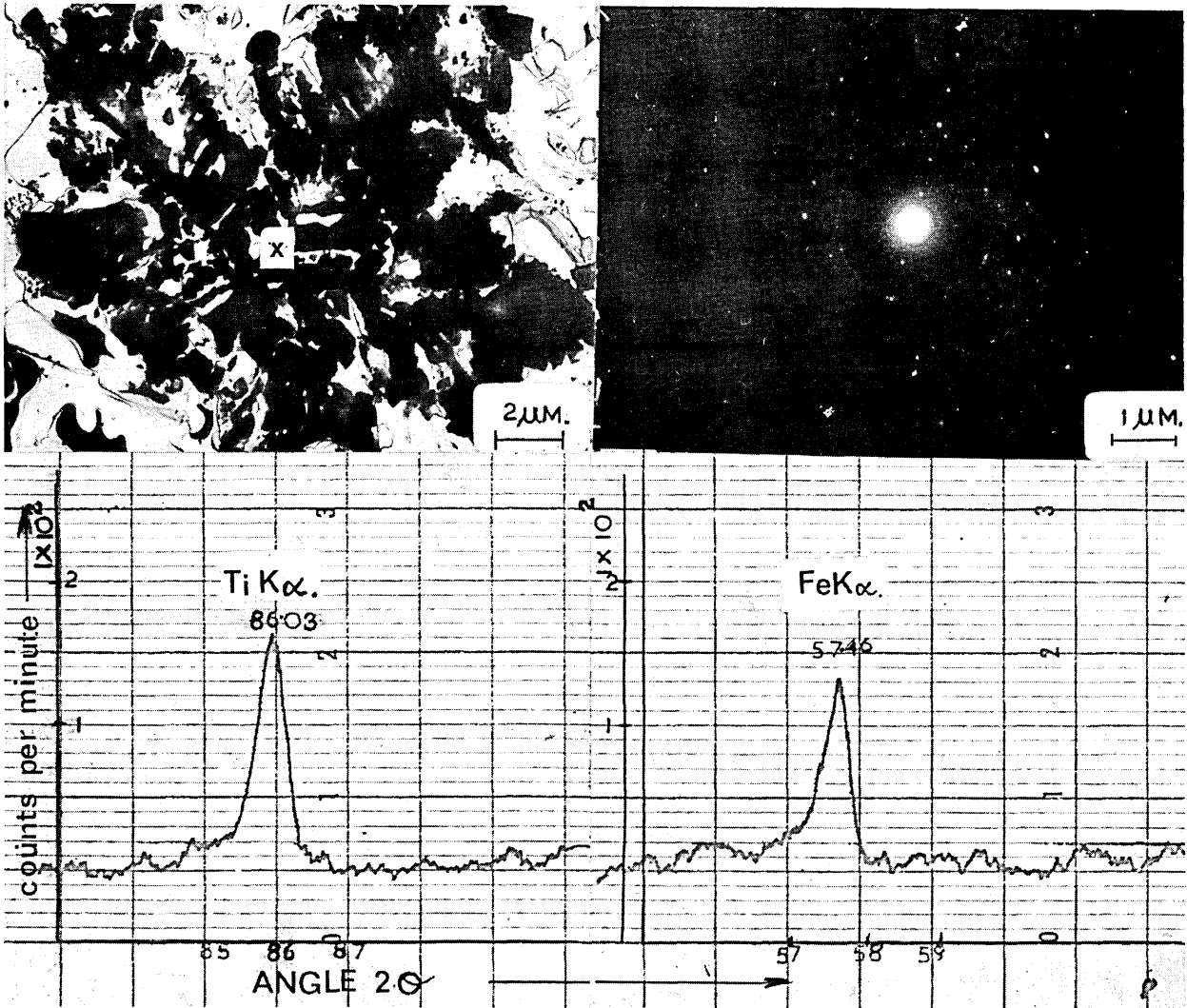
FIG. 52   SHOWS ELECTRON MICROSCOPE MICRO ANALYSIS OF Fe AND Ti PHASE
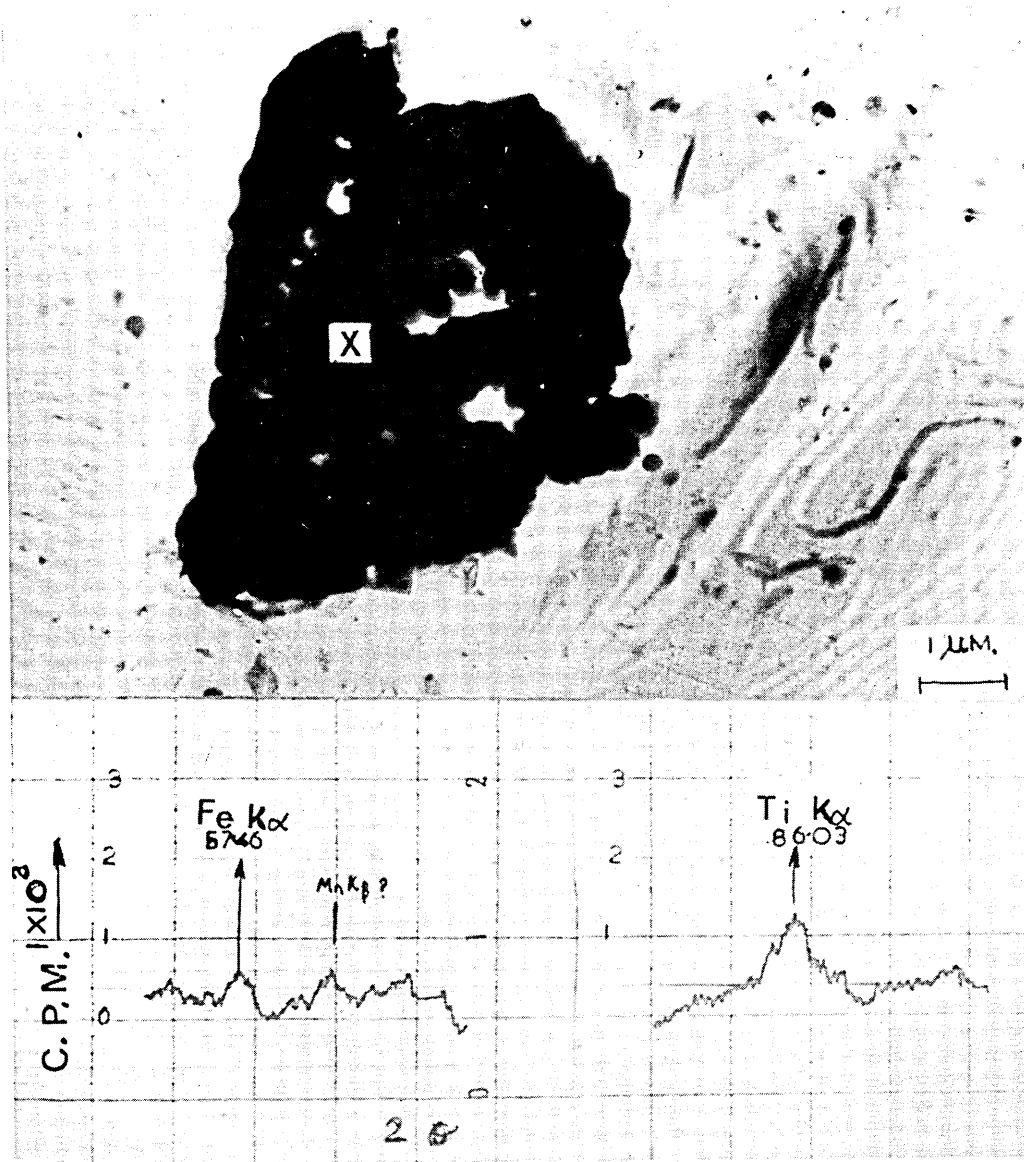
FIG. 53   SHOWS IRON TITANIUM PHASE ASSOCIATED WITH THERMAL FACETING
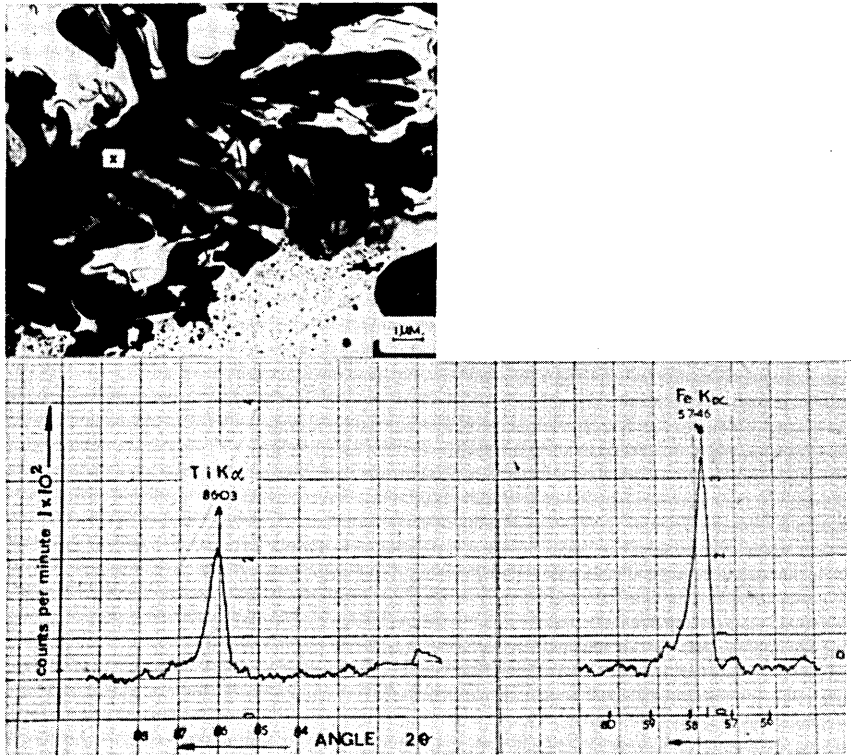
FIG. 54    DENDRITIC Fe - Ti PHASE
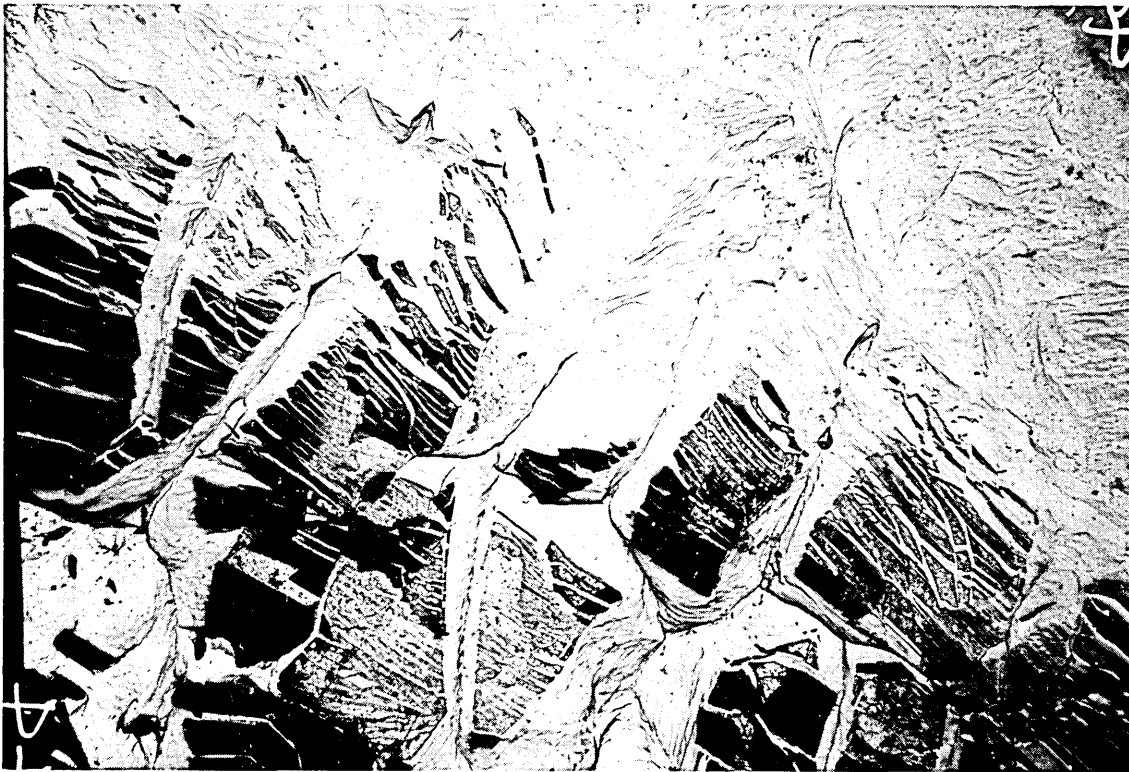
x 2000

N 693 (44)

FIG. 55   SHOWS TITANIUM VANADIUM CARBOSULPHIDE (Y PHASE) IN THE HAZ OF
A286.   THIS PARTICULAR REGION IS NEAR THE FUSION BOUNDARY
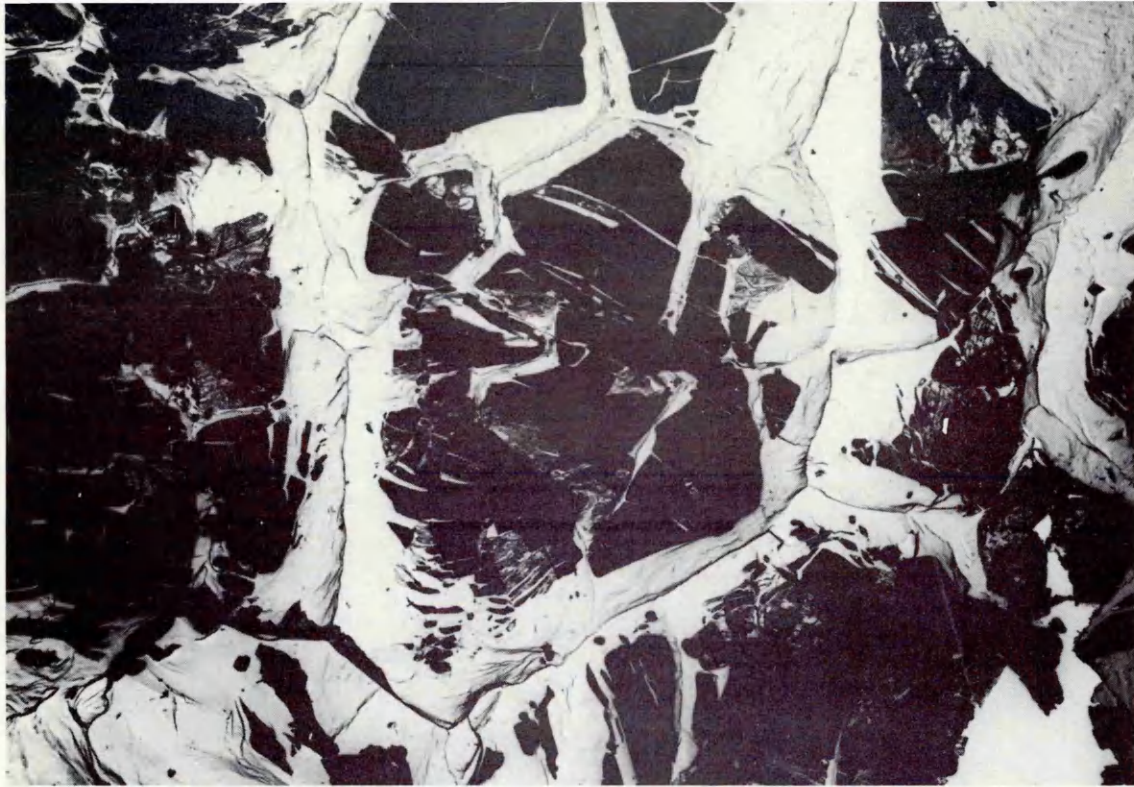
× 3600

N 692(43

FIG. 56   SHOWS INTERGRANULAR DUCTILE RUPTURE ALONG WHITE ETCHING REGIONS

IN THE HAZ . THE DARK FILMS ARE THE BRITTLE TITANIUM VANADIUM

CARBOSULPHIDES "Y PHASE"



N 419(10)

FIG. 57   SELECTED AREA ELECTRON DIFFRACTION INDICATES $\begin{bmatrix} 0001 \end{bmatrix}$ ZONE

(BASAL PLANE) OF Y PHASE
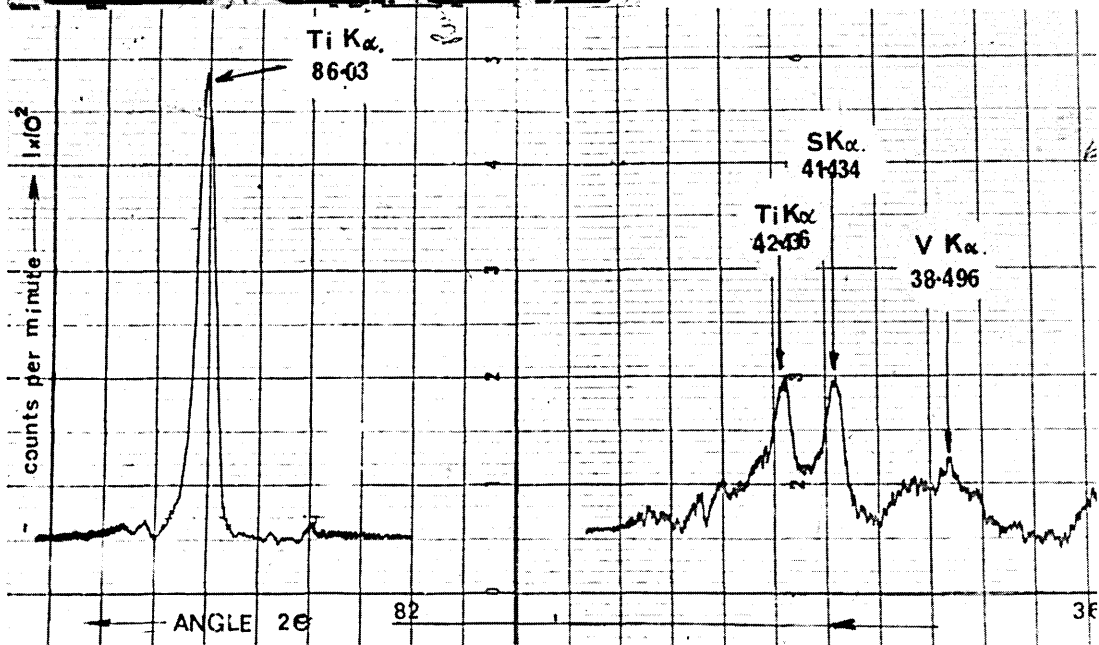
FIG. 58   ELECTRON – MICROSCOPE – MICRO – ANALYSIS INDICATES Ti, S AND

V WHICH WOULD SUGGEST $M_2$(CS) WHERE M = Ti OR V
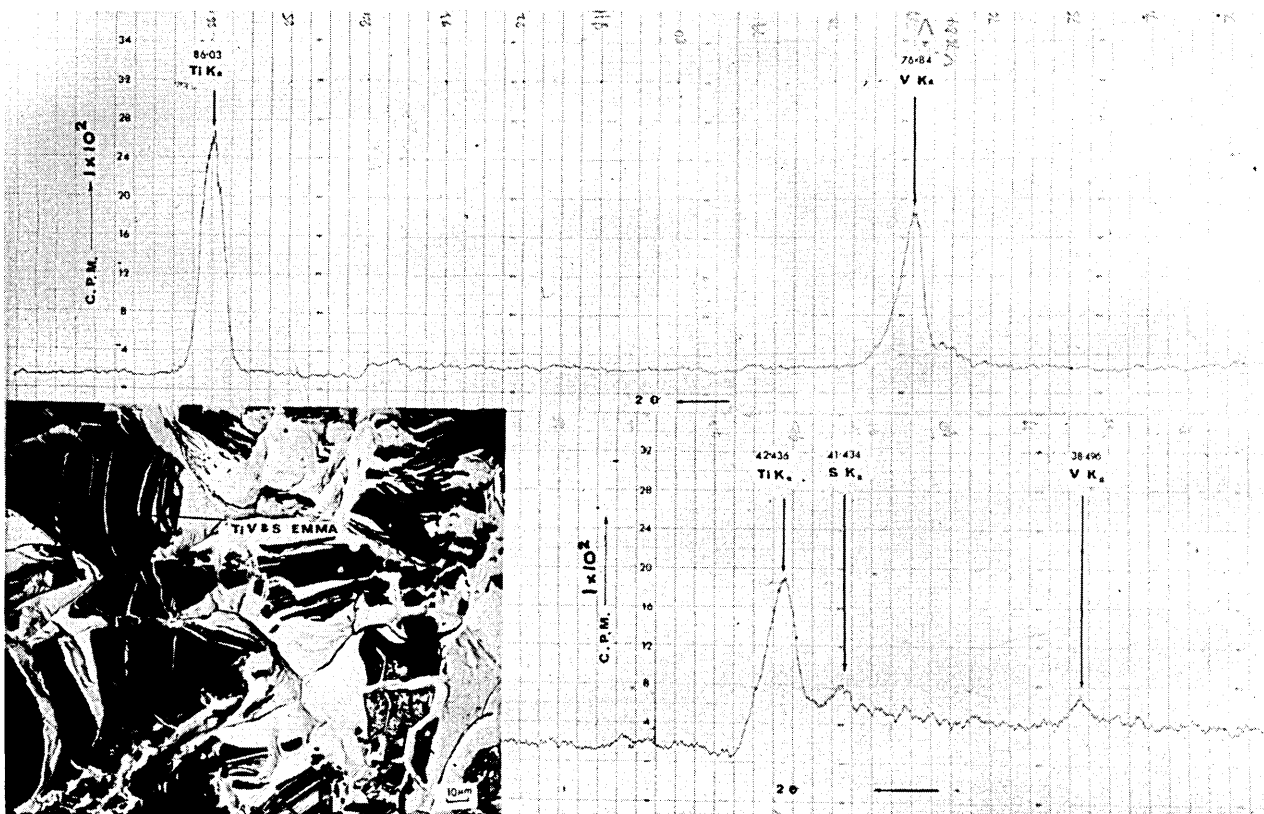
FIG. 59   ELECTRON MICROSCOPE MICRO ANALYSIS INDICATES Ti, V AND S WHICH

IS CONSISTENT WITH Y PHASE $(TiV)_2$ CS
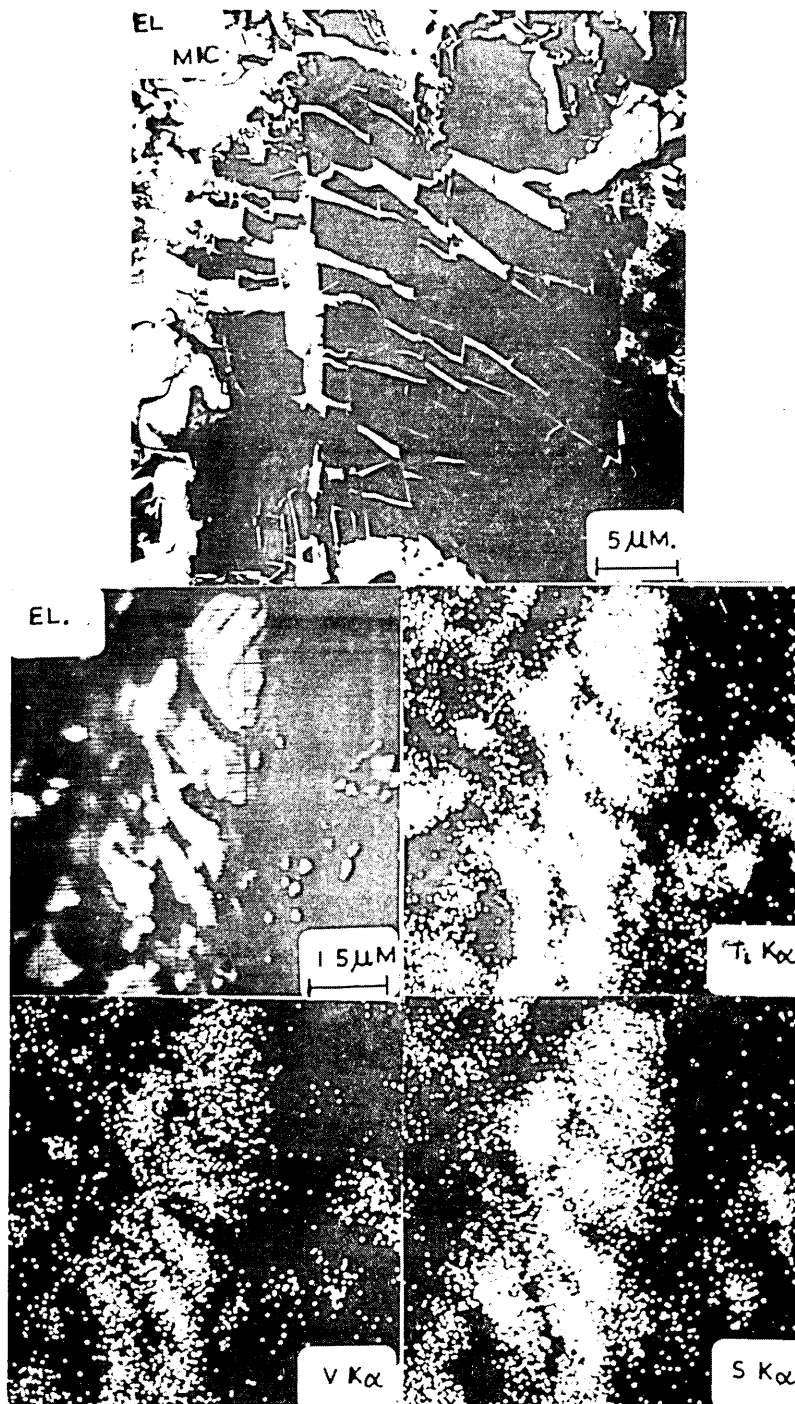
FIG. 60   Y PHASE OR SHATTERED FILMS ARE SEEN BY ELECTRON MICRO PROBE
ANALYSIS TO CONSIST OF Ti, V AND S

FIG. 61. SHOWS COLDER REGION OF HAZ (ZONE II ) THERMAL FACETS PLUS
SLIP LINES                                                    859 ( 19 )
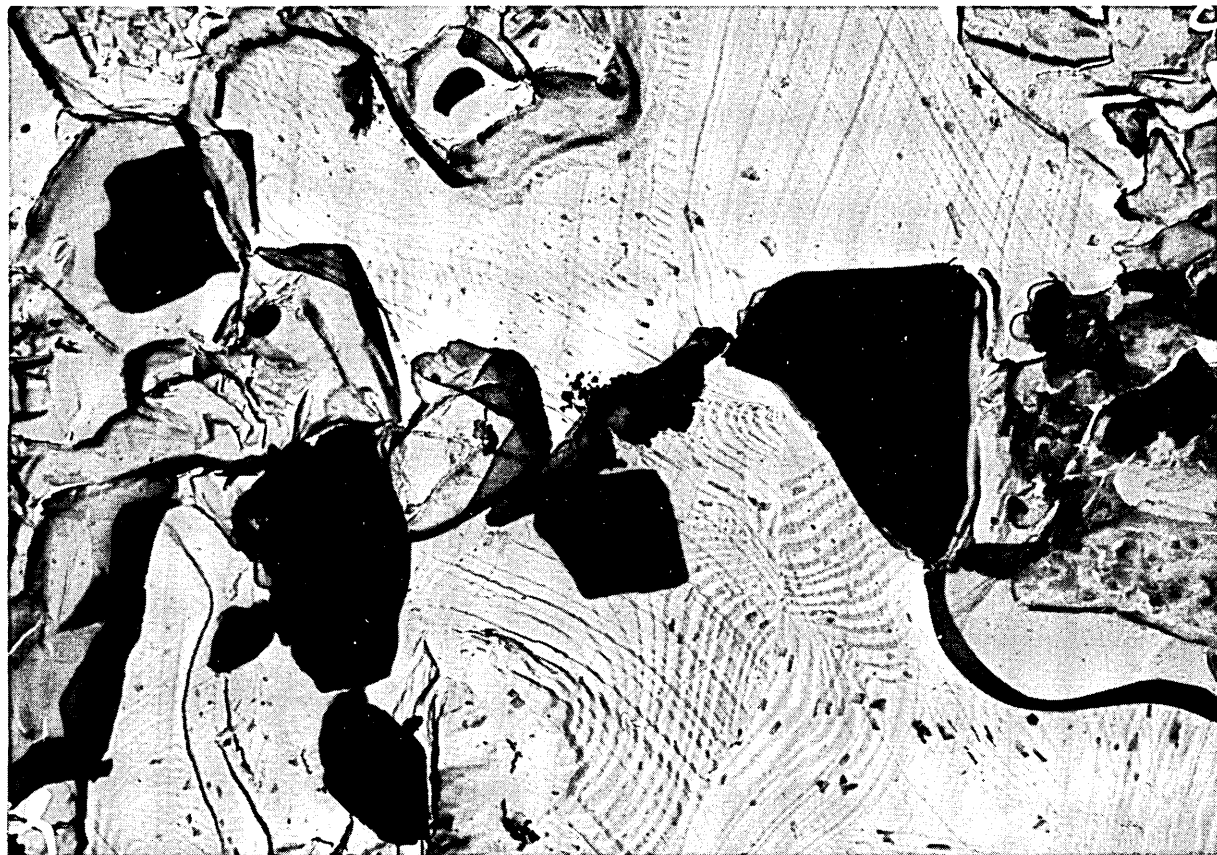


FIG. 62. DETAIL OF FIG.61. THERMAL FACETS, SLIP LINES PLUS SMALL
TITANIUM CARBONITRIDES                                   860 ( 20 )

RD/M/R118
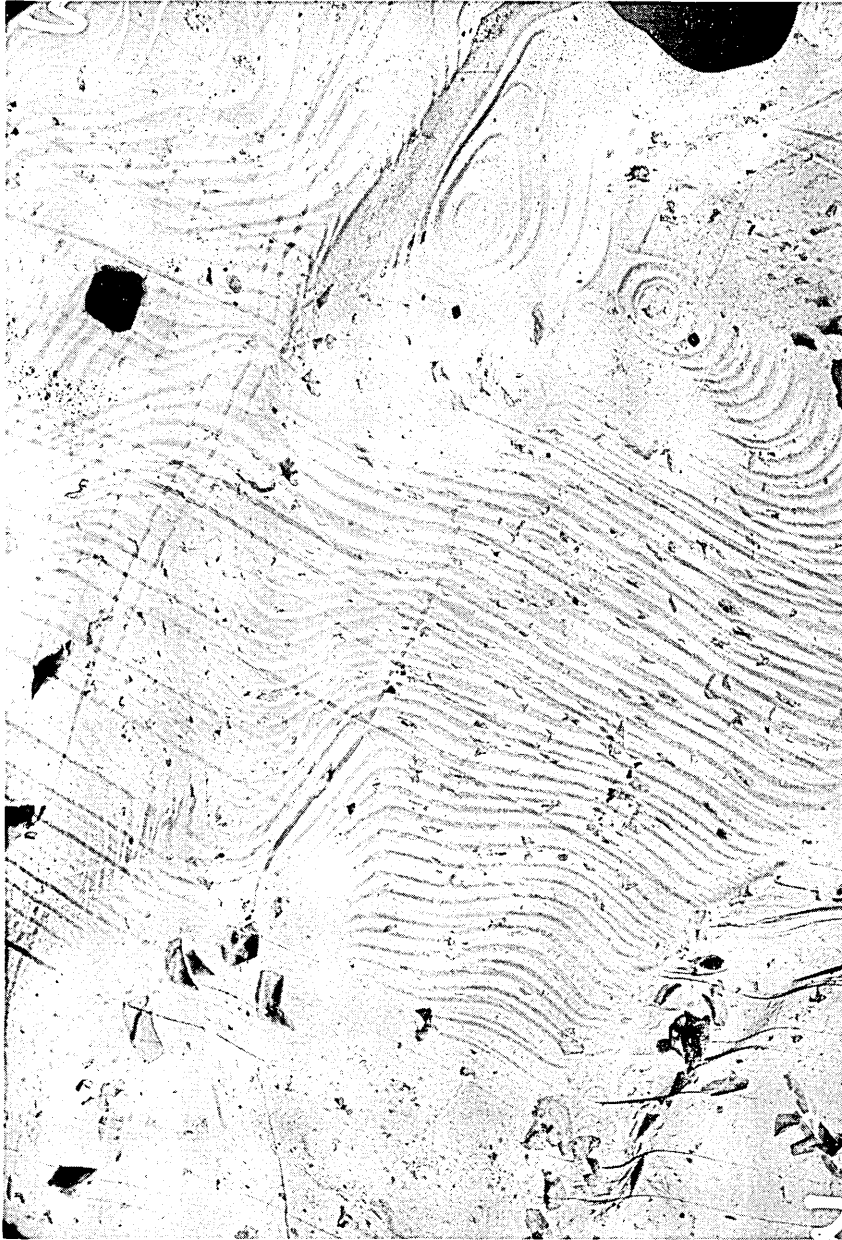
FIG. 63. THERMAL FACETING IN ZONE II    x 4200

N811(18)

FIG. 64. SLIP LINES AND THERMAL FACETS IN ZONE II

x 9000

N520(14)
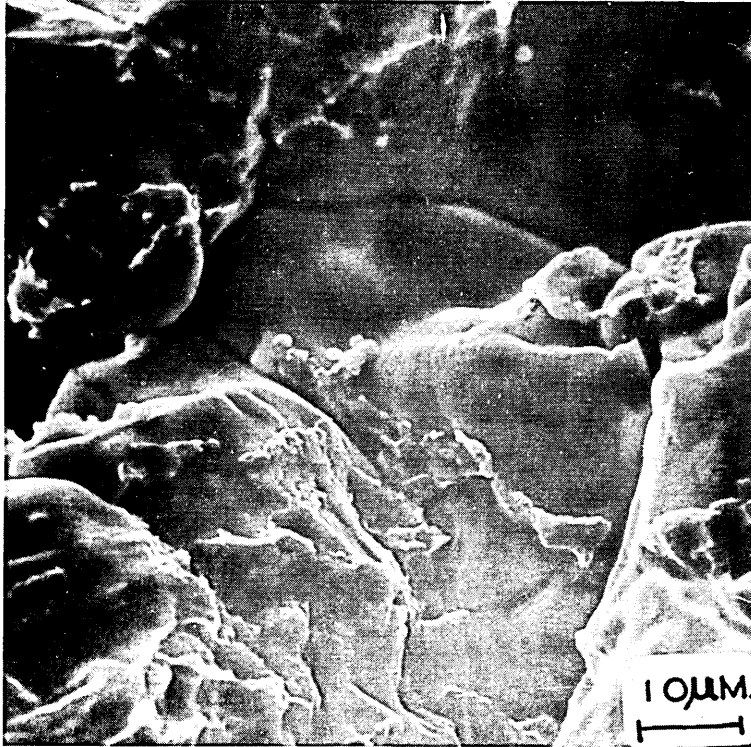
FIG. 65. SHOWS THE COLDER REGION OF (ZONE II)
OF THE FRACTURE SURFACE. NOTE THE
CRACK SURFACE IS COVERED WITH SLIP
LINES .

FIG. 66. ARRAYS OF TITANIUM CARBONITRIDES  x 6000

N1025 ( 36 )
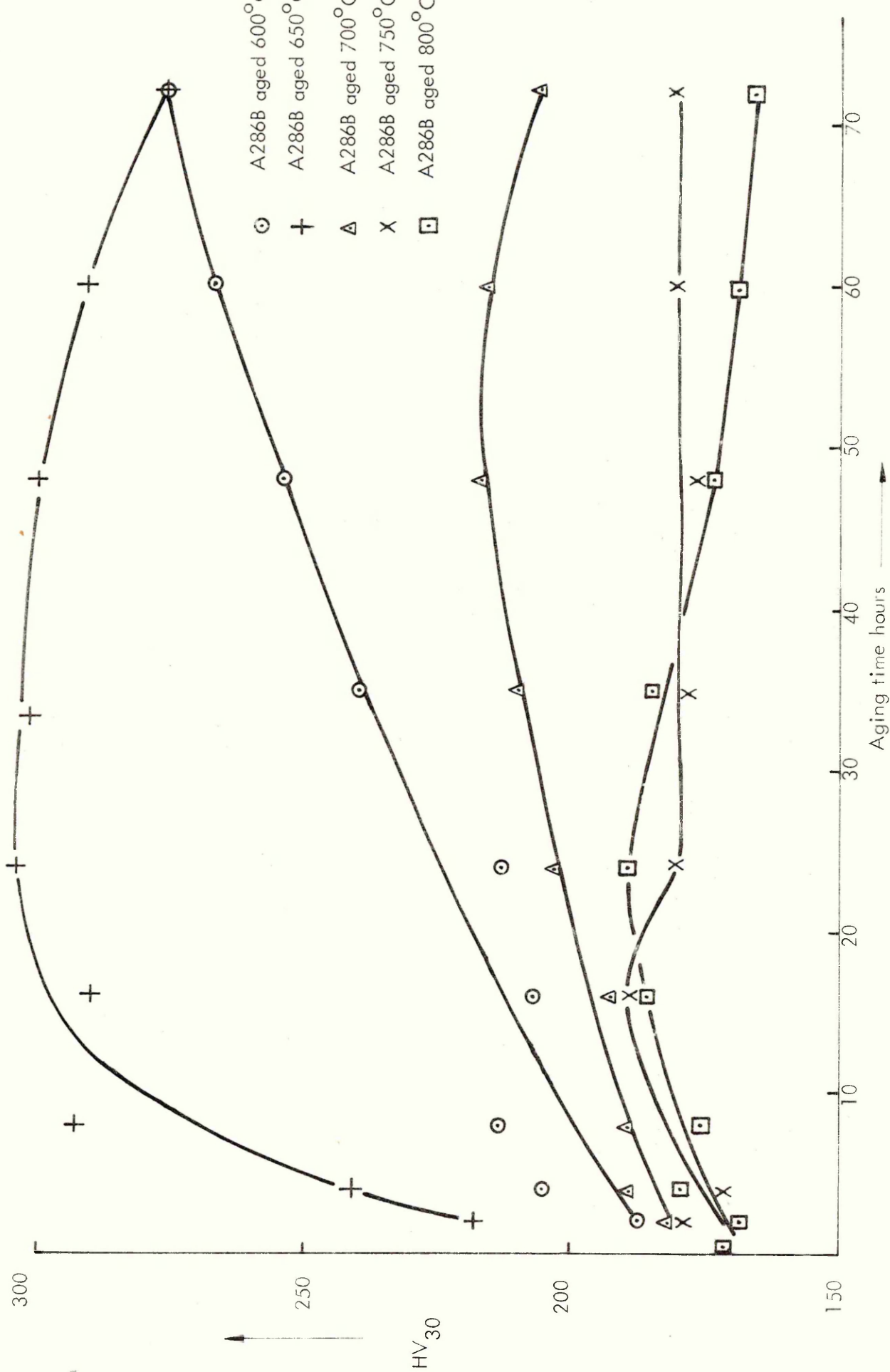
FIG. 67. PLOT OF VICKERS HARDNESS AGAINST AGEING TEMPERATURE °C

Legend:
- ⊙ A286B aged 600°C
- + A286B aged 650°C
- △ A286B aged 700°C
- × A286B aged 750°C
- ▣ A286B aged 800°C

Aging time hours

$HV_{30}$

RD/M/R118
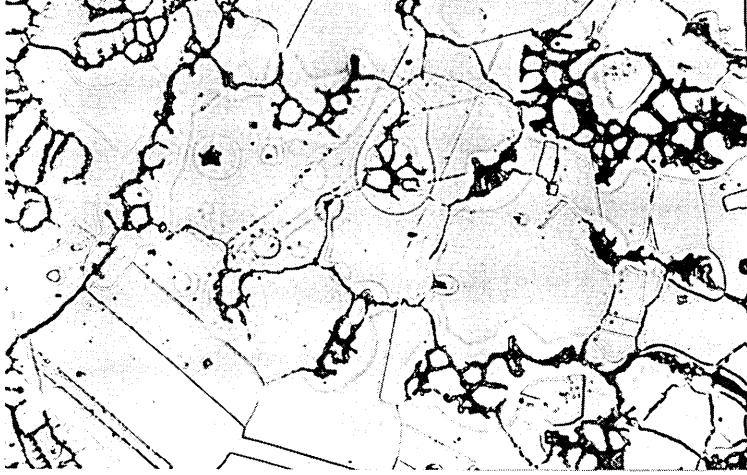
FIG. 68. SHOWS DUPLEX AUSTENITE PLUS

EUTECTIC BORIDE          x 300
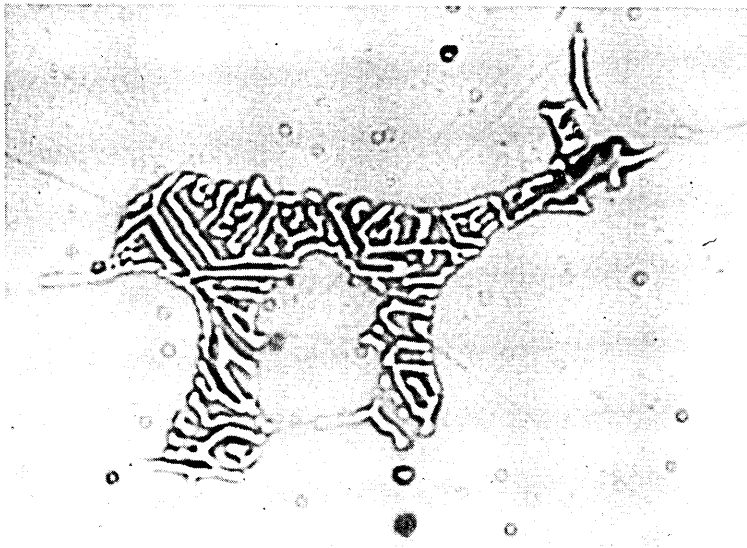


FIG. 69. SHOWS DETAIL OF EUTECTIC BORIDE

x 2000
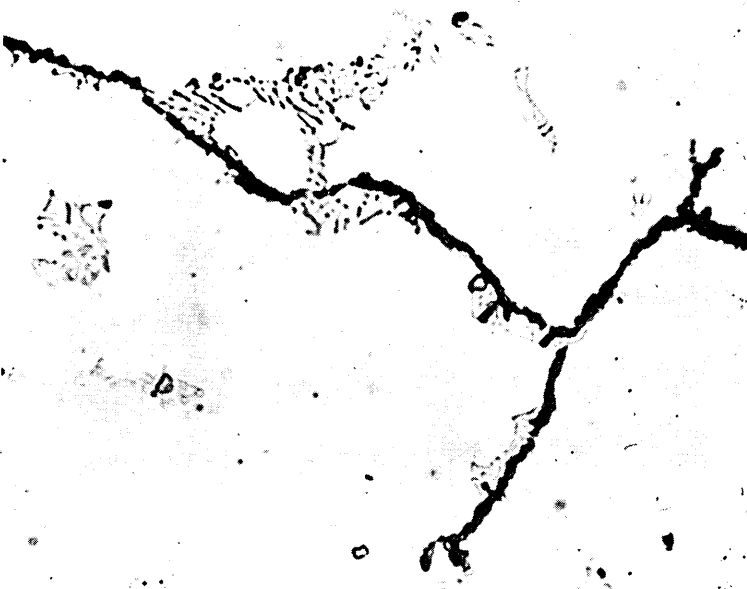


FIG. 70. SHOWS CRACKING ALONG EUTECTIC

BORIDE          x 1000

RD/M/R118
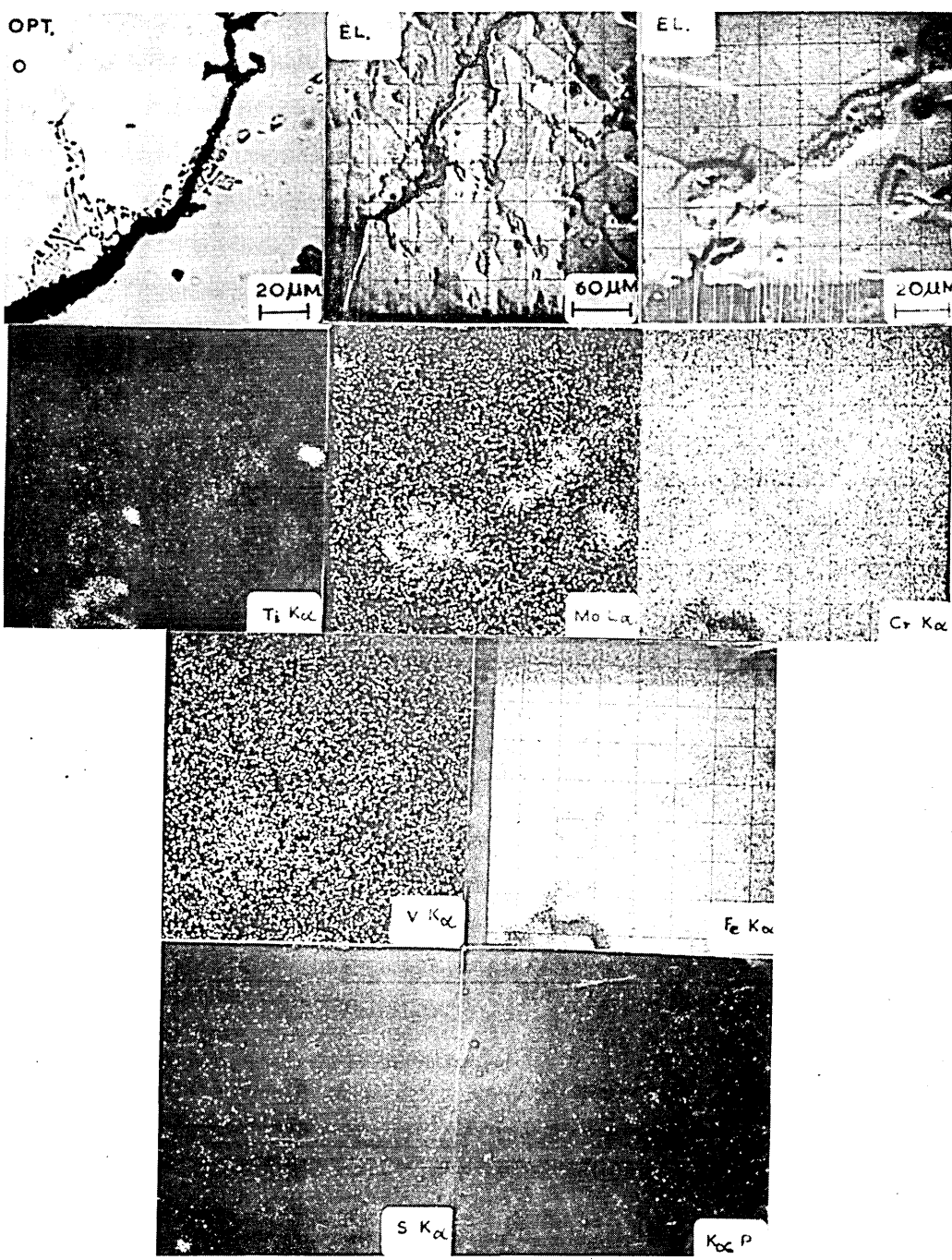
FIG. 71. ELECTRON-MICRO PROBE ANALYSIS OF THE EUTECTIC
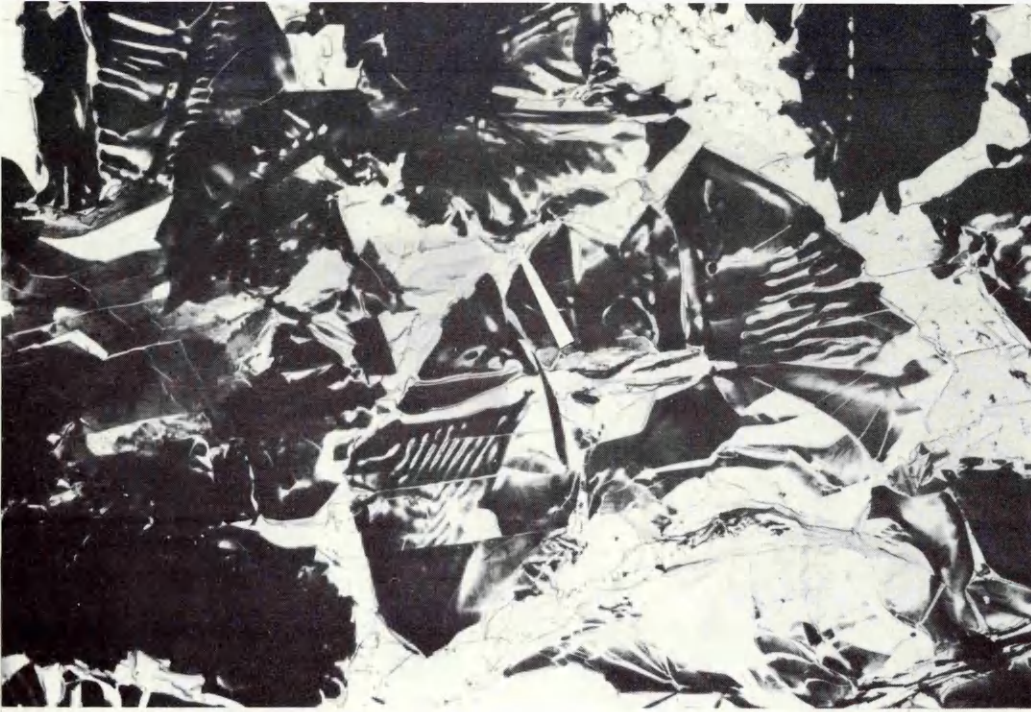
BORIDE

FIG. 72. ELECTRON FRACTOGRAPHY REVEALS DENDRITIC MORPHOLOGY
OF EUTECTIC BORIDE                                    x 1800

N1013 ( 24 )



FIG. 73. SHOWS BRITTLE FRACTURE OF EUTECTIC BORIDE. (STEREOSCAN
ELECTRON MICROSCOPE)
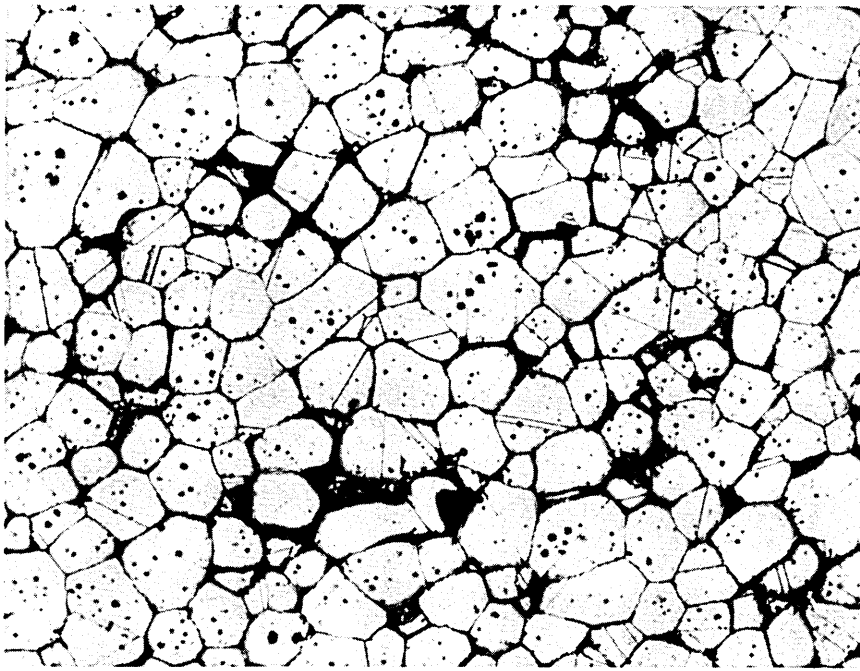
FIG. 74. A286 PLUS 0.39 wt % BORON AFTER A 1350°C

WATER QUENCH HEAT TREATMENT          x 150

N1657
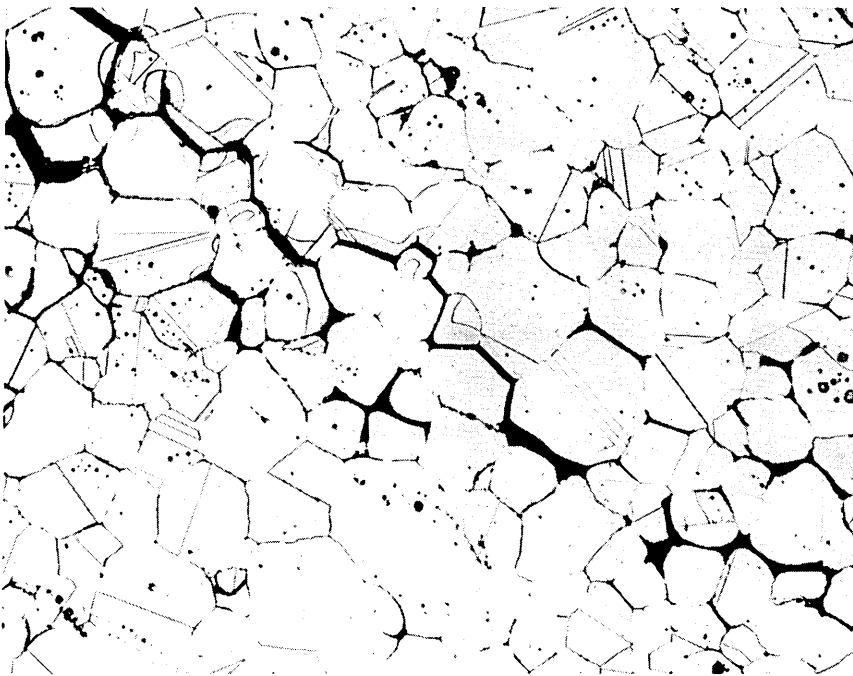


FIG. 75. A286 HEAT TREATED 1350°C WATER QUENCH.

EXTENSIVE INTERGRANULAR CRACKING NOT

TYPICAL OF HAZ CRACKS.          x50

N165

FIG. 76. SHOWS DENDRITIC PARTICLES IN A BURNT SAMPLE OF

A286. ( 1350°C 1 HOUR WATER QUENCH )          x 1800

N851 (11)

FIG. 77.  DETAIL OF A DENDRITIC TITANIUM, VANADIUM
CARBOSULPHIDE IN THE BURNT SPECIMEN OF
A286.                                           x 2800
                                               N700 (3)
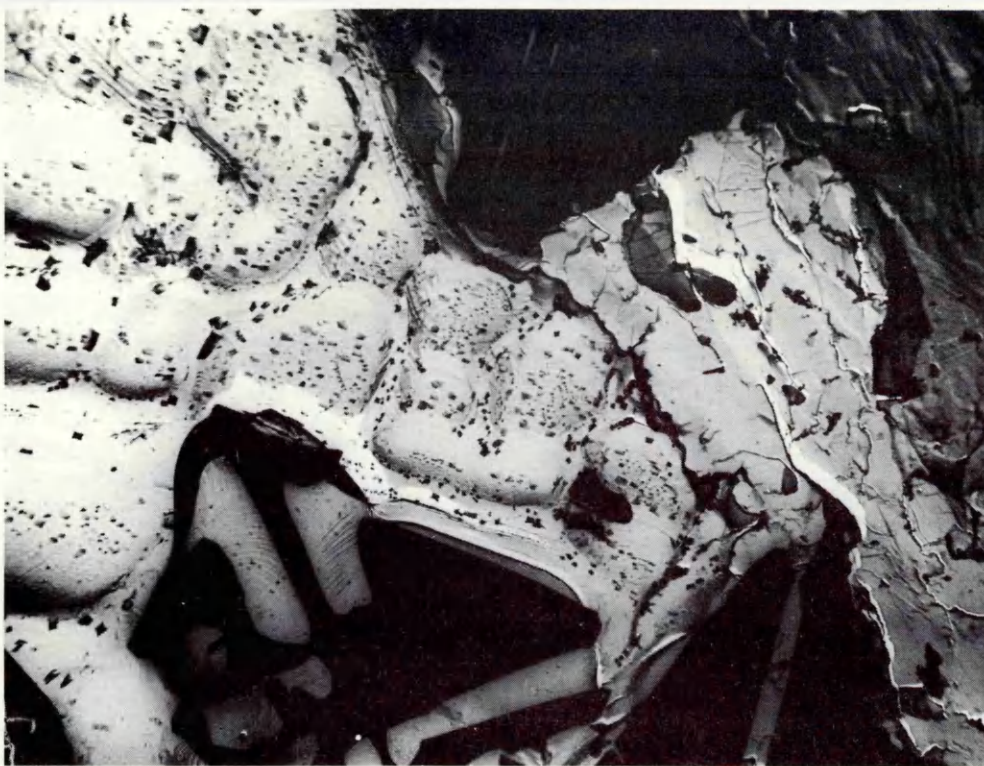
FIG. 78. SHOWS FRACTURE SURFACE OF CRACKS FORMED
DURING 1350°C HEAT TREATMENT            x 2000
                                        N1033(44)
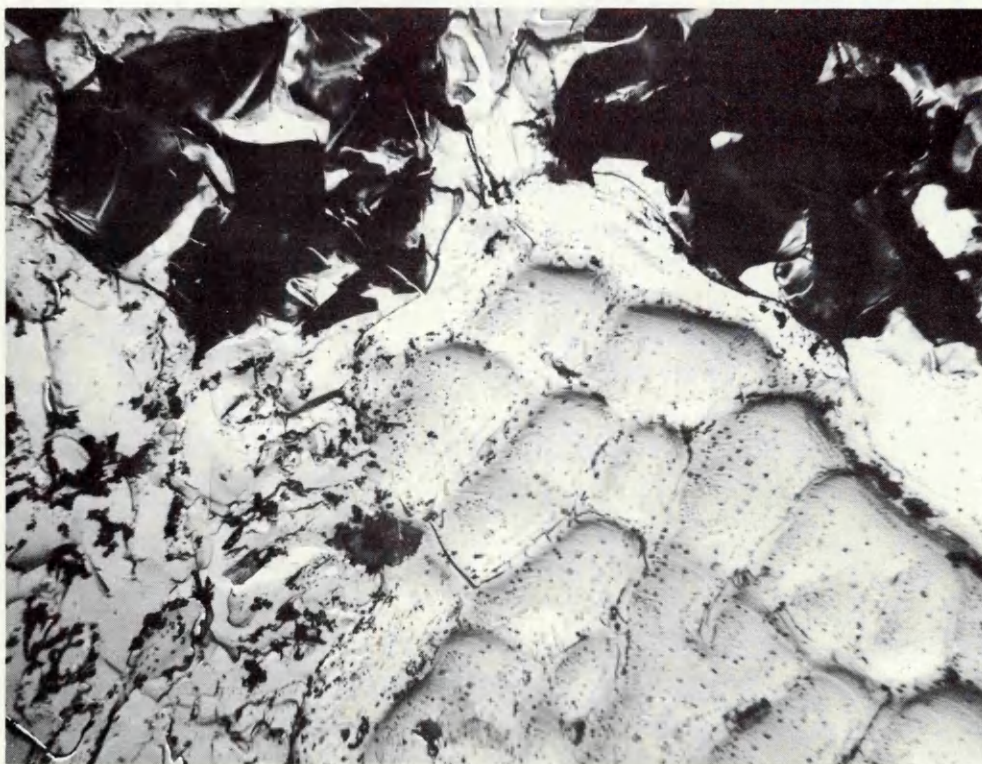


FIG. 79. DETAIL OF THERMAL FACETING        x 2000
                                           N1029(40)
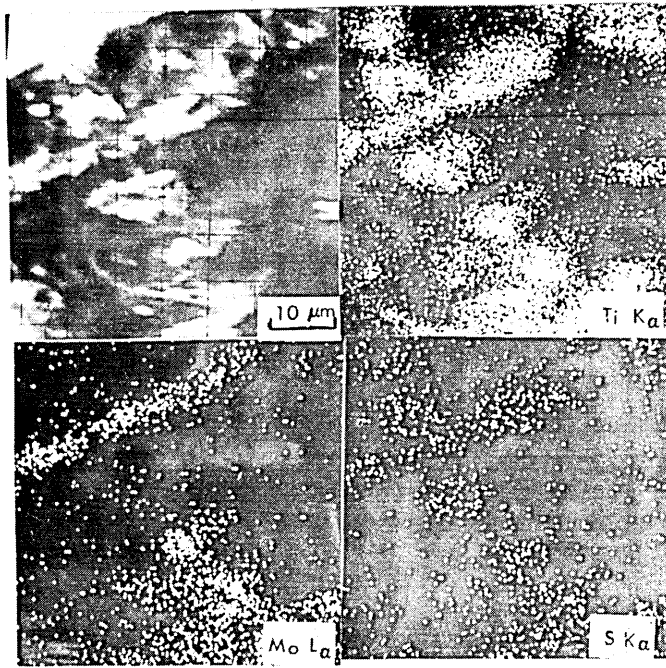
COMPLEX [Ti Mo] CARBOSULPHIDE

FIG. 80. DENDRITIC CARBOSULPHIDES
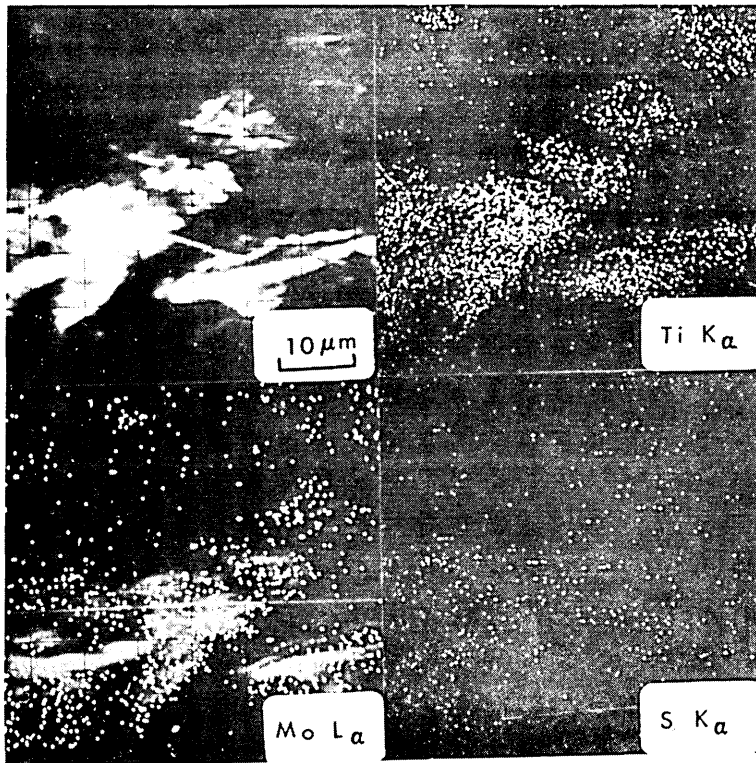
DENDRITIC [Ti - Mo]C

FIG. 81. DENDRITIC CARBIDES OR CARBOSULPHIDES
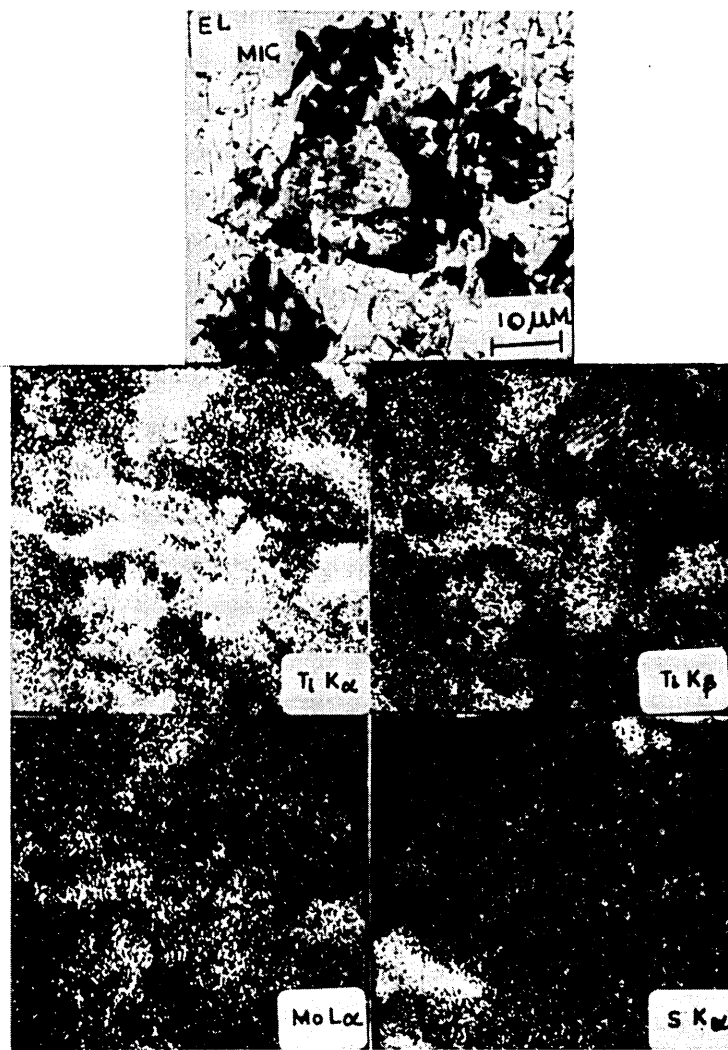
FIG. 82. SHOWS DENDRITIC CARBOSULPHIDES
IN OVERHEATED SPECIMENS. (1350°C
1 HOUR WATER QUENCH)
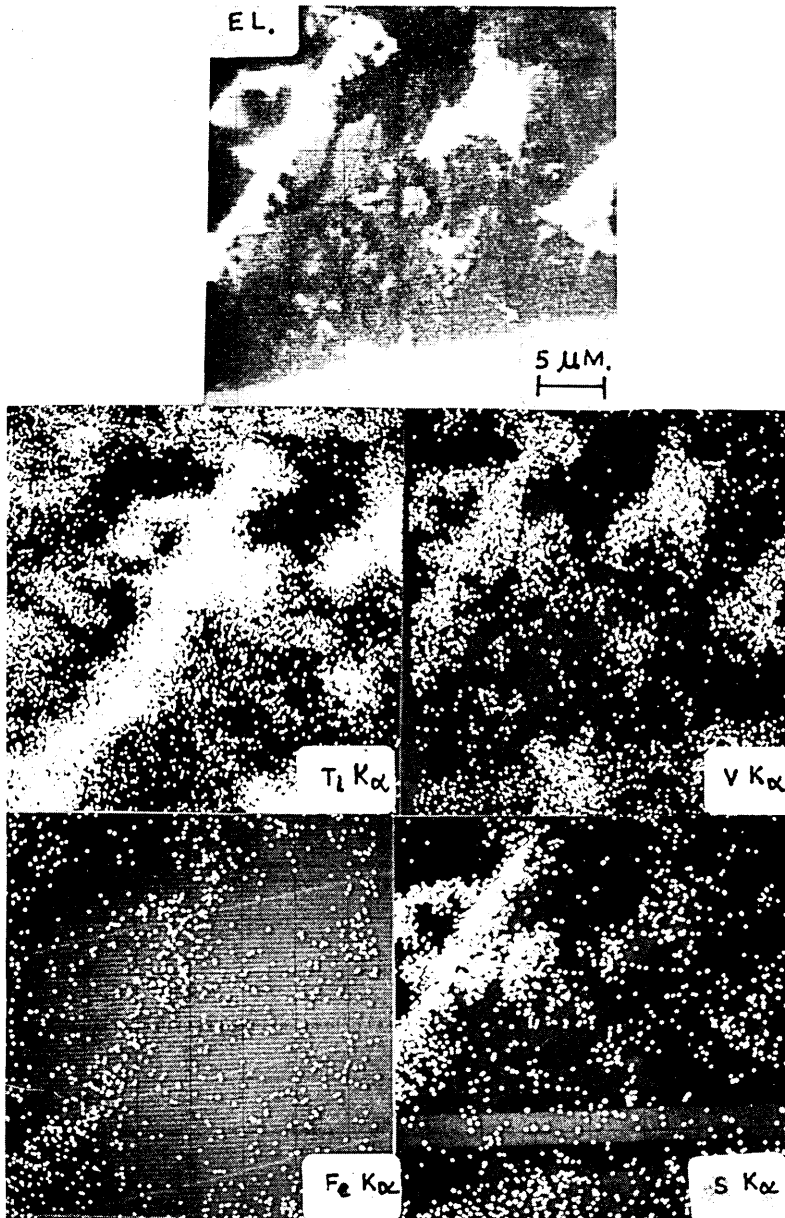
FIG. 83. SHOWS DENDRITIC ( Fe Ti V ) SULPHIDES OR
POSSIBLY CARBOSULPHIDES IN THE BURNT
SPECIMEN OF A286. ( 1350°C 1 HOUR
WATER QUENCH )
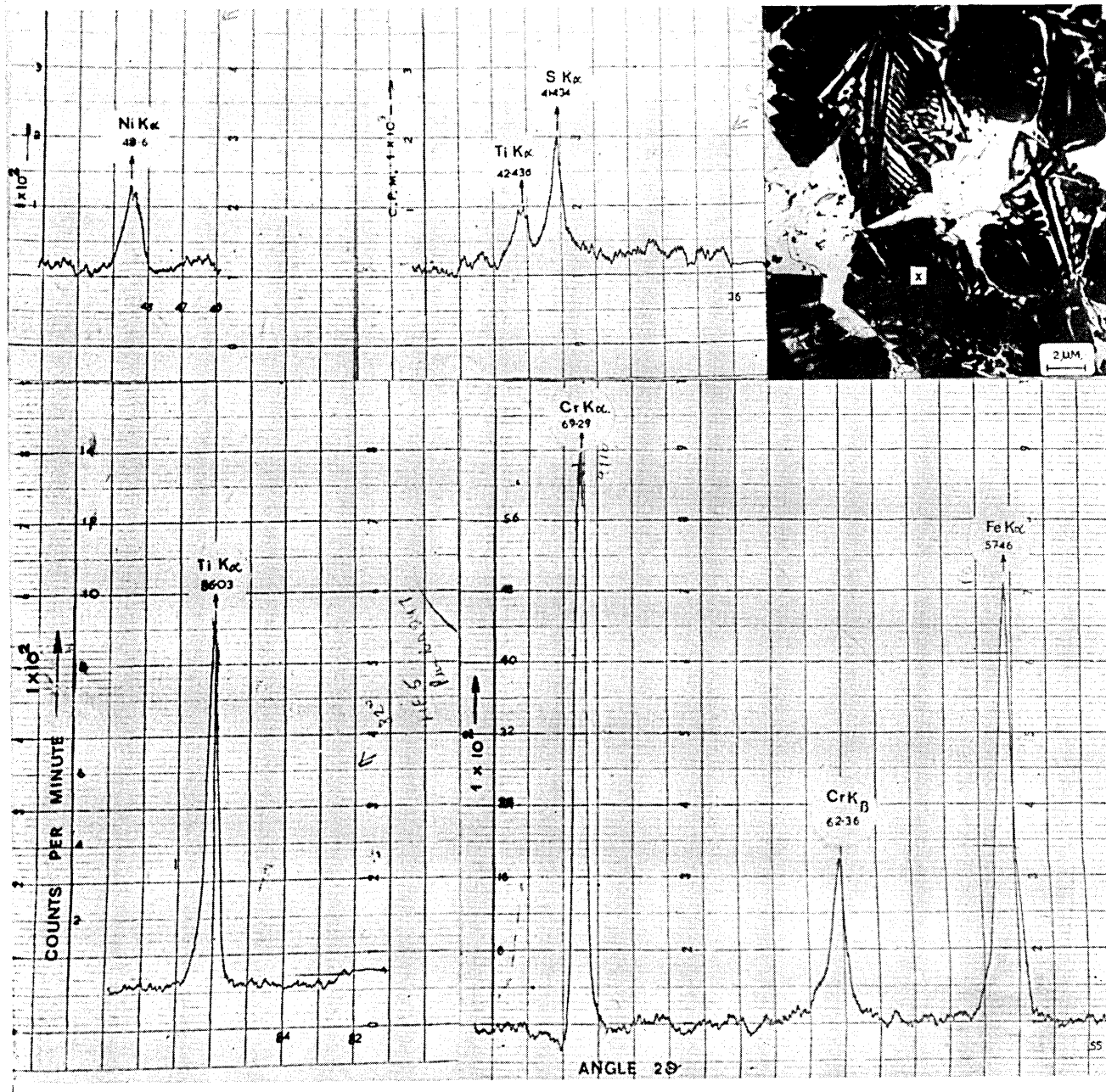
FIG. 84. SHOWS COMPOSITION OF THE EUTECTIC BORIDE

RD/M/R118